TAMPEREEN TEKNILLINEN YLIOPISTO
TAMPERE UNIVERSITY OF TECHNOLOGY

Jari Pohjola

Probabilistic Modeling of Landscape Development and Surface Water Body Formation

Julkaisu 1266 • Publication 1266

Tampere 2014

Tampereen teknillinen yliopisto. Julkaisu 1266
Tampere University of Technology. Publication 1266

Jari Pohjola

Probabilistic Modeling of Landscape Development and Surface Water Body Formation

Thesis for the degree of Doctor of Science in Technology to be presented with due permission for public examination and criticism in Auditorium 125, at Tampere University of Technology - Pori, on the 28th of November 2014, at 12 noon.

Tampereen teknillinen yliopisto - Tampere University of Technology
Tampere 2014

ISBN 978-952-15-3409-6 (printed)
ISBN 978-952-15-3420-1 (PDF)
ISSN 1459-2045

Thesis advisor
Tarmo Lipping

Author
Jari Pohjola

Probabilistic Modeling of Landscape Development and Surface Water Body Formation

Abstract

Biosphere development estimation is a major factor in assessing the long-term safety of a final repository of spent nuclear fuel in the time scale of thousands of years. In this thesis the future evolvement of the Olkiluoto modeling area, situated in Western Finland, is studied. The main reason for the change in the landscape is the ongoing post-glacial uplift. Due to this uplift, the shoreline will be shifted westwards by several kilometers during the next 10 000 years. The focus of the study is on the newly formed surface water bodies since they are the most significant carriers of radiating particles in potential risk scenarios of canister failures.

The thesis has been divided into three parts: 1) creation of a probabilistic digital elevation model, 2) optimization of the components and parameters of a mathematical land uplift model and 3) estimation of surface water body formation based on the aforementioned models. The probabilistic digital elevation model is created using measurement data from numerous sources. Thin plate spline method is used for interpolation and the uncertainties in the source data are taken into account using Monte Carlo simulation. The mathematical land uplift model used in the thesis is based on past shore level information. An alternative eustatic model, using more precise data from the Baltic Sea area, and updated ice retreat and crust thickness models are presented to be used in the land uplift model optimization process. The parameters of the land uplift model are optimized using data from past shore level displacement and archaeological findings. The parameter optimization is done in a probabilistic way using Monte Carlo simulation.

The probabilistic digital elevation and land uplift models are combined in the surface water body estimation where four main lakes are shown to be formed in the vicinity of the present Olkiluoto Island. The study results reveal that the landscape development tracks produced by the different modeling schemes estimated using alternative eustatic models are mostly similar indicating the robustness of the modeling.

Contents

Acknowledgments

The research work for this thesis was carried out at Tampere University of Technology (TUT) - Pori during the period 2010-2014. First I would like to thank my thesis advisor Professor Tarmo Lipping (TUT) for his guidance and support on this thesis. Tarmo has provided the possibility to conduct the research work related to this thesis.

I would like to express my gratitude to Adjunct Professor Jari Turunen (TUT) for his advice and encouragement throughout the thesis process. I would also like to thank Ari Ikonen (Posiva) for his interest and support on the subject.

In addition, I wish to express my gratitude to the pre-examiners Adjunct Professor Petteri Alho (University of Turku) and Senior Geologist Gustav Sohlenius (Geological Survey of Sweden) for their valuable comments on the thesis. I would also like to thank Professor Markku Poutanen (Finnish Geodetic Institute) for agreeing to act as an opponent for this thesis.

Posiva Oy, together with the Satakunta University Foundation, have provided long-term funding for the research work. Also the financial support from the Satakunta Regional Fund of the Finnish Cultural Foundation is gratefully acknowledged.

Finally, I would like to thank my family, especially my mother Lahja, for supporting me throughout my life.

Ulvila, October 6, 2014,

Jari Pohjola

List of Abbreviations and Symbols

Abbreviations

AP	year After Present
BIFROST	Baseline Inferences for Fennoscandian Rebound, Sea-level, and Tectonics
BP	year Before Present
DEM	Digital Elevation Model
DGPS	Differential Global Positioning System
DSM	Digital Surface Model
DTM	Digital Terrain Model
FEA	Finite Element Analysis
GIA	Glacial Isostatic Adjustment
GIS	Geographical Information System
GPS	Global Positioning System
GTK	the Geological Survey of Finland
IAEA	International Atomic Energy Agency
IDW	Inverse Distance Weighting
IOW	Institut für Ostseeforschung Warnemünde
KKJ	Finnish coordinate system
LiDAR	Light Ranging and Detection
MEE	Ministry of Employment and the Economy
NLS	the National Land Survey of Finland
RTK	Real Time Kinematic
TIN	Triangulated Irregular Network
TPAPS	MatLab routine for implementing thin plate spline interpolation
TVO	Teollisuuden Voima Oyj
UNTAMO	GIS-based toolbox for biosphere modeling

Symbols

Land uplift model

A_f	total subsidence in fast uplift (m)
A_s	download factor in slow uplift (m)
B_f	inertia factor in fast uplift (year^{-1})
B_s	inertia factor in slow uplift (year^{-1})
ct	crustal thickness (km)
E	eustatic sea level rise (m)
t	time (years BP)
T_f	time for the turning point from subsidence to uplift in fast uplift (years)
T_s	time for maximal uplift rate in slow uplift (years)
U	land uplift (m)
U_f	fast uplift (m)
U_s	slow uplift (m)
v_0	recent uplift rate (m/year)

Chapter 1

Introduction

This thesis is about modeling the future development of the geomorphic landscape in the Olkiluoto area in Finland using a time scope of thousands of years. Geomorphic landscape contains the geomorphology and the water body distribution in the area. It can be considered as a part of the whole landscape which contains also e.g. fauna, flora and human activities. The main reason for the change in the geomorphic landscape is the post-glacial uplift of the earth's crust. Due to this uplift, the shore level will be shifted westwards by several kilometers, new water bodies will be formed and land usage on the present land area will most probably change during the following 10 000 years. The location and the extent of the modeling area are presented in Figure 1.1.

The size of the Olkiluoto Island is approximately 12 km^2. The majority of the western part of the island is constructed area. The other parts of the island are mainly covered by forests and farmland. There is also human settlement in the island. Especially at the coastal part of the island there are summer houses.

A map illustrating the present soil type locations in Olkiluoto area is shown in Figure 1.2. From the map it can be identified that the shores of Olkiluoto Island are covered with rock and till. There are also large deposits of gyttja, mud and clay near the shoreline. The bedrock types in Olkiluoto area are shown in Figure 1.3. Biotite paragneiss is the main bedrock type in the Olkiluoto Island. There are also significant deposits of granite, granodiorite and dolerite in the Olkiluoto area.

The two rivers having an eustary in Eurajoensalmi Bay, located in the vicinity of

the Olkiluoto Island are called Eurajoki and Lapinjoki. The River Eurajoki originates from the northern part of Lake Pyhäjärvi, which is located about 35 km from Olkiluoto Island. The source for River Lapinjoki is Lake Koskeljärvi situated approximately 45 km from Olkiluoto Island.

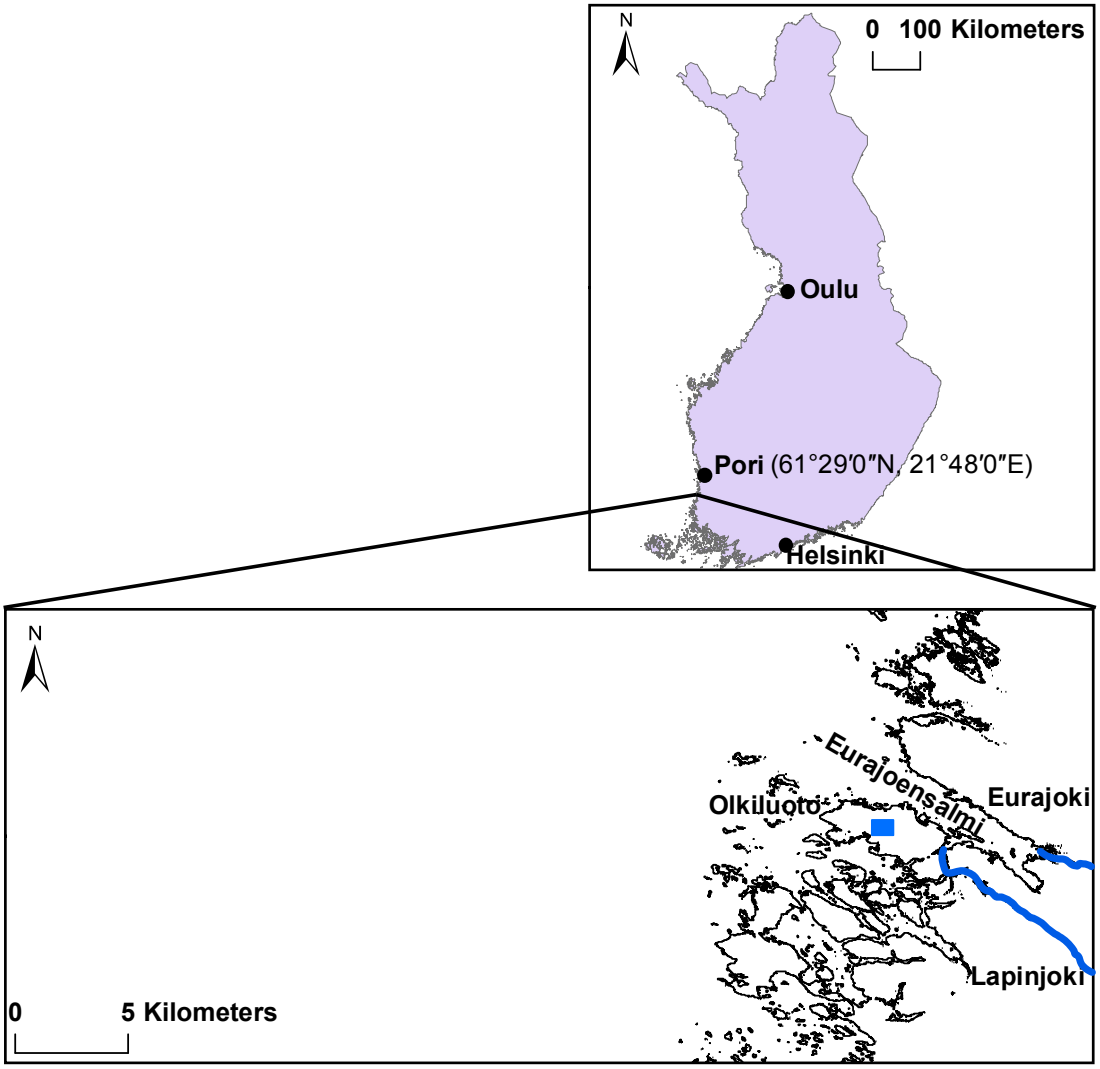

Figure 1.1: The location of the modeling area. The blue rectangle indicates the approximate location of the repository of spent nuclear fuel.

While there may be several reasons to model the future development of the geomorphic landscape, the main driving force for the research presented in this thesis is the need to assess the safety of the repository for spent nuclear fuel in Olkilu-

oto. Therefore, the regulations and requirements concerning the safety analysis of the repository set the framework also for the geomorphic landscape modeling effort presented.

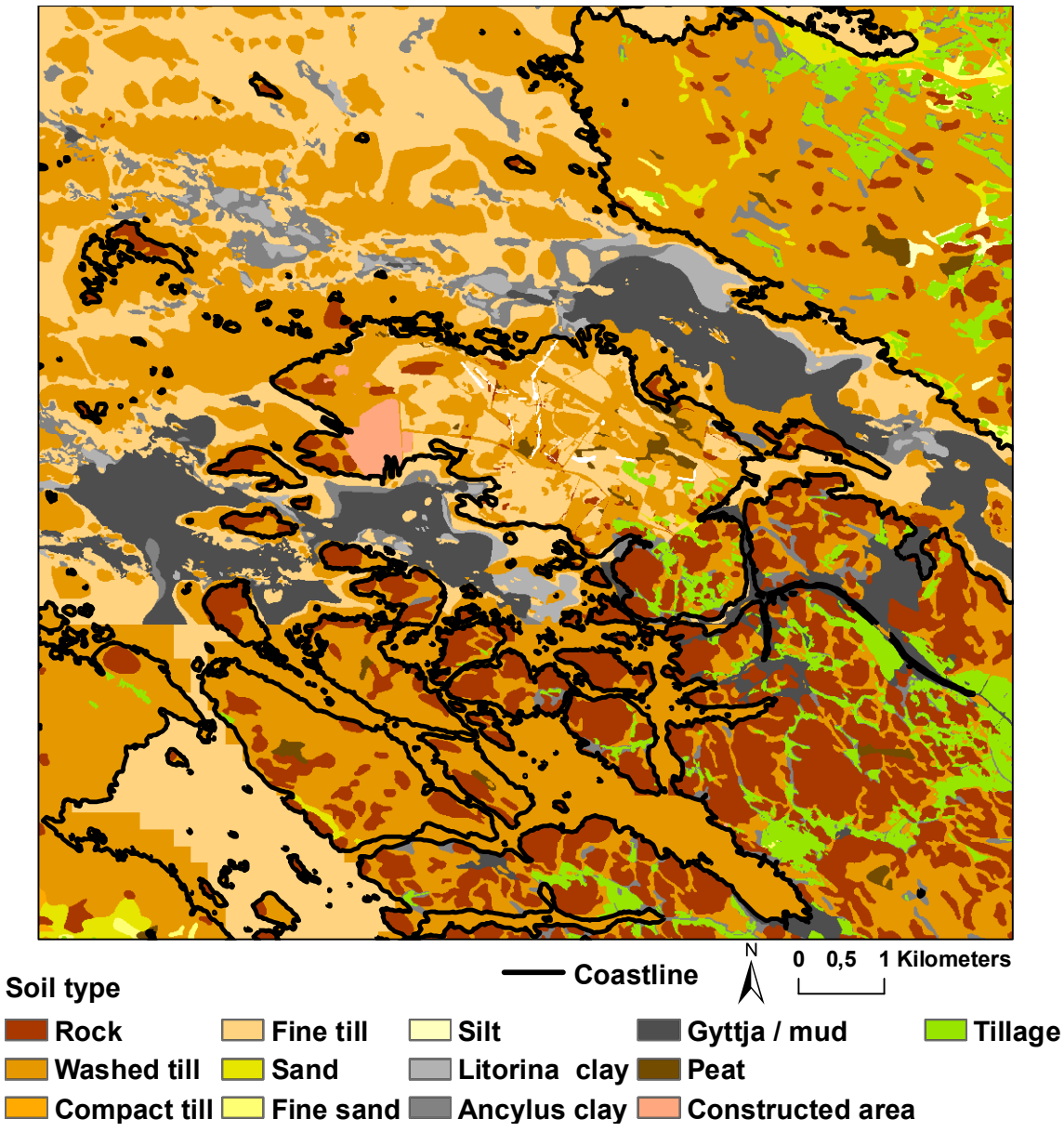

Figure 1.2: Soil type map of the Olkiluoto area. The map includes edited material from (Rantataro, 2001, 2002; Rantataro and Kaskela, 2009) and the Soil map 1:200 000 ©Geological Survey of Finland 2013.

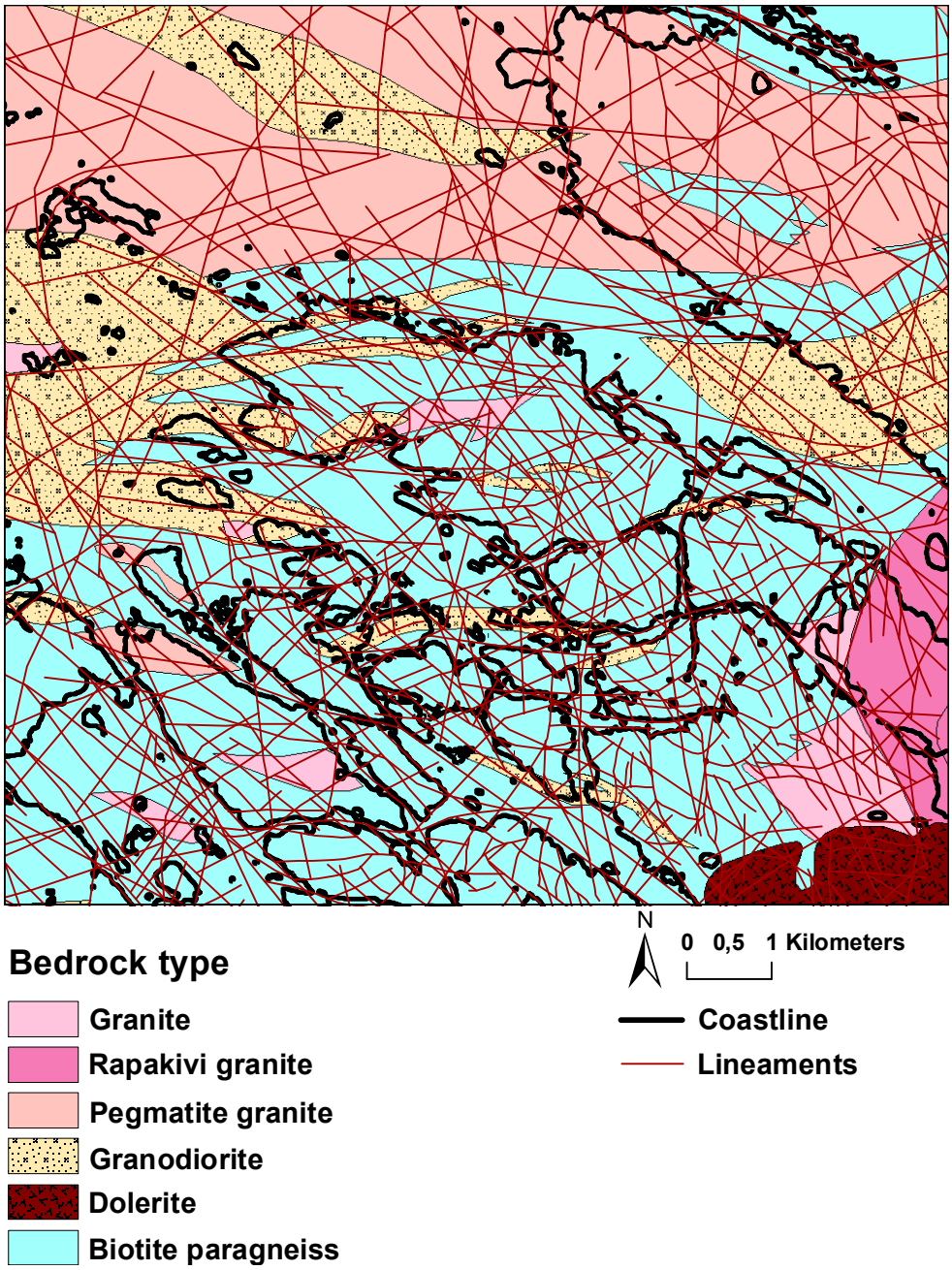

Figure 1.3: Bedrock type map of the Olkiluoto area. The map includes edited material from the Digital bedrock map 1:200 000 ©Geological Survey of Finland 2010 and (Korhonen et al., 2005).

1.1 Safety assessment of the spent nuclear fuel repository

According to the Finnish Nuclear Energy Act (990/1987), Act (342/2008) amending the Nuclear Energy Act and the Nuclear Energy and Government Decrees (161/1988) and (736/2008), nuclear waste generated in Finland shall be handled, stored and permanently disposed in Finland. The Nuclear Energy Act (990/1987) moment 34 enforces the atomic energy companies to maintain safety and its assessments after nuclear waste disposal. Finland is a member of the International Atomic Energy Agency (IAEA) and the Nuclear Energy Agency and follows their guidelines according to nuclear energy and waste disposal.

Posiva Oy was established in 1995 to maintain and process nuclear waste and its safety aspects for two nuclear energy companies, Teollisuuden Voima Oy and Fortum Power and Heat Oy. Posiva has been granted permission from the Ministry of Employment and the Economy (MEE) to build nuclear disposal tunnel, ONKALO, in Olkiluoto. The purpose of the ONKALO excavation repository is to keep nuclear waste from 5 power plants, Olkiluoto $1-3$ and Loviisa $1-2$, safely over 10 000 years. Posiva filed Decision-in-Principle applications to MEE to enlarge the ONKALO repository to dispose nuclear waste from planned two new reactors, Olkiluoto 4 and Loviisa 3.

IAEA has set guidelines for long term disposal. IAEA Safety standard 5 states in moment 2.15 (IAEA, 2011):

> *The safety objective is to site, design, construct, operate and close a disposal facility so that protection after its closure is optimized, social and economic factors being taken into account. A reasonable assurance also has to be provided that doses and risks to members of the public in the long term will not exceed the dose constraints or risk constraints that were used as design criteria.*

Posiva Oy is planning to seal the nuclear waste in cast iron (inner core) and copper (outer edge) capsules in the ONKALO tunnel. These capsules are then buried in boreholes drilled in crystalline rock, and the empty space between the borehole

and copper is filled with bentonite clay (Palomäki and Ristimäki, 2013). Finnish Radiation and Nuclear Safety Authority (STUK) regulates the use of nuclear energy in Finland and it is stated in the Guide for Disposal of Nuclear Waste (STUK, 2013) in moment 316:

> *The unlikely events potentially impairing long-term safety induced by natural phenomena to be considered shall at least include rock movements jeopardizing the integrity of disposal canisters. Unlikely events caused by human actions to be considered shall at least include the boring of a medium-deep water well at the disposal site and core drilling or boring hitting a disposed waste package. In such a case, it is assumed that the existence of the disposed waste is not known and that the incident may only occur 200 years following the closure of the disposal facility at the earliest.*

It is also stated in the Guide for Disposal of Nuclear Waste (STUK, 2013) in moment 309:

> *In applying the dose constraints, the exposure shall be assumed to arise from radioactive materials released from the repository and migrated to near-surface groundwater bodies and further to above-ground watercourses. At least the following potential exposure pathways shall be considered:*
> - *the use of contaminated water as household and irrigation water and for animal watering; and*
> - *the use of contaminated natural or agricultural products originating from terrestrial or aquatic environments.*

Moment 309 in (STUK, 2013) provides the basis for this research work. In the 'worst-case' scenario, the waste canister is broken and it will leak radionuclides to groundwater, which transfers them to different water bodies such as wells, rivers and lakes. Eventually plants will consume the polluted water, and herbivores eat the plants and finally the local biosphere around the nuclear waste disposal will be a potential source of radionuclides to humans.

The surface environment, or the local biosphere itself has no safety function for nuclear waste disposal, but in long-term safety analysis the potential radiation and ionizing radiation risks have to be assessed. Olkiluoto Biosphere Description report states several issues considering the potential risks at surface (Posiva Oy, 2013a):

How does the surface environment evolve after closure of the repository?

How do hypothetical radionuclide releases from the geosphere migrate and accumulate in the geological-hydrological-biological cycles of the surface environment?

How do humans utilize and change the surface environment and to what extent might people be exposed to radionuclide releases from the repository ending up in the surface environment?

What kind of biotopes might there be available for plants and animals and to what extent might they be exposed to radionuclide releases from the repository ending up in the surface environment?

Groundwater will also accumulate into water bodies such as ponds and lakes, so the fish and benthic vegetation also take part in the radiation circulation process. An example of the radiation circulation process is illustrated in Figure 1.4. Due to the reasons discussed above, biosphere modeling is an essential part of assessing the safety of nuclear waste management in the time span of thousands of years. Especially the risks for humans and environment due to possible radionuclide releases have to be studied carefully (IAEA, 2011).

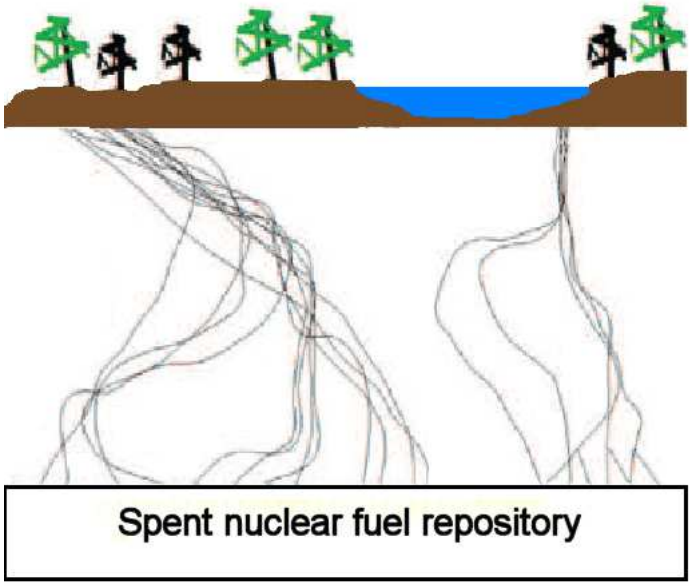

Figure 1.4: Illustration of radioactivity propagation.

1.2 Objectives and structure of the thesis

The main objectives of this thesis can be summarized as follows:

- ***How does the geomorphic landscape at the Olkiluoto site evolve during the next 10 000 years?***
- ***What are the probable locations, volumes and surface areas of the future water bodies?***

An effective way to study the future development of the biosphere is to calculate the probability of various development scenarios and to determine those of high probability. To address the objectives of the thesis in a quantitative way, numerical simulations must be carried out. The overall task of predicting the future geomorphic landscape development and surface water body formation can be separated into the following three subtasks:

- to generate a probabilistic digital elevation model of the study area based on available measurement data
- to develop a probabilistic model for the post-glacial land uplift process for the study area
- to simulate the formation of surface water bodies in the vicinity of the Olkiluoto Island using the results of the previous subtasks.

These subtasks are addressed separately in this thesis in chapters 2, 3 and 4, respectively. As each subtask has its own separate methodology and scientific framework, each of the mentioned chapters contains an overview of previous literature and methodology related to the particular subtask, followed by the description of the work performed in the course of this thesis.

In chapter 2 the data models and main procedures for DEM generation are shortly presented first. As most of the study area currently constitutes seabed, numerous different source data sets had to be considered to create the DEM. These data sources are described one by one with particular interest in their reliability. Several interpolation methods are presented next with some comparison and the selection of the thin plate spline interpolation algorithm for the DEM generation task is justified. It was found during the research that the selection of the interpolation neighborhood has a

crucial impact on the resulting DEM; therefore, a detailed procedure was developed for this purpose. The uncertainties in the source data are taken into account by using the Monte Carlo simulation to obtain a probabilistic DEM. Finally in chapter 2 the developed probabilistic DEM is presented and new updates to the DEM, not yet exploited in the future geomorphic landscape simulations, are also presented.

In chapter 3 two different approaches to land uplift modeling - geodynamical modeling and fitting a mathematical model to the source data on past shoreline displacement - are discussed first. The mathematical model proposed by Tore Påsse (Påsse, 2001) is described next with the emphases on the origin, meaning and optimization of the model components and parameters. An alternative eustatic curve is compiled based on more precise data on the Baltic Sea area. The source data on past shore level displacement, used for land uplift model parameter optimization, is presented next. Finally, the developed parameter optimization procedure is described and the resulting probabilistic land uplift model is presented and discussed.

In chapter 4 a brief overview on biosphere modeling is given first. Three scenarios for geomorphic landscape and surface water body development are specified next corresponding to different model parameter optimization schemes and different eustatic curves. A method developed for drawing realizations from the probabilistic DEM and land uplift model is also described. Finally, the simulation results indicating the formation of four main lakes in the vicinity of the Olkiluoto Island are presented; the development of these lakes is described by means of their surface area and volume for all three geomorphic landscape development scenarios.

1.3 Author's publications related to the thesis

Although this thesis is presented in the form of a monograph, the research work has also been presented in several international peer-reviewed publications and as parts of the Working Report series by Posiva Oy. The probabilistic DEM creation (described in chapter 2 in the thesis) has been discussed in (Pohjola et al., 2009a,b). In (Pohjola et al., 2009b) the basic principles of the creation of the probabilistic DEM are presented in a 1.8 km $\times$ 1.5 km test area inside the modeling area of Olkiluoto.

The results of (Pohjola et al., 2009b) show that the applied methods (thin plate spline interpolation, overlapping computational packets and the use of Monte Carlo simulation) work well for producing a smooth and reliable DEM with an error model. A broader look at the process of creating a DEM in the Olkiluoto area is given in (Pohjola et al., 2009a).

The refinement of land uplift model (chapter 3 in the thesis) has been discussed in (Pohjola et al., 2012a,b, 2013). In (Pohjola et al., 2012a,b, 2013) the parameters of the mathematical land uplift model by Påsse (2001) are optimized using data on past shore level displacement. Also new models for ice retreat estimation and eustatic sea level rise are included into the optimization process. The resulting probabilistic land uplift parameter maps in (Pohjola et al., 2012a,b, 2013) indicate the possibility of local deviations in land uplift in Finland.

In (Pohjola et al., 2014a,b) the probabilistic estimation process of geomorphic landscape development and surface water body formation (chapter 4 in the thesis) based on the digital elevation and land uplift models is presented. The results show that the geomorphic landscape development tracks produced by the different modeling schemes estimated using alternative eustatic models are mostly similar. However, the results also reveal some more improbable realizations, which differ significantly from the main development tracks.

Chapter 2

Creation of probabilistic digital elevation model

Digital elevation model (DEM) is a representation of the surface of a terrain. It is a substantial component of geographical information systems (GIS) for many applications (Li et al., 2005). In the literature the terms *digital elevation model* and *digital terrain model* (DTM) are often used interchangeably while *digital surface model* (DSM) denotes the upper surface of the terrain together with the objects belonging to it (trees, buildings)(Maune, 2001).

There are two ways of representing a DEM: the raster model and the triangulated irregular network (TIN) model. In the raster model the area to be modeled is divided into regular-size squares (pixels), where each square has a height value. The spatial resolution of the raster model may vary from centimeters to kilometers depending on the area and the use of the model. In the TIN model the surface is represented by a network of triangles connecting the points with given elevation. The most common way to obtain the TIN representation of a surface is to determine the key elevation points and to use the Delaunay triangulation method (de Berg et al., 2008). The method was first presented in (Delaunay, 1934) where the theory was established using volumes.

While, in general, any terrain surface can be represented using either the raster or the TIN model, either representation has its advantages and disadvantages some

of which can be listed as:

- the TIN model is more straight forward to create based on irregular measurement data
- the TIN model is often easier to render and with the TIN model the resolution of representation (and therefore the required memory storage) scales according to the landscape: flat areas are represented by large triangles while rugged terrain is represented by small triangles
- it is easier to incorporate new data into the TIN model; also the features of the landscape (rivers, roads etc.) are easier to integrate into the TIN model compared to the raster representation
- the raster model is more convenient from the point of view of several analysis tasks (for example, slope and aspect of the terrain are easier to calculate based on the raster model).

In the DEM creation and analysis effort presented in this thesis both representations were used, however, the final result was produced in the raster format for further calculations. The terrain model, either raster or TIN, may be viewed as a 2.5 dimensional object as it does not involve 3D topology.

The development of LiDAR (*Light Ranging and Detection*) technology has taken the DEM creation efforts to a new level: instead of measuring the elevation of individual points, large areas can be scanned from airplanes or helicopters in short time and with superior accuracy (Shan and Toth, 2009). In Finland the National Land Survey (NLS) is currently carrying out the campaign of LiDAR scanning the whole territory of the country in order to develop a 2 m $\times$ 2 m digital elevation model. The campaign started in 2010 and by the end of 2013 235 000 square kilometers of the total 338 000 have been scanned. The maximum error of the acquired data is 60 cm in the x-y directions and 15 cm in the z direction by specifications. The Olkiluoto area was scanned in spring 2012.

The modeling work presented in this thesis was started in 2008 when LiDAR data were not available from the area of interest. The first versions of the DEM model were composed based on various sets of elevation data either in the form of individual points, height contours or lines of sonar measurements (in sea areas). To obtain the

elevation model in the form of a regular grid the following issues had to be solved:

- the selection of proper interpolation method
- determination of the neighborhood for interpolation purposes
- specifying the confidence interval for the resulting probabilistic DEM.

In this chapter these issues will be considered one by one providing also the theoretical background where appropriate.

From the point of view of terrain modeling the area of interest (see Figure 1.1) can be divided into two parts: the area currently above the sea level (i.e., dry land) and the area currently under the water (i.e., seabed). In the latest version of the DEM the LiDAR data by the NLS were incorporated into the original model in the area of dry land. Due to the superior accuracy of the LiDAR measurements there is no need to consider measurement error in this area. It should be noted, however, that the interpolation methodology presented is still relevant as major part of the area considered in the landscape development modeling effort is currently under the water and thus cannot be mapped using the LiDAR technique except for shallow coastal waters that can be measured using bathymetric LiDAR. In the final section of this chapter the updated elevation model is presented and the interpolation error is studied by comparing the original interpolated DEM with the LiDAR data in the dry land area.

2.1 Source data used in DEM creation

The source data used in the creation of the Olkiluoto area DEM contain data sets from various sources. These data sets include elevation data on regular grid, spatially irregular measurement points, contour lines, as well as lines of sonar measurements at sea areas. The majority of the data represents land areas while the coverage is much more sparse and more irregular at sea areas. Precision and reliability of the data sets vary a lot. Normal probability distribution was assigned to all the other data sets except for the data obtained from the Finnish Marine Administration (©Finnish Marine Administration 2005; permission number 529/721/2005), for which an asymmetric distribution was generated. This was justified as the values of this

data set give the guaranteed minimum depth of the water for marine traffic. The effect of land uplift to data set points was taken into account by multiplying the age (in years) of the data set in question with the current uplift rate in Olkiluoto area (approximately 6 mm per year), and adding this number to the elevation values.

In the following, the data sets are presented one by one and the preprocessing steps taken before their application to DEM creation are described. An overview of the data sets is presented in Table 2.1 and in Figure 2.1 a sample of the spatial distribution of the source data from the northern part of the Olkiluoto Island is presented. In Table 2.2 the proportional shares of the data sets are shown.

2.1.1 Data from the National Land Survey of Finland

The data from the National Land Survey of Finland (*Elevation model* 25 *m* ©National Land Survey of Finland (NLS), permission 41/MYY/08-09) mainly from 1997 contain individual elevation and sea depth points as well as elevation and sea depth contour lines covering the whole area of interest except the westernmost sea areas. The *Elevation model* 25 *m* is created based on the digitized elevation contours and water system elements of the base map by means of triangulated network interpolation on the raster of 25 meter resolution. In the triangulated network interpolation a contiguous network of triangles is formed between the available data points. The elevation of the interpolated points is obtained from the information about the slope and orientation of the triangles. The elevation contours of the source data occurred in 5 meter steps. The factors determining the precision of the *Elevation model* 25 *m* data include the method used for obtaining the elevation contours, the density of the contours, the quality of the source data and the interpolation method. The mean and standard deviation of the precision of the *Elevation model* 25 *m* data at the area of interest is stated to be 1.76 and 1.39 meters, respectively (National Land Survey of Finland, 2013).

2.1.2 Seismic measurements

This data set contains seismic measurements performed in different parts of the Olkiluoto Island during 1975-1978 and 2002-2007. In the case of the data acquired during 1975-1978, the positioning of the measurement points was performed by the Olkiluoto power plant operator. It was a common practice then to use local reference points and to determine the elevation and coordinates of the so-called pole points by means of theodolite. Theodolite is a common tool in geodetic measurements for measuring angles between landmarks. The lines of seismic measurement points are oriented in 45 degree angles with respect to the KKJ coordinate system causing about $10 - 15$ meter interpolation error in the spatial location of the points. The measurements cover the power plant areas owned at the time by the energy corporations Teollisuuden Voima Oy (TVO) and Imatran Voima Oy (IVO). The vertical precision of the measurements was specified as $\pm$ 1 meters with 95 % confidence based on comparison with the information contained in other data sets and the knowledge on the acquisition method of the data (Lehtimäki, 2003).

The more recent seismic measurements were performed during 2001-2003 and in 2005. These measurements were made along lines separated by 50 meters and oriented according to the KKJ1 coordinate system. The Real Time Kinematic (RTK) GPS device was used for positioning the measurement points. The measurements cover a significant part of the island. The elevation of the measurement points was obtained using a hosepipe-based water level device. The precision of the measurements was specified as $\pm$ 0.5 meters with 95 % confidence based on the knowledge on the measurement procedure and comparison with other data (Öhman et al., 2006). During 2006-2007 another seismic measurement campaign was carried out. The measurement points were again positioned using the RTK-GPS device. The precision of the elevation data was specified as $\pm$ 0.3 meters with 95 % confidence based on the knowledge on the measurement procedure and comparison with other data (Öhman et al., 2008).

2.1.3 Acoustic-seismic measurements

The acoustic-seismic measurements performed by the Geological Survey of Finland (GTK) for Posiva Oy in July 2000 covered about 360 line kilometers. The studies covered sea areas around the Olkiluoto Island. In addition, in September 2000 measurements along another 90 line kilometers were performed at sea areas south west, west and north west to Olkiluoto. The depth of the seabed was measured using a sonar device (MeriData, 28 kHz sensor). Positioning was done using differential GPS (DGPS). The precision of the data was estimated at $\pm$ 2.0 meters with confidence 95 % in the report of the measurement campaign in (Rantataro, 2001, 2002). The measurement results were corrected for the sea level data of the day the measurements were performed before the data were used for DEM generation. Depth contours with the step size of 5 meters as well as the coastline estimate were produced as the result of the campaign. These contours were also used in the generation of the high resolution DEM.

Similar measurements were performed also in 2008 by GTK. The positioning was done using DGPS and a similar sonar device as in earlier measurements (MeriData, 28 kHz sensor) was used in measuring the depth of the sea. Based on the available information the precision of the data was specified as $\pm$ 2.0 meters with 95 % confidence (Rantataro and Kaskela, 2009).

2.1.4 IOW data

The Leibniz Institute for Baltic Sea Research (Institut für Ostseeforschung Warnemünde, IOW) has produced data about the ground elevation at 1.8 km $\times$ 1.8 km resolution for the whole Baltic sea area covering sea as well as land areas. The data has been produced based on various source data sets the resolution of which has varied significantly. For each data point a number of variables are provided including the mean elevation, minimum elevation, maximum elevation and standard deviation of the elevation data over the area represented by the point. For the purpose of this work each data point of the IOW data was assigned standard deviation separately based on these variables (Seifert et al., 2001).

2.1.5 Sonar measurements

Sonar measurements arranged by TVO in 1972 contain measurement lines at the sea areas surrounding the Olkiluoto Island at two different places. The results of the measurements are given with 10 centimeter precision. The measurements are performed using a sounding line. Possible factors causing errors in the measurement results include the sea level at the moment of data acquisition and deviations in the angle of the sounding line. Based on these arguments the precision of the data was specified as ± 1 meter with 95 % confidence. Depth contour lines were produced for TVO in 1973 and they cover sea areas near the Olkiluoto Island. The step size of the contour lines is 1 meter. The precision of the data was specified as ± 1 meter with 95 % confidence based on comparison with other data and the year of measurement.

In 2007 TVO arranged a sonar measurement campaign of coastal water areas near the Olkiluoto Island. Depth contours of the seabed covering various regions around the island were produced based on the results. The areas covered are of relatively small size and include mainly coastal areas and straits. The contour lines were produced at every 0.2 meters of depth. The precision of these data was specified as ±0.5 meters with 95 % confidence based on the knowledge on the measurement procedure and comparison with other data.

In 2009 Posiva Oy collected additional sonar measurement data especially from coastal areas where the source data previously was sparse or non-existent.

2.1.6 Data from the Finnish Maritime Administration

The data obtained from the Finnish Maritime Administration (MKL) and produced in 2005 (©Finnish Maritime Administration; permission number 529/721/2005) includes depth contour lines and individual measurement points from the area of interest. The contour lines are composed so that the sea at the location of the lines is at least as deep as indicated by the assigned depth value. At depths below 10 meters it can be assumed that the sea is actually at least 1 meter deeper than the indicated number would suggest. At deeper sea areas it can be assumed that there is at least 2 meters more water than the indicated number would suggest. Due to

this property, asymmetrical probability distribution was assigned to the data, limited from above by the value indicated at the contour line but having a longer tail towards lower values. Using this kind of probability distribution allows values indicated on the depth contour line to occur, however, their probability in the Monte Carlo simulation procedure is low.

2.1.7 Precision leveling

Several precise leveling campaigns have been performed in Olkiluoto. The first one took place in 2003 and the latest in 2011 (Saaranen et al., 2012). The data includes several measurement points at the Olkiluoto Island measured using GPS stations. The precision of the data was estimated as ± 0.01 meters with 95 % confidence.

2.1.8 Ground penetrating radar measurements

The aim of the ground penetrating radar measurements performed by GTK in 2001 was to determine the thickness of the peat layer as well as other soil layers at the mire area of Olkiluodonjärvi. The measurement points were positioned using GPS. The measurements were performed using the ground penetrating radar SIR-2 produced by the Geophysical Survey Systems Inc. (GSSI) and the antenna Subecho-150 produced by Radarteam AB. Measurement time was set to 200 ns. The power lines located at the measurement site caused interference in the GPS positioning as well as in the radar measurements (Leino, 2001). Based on this information the precision of the data was specified at ± 0.5 meters with 95 % confidence.

Table 2.1: Summary of the source data sets

Name	Acquisition year	Data set type	Precision (95 % confidence)
Elevation model 25 m (NLS)	1997	Elevation and depth contour lines and data points	Mean precision = 1.76 m, Standard deviation = 1.39 m
Seismic measurements	1975-78	Elevation data points	± 1 m
	2002		± 0.5 m
	2006-07		± 0.3 m
Acoustic-seismic data (GTK)	2000, 2008	Sonar measurement and depth contour lines	± 2 m
IOW data	2001	1.8 km × 1.8 km data grid	Point-wise assigned standard deviation
Sonar measurements	1972-1973 (TVO)	Sonar measurement and depth contour lines	± 1 m
	2007 (TVO)		± 0.5 m
	2009 (Posiva)		± 0.5 m
Finnish Maritime Administration data	2005	Data points	± 1 m
		Depth contour lines < −10 m	−1 m
		Depth contour lines >= −10 m	−2 m
Precision leveling	2011	Elevation data points	± 0.01 m
Ground penetrating radar data	2001	Lines of data points	± 0.5 m

Table 2.2: Source data set proportions

Name	Proportion (%)
Elevation model 25 m (NLS)	46.00
Seismic measurements	1975-78: 0.07
	2002: 0.25
	2006-07: 0.08
Acoustic-seismic data (GTK)	17.33
IOW data	0.01
Sonar measurements	1972-1973 (TVO): 0.12
	2007 (TVO): 3.06
	2009 (Posiva): 28.78
Finnish Maritime Administration data	4.14
Precision leveling	0.01
Ground penetrating radar data	0.16

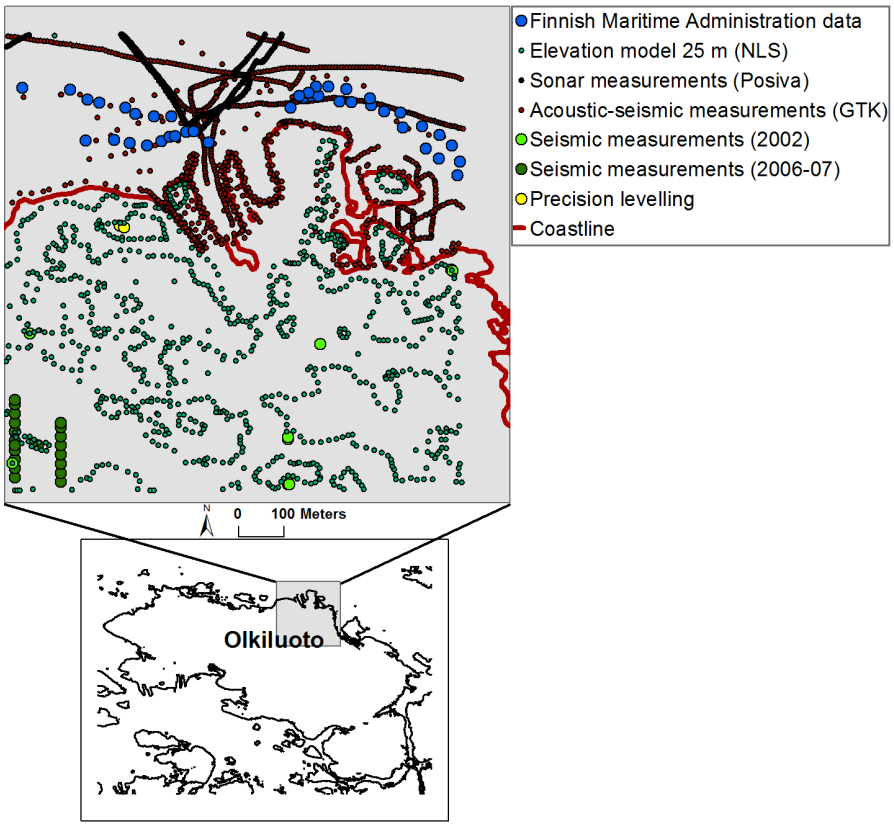

Figure 2.1: A sample of the spatial distribution of the source data.

2.2 Selection of the interpolation method

In DEM creation interpolation is usually considered to be a way to produce a regular grid from source data points. The quality of interpolation depends mainly on the following factors:

- data measurement accuracy
- data density
- data distribution and
- spatial variability of the data.

The interpolation process is usually based on calculating the weighted sum of the values of the data points neighboring the point at which the interpolation result is calculated. The general form of the interpolation equation is:

$$z_i = \sum_{j=1}^{n} \lambda_j z_j \tag{2.1}$$

In Equation 2.1 z_i is the elevation value of the point to be interpolated, the λ_j are the weights assigned to the neighboring points (the sum of the weights is usually 1 for normalization) and z_j are the known elevation values of the neighboring points. The resulting elevation z_i will lie within the range of the elevation values of the neighboring points if $\lambda_j > 0$ (de Smith et al., 2007).

2.2.1 Inverse distance weighting

In the case of the Inverse Distance Weighting (IDW) interpolation method, weighted sum is taken over the source data points in such a manner that the closer the data point is to the point to be interpolated the higher is its weight. The idea has its basis in the Tobler‘s law stating that the closer the points are located to each other on the ground (or sediment) surface the more related they are (Tobler, 1970). Due to its simplicity IDW is fast to calculate and therefore especially suitable in applications where computational power is limited. IDW can be expressed mathematically in the form of Equation 2.2:

$$z_i = \frac{\sum_{j=1}^{n} \frac{1}{d_j^p} z_j}{\sum_{j=1}^{n} \frac{1}{d_j^p}}, \tag{2.2}$$

where d_j denotes the distances between the source data points and the point to be interpolated. The distances are taken into account inversely. The value of the parameter p specifies the decay rate of the weights as the distance from the point to be interpolated becomes larger. Usually values 1, 2 or 3 are used for p, corresponding to linear, squared or cubic decay of weights, respectively. IDW is considered an exact interpolation method as the calculation scheme respects the values of the source data points strictly. However, this property can cause problems in the presence of peaks or holes in the true landscape as the output of the IDW is always inside the range of the values of the source data points. Therefore, IDW interpolation can produce a local hole in a location where there is actually a peak in the true landscape and vice versa. The IDW interpolation method is suitable for DEM production if the true landscape is relatively smooth and the source data points are located relatively evenly.

2.2.2 Kriging

Kriging is a geostatistical interpolation method, which is based on minimum mean square error data fitting. As in the IDW interpolation method, weights are assigned to the source data points based on the distance between them and the grid data points to be interpolated as expressed in Equation 2.1 (Cressie, 1993). There exist many variants of kriging, the ordinary kriging method being the most common among them.

In kriging, the optimal weights in Equation 2.1 are obtained based on the statistical properties of the elevation data. The statistical properties are analyzed in the form of semivariance computed as:

$$\gamma(h) = \frac{1}{2}(z_i - z_j)^2, \tag{2.3}$$

where h is the distance between points z_i and z_j. As presented in Equation 2.3, semivariance forms a relationship between the distance and elevation value of the

data points. A plot of $\gamma(h)$ against h is called semivariogram. Semivariogram can be obtained by considering all the possible pairs of data points, however, in the case of relatively large data sets and in order to obtain equally sampled function $\gamma(h)$ it is more practical to bin the semivariance function according to the distance parameter h. Example of a semivariogram (number of bins = 100) obtained for a set of elevation points in Olkiluoto area (Figure 2.1) is presented in Figure 2.2.

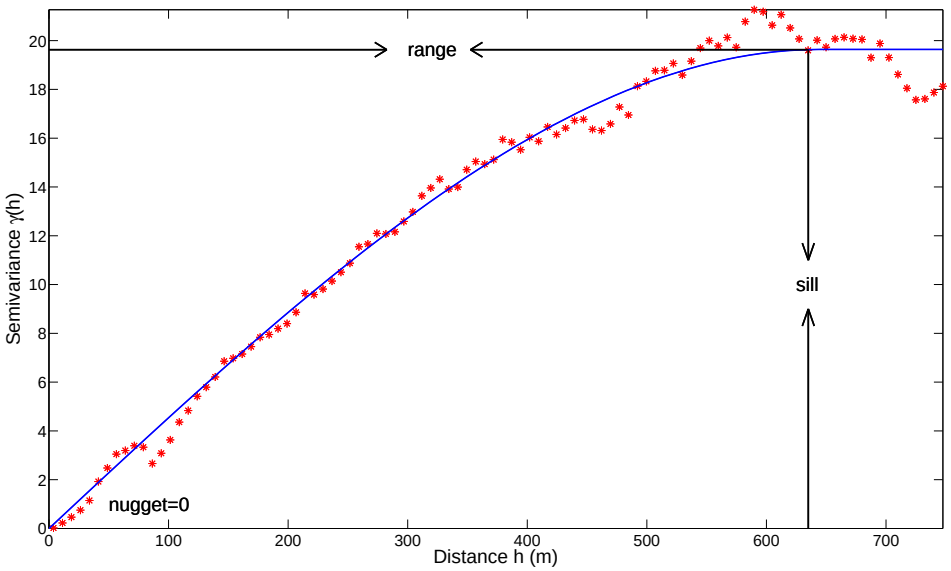

Figure 2.2: A spherical semivariogram of a set of elevation data points in the Olkiluoto area.

To obtain a smooth and mathematically well defined representation of the semivariogram, $\gamma(h)$ is modeled by some function such as exponential, for example. In Figure 2.2 a spherical model of the semivariogram is presented. The modeled semivariogram is denoted by $\gamma_m(h)$. The model of the semivariogram can be described by the following parameters (see Figure 2.2):

- *nugget*: the semivariance value at distance 0
- *range*: the distance at which semivariogram starts to level off
- *sill*: semivariance value at the distance equal to range.

In ordinary kriging the optimal weights in Equation 2.1 are obtained by solving a set of equations of the form:

$$\left(\sum_{j=1}^{n} w_j \gamma_m(h_{ij})\right) + \lambda = \gamma_m(h_{i0}); \qquad i = 1 \ldots n \tag{2.4}$$

with the constraint:

$$\sum_{j=1}^{n} w_j = 1. \tag{2.5}$$

In Equation 2.4 $\gamma_m(h_{ij})$ is the value of the semivariogram model at the distance separating the data points i and j, $\gamma_m(h_{i0})$ is the value of the semivariogram at the distance separating the i-th data point and the point of interpolation, and λ is a dummy variable called Lagrange multiplier. The weights w_j can be either positive or negative. The elevation value of the point of interpolation is calculated as:

$$z_0 = \sum_{i=1}^{n} z_i w_i. \tag{2.6}$$

Alternatively, semivariogram can be replaced by estimated covariances in finding the optimal weights for interpolation. In that case, Equation 2.4 changes to:

$$\left(\sum_{j=1}^{n} w_j C(i,j)\right) + \lambda = C(0,i); \qquad i = 1 \ldots n \tag{2.7}$$

In Equation 2.7 $C(i,j)$ is the covariance matrix where the indices i,j denote that the covariance is computed between data points i and j. The constraint of Equation 2.5 still holds (Cressie, 1993; Jones et al., 1998; LeMay, 1995).

As with the IDW method the optimal weights depend on the location of the data points in the neighborhood with respect to the point of interpolation. However, in kriging the overall statistical properties of the data set are also taken into account by means of the semivariogram and the optimization procedure involves the (semivariogram-modeled) mutual distances between the neighborhood data points.

In both, the semivariogram and the covariance method, the minimization procedure requires the knowledge of the distribution of the elevation values in the data set. If the distribution of the source data points is unknown or the number of the source data points is too small to estimate the distribution, the data points can be

assumed to be outputs of a Gaussian process with known covariances. This assumption guarantees that the linear estimator is the optimal unbiased estimator in the minimum mean squared error sense (Cressie, 1993). However, if the assumptions do not hold, there might be better nonlinear methods. If there is no spatial correlation between the source data points, the kriging interpolation becomes equal to calculating the mean value of the source data points. There is a chance to choose the wrong variogram function and in this case no properties are guaranteed (Cressie, 1993).

2.2.3 Thin plate spline interpolation

The third interpolation scheme considered in this thesis is the thin plate spline interpolation. Thin plate spline interpolation is a method based on fitting a surface through available data points by applying the minimal energy principle. The method was first introduced for geometric design applications in (Duchon, 1977). In this thesis the method was implemented using the `tpaps` routine of the Curve Fitting toolbox of the MatLab software. The routine takes the source data points (x- and y-coordinates and the elevation), the x- and y-coordinates of the grid points of the new DEM and the relaxation parameter p as inputs. The relaxation parameter p determines how strictly the approximated surface follows the source data points and its value is between 0 and 1. In the case $p = 1$ the surface passes exactly through the z-values of the source data points while in the case $p = 0$ linear interpolation by minimizing the sum of squared errors between the source data point values and the approximated surface is performed (Mathworks, 2014).

The thin plate spline interpolation method employs a commonly used basis function for representing coordinate mappings. It minimizes the weighted sum:

$$pE(f) + (1 - p)R(f), \tag{2.8}$$

where $E(f)$ is an error of the form:

$$E(f) = \sum_j |z_j - f(x_j, y_j)|^2 \tag{2.9}$$

and $R(f)$ is a roughness measure of the estimated surface:

$$R(f) = \int \left(|D_x D_x f|^2 + 2\,|D_x D_y f|^2 + |D_y D_y f|^2 \right). \tag{2.10}$$

Here f is the approximating function, z_j denotes the measured value of the j-th source data point and $D_i f$ denotes the partial derivative of f with respect to the i-th component of f. The value of the smoothing parameter p lies between 0 and 1, and is chosen by the user (Donato and Belongie, 2002).

In preliminary tests it appeared that if the value of the smoothing parameter was close to one and there was a sharp change in the slope of the landscape, the interpolated surface tended to oscillate. It was found that the oscillation artifact could be eliminated by adjusting the value of the smoothing parameter according to the variance of the source data points used in the interpolation process. The tests showed that good results were obtained by mapping logarithmically the variance range of $0.05 \ldots 0.7$ m^2 of the source data points to the range of $0.99 \ldots 0.01$ of the smoothing parameter value, respectively. In this mapping the smoother the terrain (i.e., the lower is the variance of the source data values), the higher the smoothing parameter value (i.e., the more strictly the interpolated surface is forced to follow the values of the source data points) and vice versa.

2.2.4 Interpolation method comparison

The three methods (IDW, ordinary kriging and thin plate spline approximation) were compared against each other by creating a 2.5 m $\times$ 2.5 m DEM grid of a LiDAR scanned area. Because LiDAR data was not yet available from the Olkiluoto area at that time, the data for the method comparison was taken from the city of Pori, which is located about 40 kilometers north of Olkiluoto. The city of Pori was LiDAR scanned by NLS in 2008, the minimum point density of the acquired data is 0.5 points per square meter (i.e., the maximum distance between points is 1.4 m) and the elevation accuracy of the data values is 15 centimeters. An area similar in size as the test area in Figure 2.1 was selected from the LiDAR data. The source data points from the LiDAR data were selected using a mask corresponding to the spatial

distribution of the source data in Figure 2.1. The rest of the LiDAR data were then regenerated using the three interpolation methods and a comparison against the original data was made. The amount of neighbors from the source data used in the interpolation was 80 in all cases. The interpolated surfaces were compared with the original surface created from the LiDAR data with a resolution of 2.5 m × 2.5 m. The error distributions between the interpolated surfaces and the original surface from the LiDAR data can be seen in Figure 2.3. Table 2.3 presents how the different methods managed against each other when comparing the results at different tolerances. The results indicate that thin plate spline approximation produces the highest amount of values inside 1 meter error tolerance. The results from IDW 3 and ordinary kriging are quite close to those from the thin plate spline approximation. Also the surfaces of the produced DEMs were inspected in terms of how they compare with natural shapes. IDW with exponent value of 3 produced several artifacts. Also, the basic property of the IDW method that the value of the interpolated cell stays always inside the range of the values of the source data points restricts its use in this kind of rapidly changing landscape. Thin plate spline approximation and ordinary kriging produced quite similar surfaces. However, thin plate spline approximated surface follows the original landscape shapes better than that obtained by ordinary kriging. Typically, this can be seen in the vicinity of steep slopes. Also, when the surface of the whole test area was inspected it appeared that ordinary kriging tends to flatten the shapes of the terrain whereas thin plate spline approximation gives more realistic results. Based on these results thin plate spline approximation was chosen as the interpolation method to be used in this thesis.

Table 2.3: The number of points within respective error tolerances. (The total number of points was 184 836.)

Method	Tol.: ± 0.01 m	Tol.: ± 0.1 m	Tol.: ± 0.5 m	Tol.: ± 1 m
IDW 3	537	5 027	22 488	41 438
Kriging	533	4 966	22 643	42 359
Tpaps	581	5 525	24 015	43 356

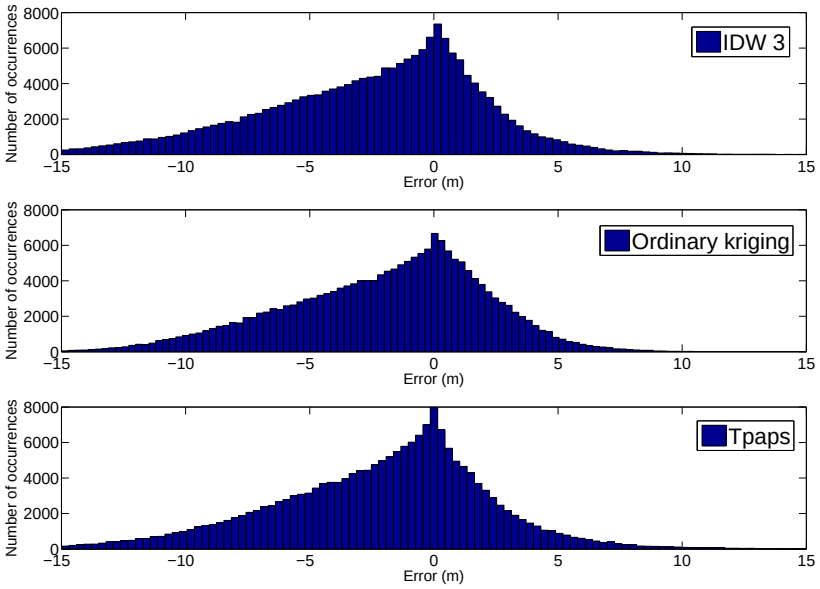

Figure 2.3: The resulting error distributions of the interpolation method comparison.

2.3 Selection of the neigborhood and computation of DEM

Because the resolution of the DEM was set as 2.5 m × 2.5 m and the size of the area is 960 km^2, it was evident that the grid points of the model had to be calculated based on a neighboring subset of source data points. In the following the set of the new grid points calculated based on a particular set of the source data points is called a *c*omputational packet. The computational packets were formed using an overlap technique where the areas of the neighboring computational packets overlap by 50 % in both directions. The reason for the use of the overlap technique was to prevent discontinuities at the borders of the areas belonging to neighboring computational packets. The size of the computational packets in terms of the new grid was 400 points (20×20 points or 50×50 meters rectangular area) and neighbors were determined for each packet separately. Each point of the grid belongs to 4 neighboring packets. In this manner the elevation value of each new grid point was approximated

from four different neighborhoods. The estimates were combined using the Inverse Distance Weighting (IDW) principle. Each of the four estimates was assigned a weight according to the distance between the estimated point of the new grid and the center of the computational packet based on which the estimate was computed. The closer the estimated point was to the center of a computational packet, the higher was the weight of the estimate computed based on this particular packet. The overlap technique is illustrated in Figure 2.4, where the elevation value of the new grid points located in the middle gray area is estimated based on four computational packets the centers of which are at points A, B, C and D. When combining the estimates for the grid points close to number 2, for example, the estimate based on the computational packet B has the highest weight as its center is closer to the points compared to the packets A, C or D.

In preliminary tests concerning the neighborhood selection, the uneven spatial distribution of the source data posed a major problem. The neighborhood had to contain source data points relatively evenly from all directions with respect to the center of the packet. This became clear in cases where the search algorithm found neighbors only from a certain direction corresponding to a sonar measurement line or an elevation contour line, for example. In these cases the interpolated surface could be bended arbitrarily in the other directions where no source data was available and large errors might occur. To avoid this problem the search area was divided into eight 45 degree sectors and a rule was introduced that at least two source data points had to be found from each sector. The minimum number of neighbors was set to 80 except at the westernmost sea areas containing mainly the IOW source data, where the minimum number of neighbors was set to 12. The maximum number of neighbors was set to 500. The minimum radius of the search area was set to 75 meters to guarantee that there are source data points available for interpolation outside the area of the particular computational packet and that the new grid points at the edge of the computational packet have also neighbors at various directions. The 75 meter rule was important in areas where the density of the source data points was high. In Figure 2.4 the rule of having source data from all directions is illustrated for the computational packet A. The 45 degree sectors are marked by numbers from 1 to 8.

Figure 2.5 presents the flow of the algorithm of neighborhood selection.

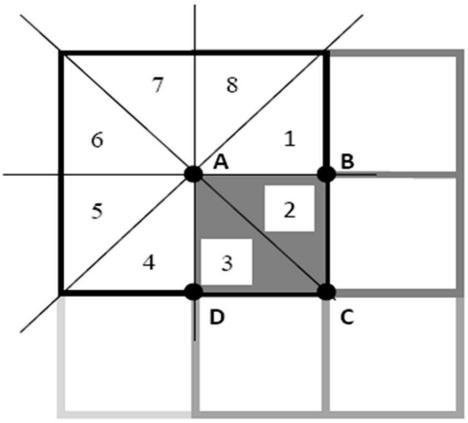

Figure 2.4: Division of the neighborhood selection area into eight 45 degree sectors in the context of the overlapping technique.

2.4 Determination of the confidence limits of the probabilistic DEM

The objective of the DEM creation in the Olkiluoto area was to create an input for the biosphere modeling. The accuracy of this kind of landscape development model is limited by the accuracy of the digital elevation model forming the basis of the analysis. The existing elevation data for the region of interest was from various different sources and of variable accuracy. The purpose of the study was to create a uniform DEM and to evaluate its accuracy (confidence limits) based on the available data. The nominal grid resolution of the final model was decided as 2.5 m $\times$ 2.5 m keeping in mind the need for further modeling of hydrological and ecological characteristics.

The method applied in this study for the creation of high resolution DEM is based on thin plate spline interpolation as described in section 2.2.3. The performance of this method can be depicted as if bending a thin metal plate over the desired grid, deviated by the values of the available source data points according to the minimal energy principle. In this way an elevation value can be assigned to every grid point of the new DEM.

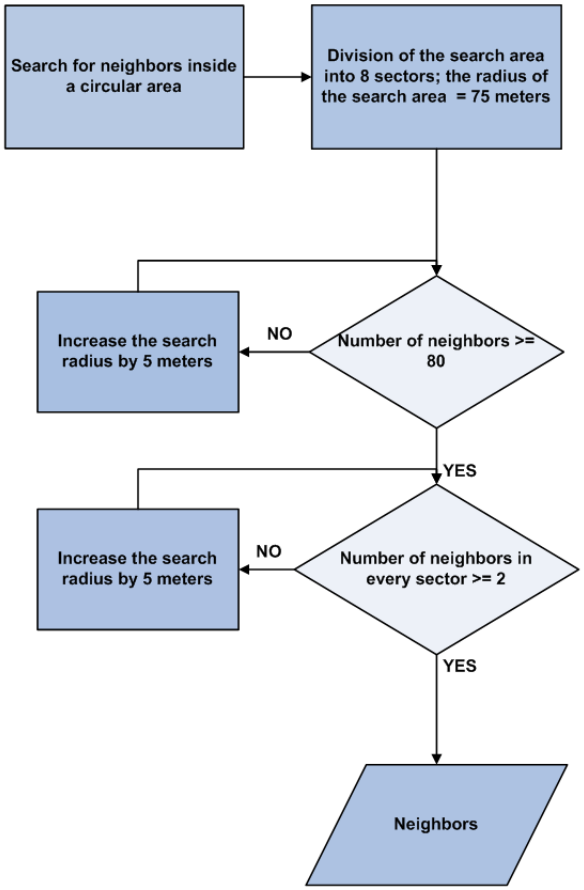

Figure 2.5: Flow chart of the neighborhood selection algorithm.

An important aspect is the need for determining the error tolerance of the created DEM in order to be able to evaluate the reliability of each DEM point. For this purpose Monte Carlo simulation was applied. The surface bended over the grid points was varied randomly in the predefined tolerances of the source data points to get statistical coverage. Each variation of the surface gives a realization of the elevation value at every new grid point and thus the error tolerances of the source data points are passed over to the points of the created high resolution DEM raster.

The computation of the elevation model was undertaken in the MATLAB environment. The MATLAB routine responsible for the computations first loaded the source data points into its memory. The source data information included x, y and z coordinates as well as the form and standard deviation of the corresponding prob-

ability distributions. The distributions were assumed to be Gaussian for all other source data sets except that obtained from the Finnish Maritime Administration, which was assigned an asymmetric probability distribution. The standard deviation was provided only for the data by the Finnish National Land Survey and IOW. The data from all the other sources were assigned standard deviations according to the 95 % confidence limits given in Table 2.1. After loading the source data the MATLAB routine downloaded the desired amount of computational packets, containing the x and y coordinates of the new grid, from the server.

The next step of the computations was selecting the source data points belonging to the neighborhood of the particular computational packet according to the algorithm presented in Section 2.3. The center point of the computational packet was calculated and the radius of the search area was increased in 5 meter steps. As soon as the conditions presented in the flow chart of Figure 2.5 were fulfilled, the neighbors were accepted. The elevation values of the source data points belonging to the neighborhood were then compensated for the land uplift according to the year of the acquisition of the data. The amount of yearly land uplift, which in the Olkiluoto area is 6 millimeters (Poutanen, 2011), multiplied by the age of the data was added to the elevation values of the source data points.

Determining the value of the relaxation parameter p of the thin plate spline algorithm was addressed next in the routine. The value of p was determined according to the variance of the source data points belonging to the neighborhood. If the variance of the data points was higher than 0.7 m^2, the value of the relaxation parameter was set to 0.01, i.e., linear approximation by minimizing the squared error was applied. If the variance was less than 0.05 m^2, the value of the relaxation parameter was set to 0.99. If the variance was between 0.7 m^2 and 0.05 m^2, the value of the relaxation parameter was determined by logarithmic mapping between the mentioned range of variance and the range of p between 0.01 and 0.99 as described in section 2.2.3.

The elevation value estimates for the points of the new data grid in the computational packet were computed next. Several estimates were calculated. The first estimate was obtained by approximating the surface according to the measured values of the neighboring source data points, i.e., without any probabilistic modeling involved.

Other estimates together with the confidence limits were obtained using the Monte Carlo simulation. The Monte Carlo simulation involved drawing 250 values for the neighboring source data points from their corresponding probability distributions and approximating the corresponding surfaces using the thin plate spline method. From these 250 realizations of the surfaces, 250 realizations of the new grid points of the computational packet were obtained. The 250 realizations enabled to estimate the error probability distributions of the points of the new high resolution grid. Mean, median and the maximum of these distributions were used as alternative estimates of the new high resolution DEM. All the mentioned estimates gave relatively similar values in the area of interest.

The realizations of the data points corresponding to different computational packets were combined next. This was performed according to the IDW principle as described in Section 2.2.1. The data was combined so that the closer the data point was to the center of a computational packet the higher was the weight of the results computed based on that particular packet in the combined data. The inverse distance was considered as such, i.e., the exponent value in the IDW algorithm was 1. In this manner each point of the new high resolution DEM was estimated based on $4 \times 250 = 1000$ realizations of thin plate spline interpolation (except for the computational packets at the edge of the modeling area where the number of overlapping computational packets was less than 4). As the final result the following DEM data was produced:

- deterministic DEM based on the exact measured values of the source data
- probability histograms containing 1 000 realizations of the probabilistic DEM
- DEM presenting the mean of the realizations of the probabilistic DEM
- DEM presenting the median of the realizations of the probabilistic DEM
- DEM presenting the maximum of the realizations of the probabilistic DEM
- 95 % confidence limits for the probabilistic DEM

This version of the probabilistic DEM was used in the surface water body estimation procedure in Chapter 4. In Figure 2.6 the resulting deterministic DEM is presented.

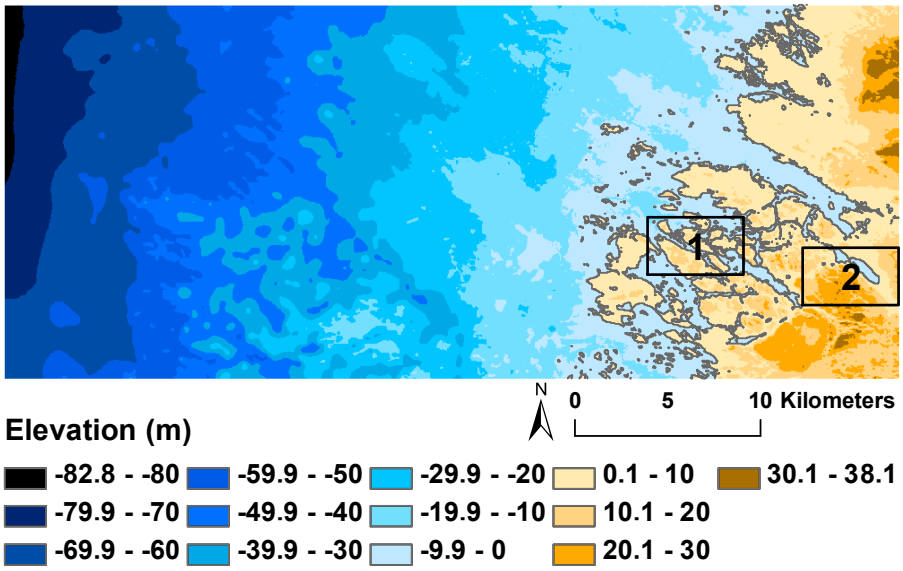

Figure 2.6: The digital elevation model used in landscape development modeling. The numbered rectangled areas refer to Figures 2.12 and 2.13.

2.5 New version of the probabilistic DEM

Recently, new elevation data have become available and a modification of the probabilistic DEM has been compiled. The new data sources include the airborne LiDAR data acquired by the National Land Survey of Finland in 2012, bathymetric LiDAR data acquired by Airborne Hydrography AB (AHAB) on September 25th in 2012, and the global topography data set (version 15.1, year 2012) obtained from the University of California, San Diego. Due to biosphere modeling needs, the modeling area was expanded 10 km to north, covering now a 30 km $\times$ 48 km area of the neighborhood of the Olkiluoto Island. The supplementary data sources incorporated into the new version of the DEM are listed in Table 2.4; the updated DEM and its 95 % confidence limit map are presented in Figures 2.8 and 2.9, respectively. In Figure 2.9 the lines of narrower confidence limit (i.e., lighter color) are due to differences in accuracy between the sonar measurement lines and the data sets surrounding them.

2.5.1 Airborne LiDAR data acquired by the NLS

The airborne LiDAR data of Olkiluoto area was scanned by the NLS in spring 2012. It covers the area above water bodies in the modeling area. The minimum point density of the NLS LiDAR data is 0.5 points per square meter and the elevation accuracy of the points is 15 centimeters (National Land Survey of Finland, 2014). In the new version of the Olkiluoto DEM the existing source data from the area above water bodies were replaced by the LiDAR data.

2.5.2 Bathymetric LiDAR data acquired by AHAB

Bathymetric LiDAR data acquisition was performed on 25th of September in 2012 by Airborne Hydrography AB (AHAB). This was a pilot study to assess the usability of bathymetric LiDAR technology in future monitoring of the Olkiluoto site. Two areas were LiDAR scanned: one close to the northern coast and the other close to the southern coast of the Olkiluoto Island. The total area scanned was 14 square kilometers. The location of the scanned area is presented in Figure 2.7 using the indicated colormap while the elevation of the surrounding areas are shown in grayscale. The survey was carried out using the HawkEye II bathymetric LiDAR system (Airborne Hydrography AB, 2014). The wavelength of the LiDAR is 532 nm and the average point density of the data is 0.4 points per square meter.

2.5.3 Global topography data set from the UCSD

The third supplementary data source was the global topography data set (version number 15.1, year 2012) from the University of California, San Diego. The data set has been collected from satellite altimetry and depth soundings data. The satellite altimetry data is based on high-resolution marine gravity information from the Geosat and ERS-1 spacecraft (Smith and Sandwell, 1997). The average precision of the data is $\pm$ 13 m (Sandwell et al., 2001). This data set was used in the western part of the modeling area where previously only the data from the IOW was available. Due to its large error variance, the IOW data was not included in the new DEM version.

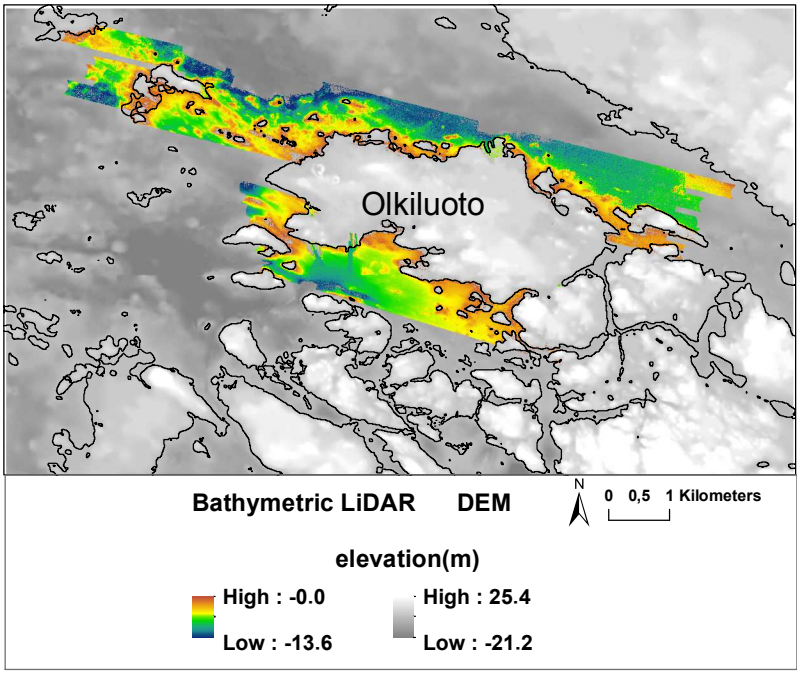

Figure 2.7: The areas scanned by AHAB using the bathymetric LiDAR.

Table 2.4: Updates to source data sets

Name	Acquisition year	Data set type	Precision (95 % confidence)
LiDAR (NLS)	2012	Point cloud	± 0.15 m
Bathymetric LiDAR (AHAB)	2012	Point cloud	± 0.25 m
Global topography data set (UCSD)	2012	Depth data points	± 13 m

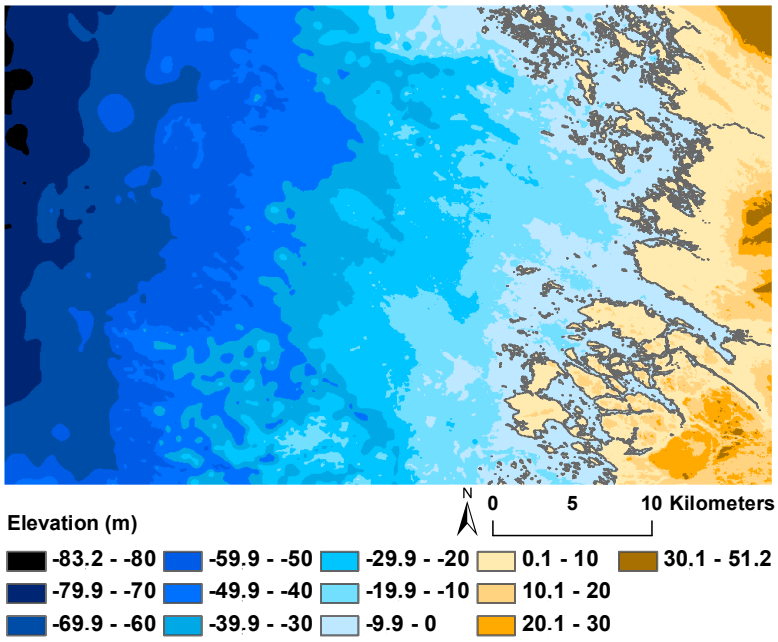

Figure 2.8: The digital elevation model after incorporating the LiDAR data.

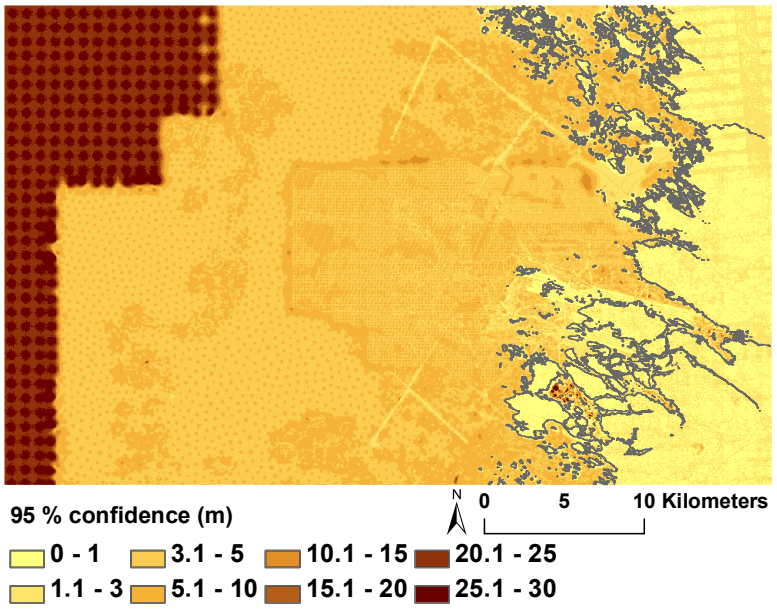

Figure 2.9: The 95 % confidence limit map of the updated DEM.

2.5.4 Error analysis between the interpolated DEM and the LiDAR data

The error between the LiDAR data from the NLS and the DEM presented in Figure 2.6 is presented in Figure 2.10. Only land areas are covered as the NLS LiDAR data does not cover seabed. In Figure 2.11 the error between the LiDAR data and the source data used in the generation of the DEM of Figure 2.6 is presented. The major error sources between the LiDAR data and the previous source data are in the Olkiluoto Island where earthwork has been done due to the construction of the new nuclear power plant. This is also seen in Figure 2.10. Other major errors are in places where there has not been any source data points. Two enlargements from Figures 2.6, 2.10 and 2.11 presenting error sources can be seen in Figures 2.12 and 2.13. In Figure 2.12 a part of the archipelago south of Olkiluoto is illustrated. Especially in the largest island the elevation of the top of the hill, where source data points have not been available, has been estimated to be too high by the thin plate spline interpolation method. In Figure 2.13 the largest error source is a gravel pit where the surface elevation has been lowered artificially.

The errors between the interpolated DEM and the LiDAR data have, in principle, three sources:

- errors caused by changes in the terrain due to construction work, for example
- errors due to measurement inaccuracies of the source data
- interpolation errors.

From the point of view of this thesis the interpolation errors are of greatest interest as these are related to the selection of the interpolation algorithm and developed methodology for DEM generation. In Figure 2.10 there are several regions of relatively high error (about 5 meters in absolute value). When comparing this with Figure 2.11 it can be seen that in many cases source data of relatively high error can be found in those areas and thus the interpolation algorithm has just filled the gaps and spread the error to larger areas. In some areas, however, the interpolated DEM deviates significantly from the LiDAR data while there seem to be no source data available (dark blue area in the lower right quarter of the figure, for example). Given

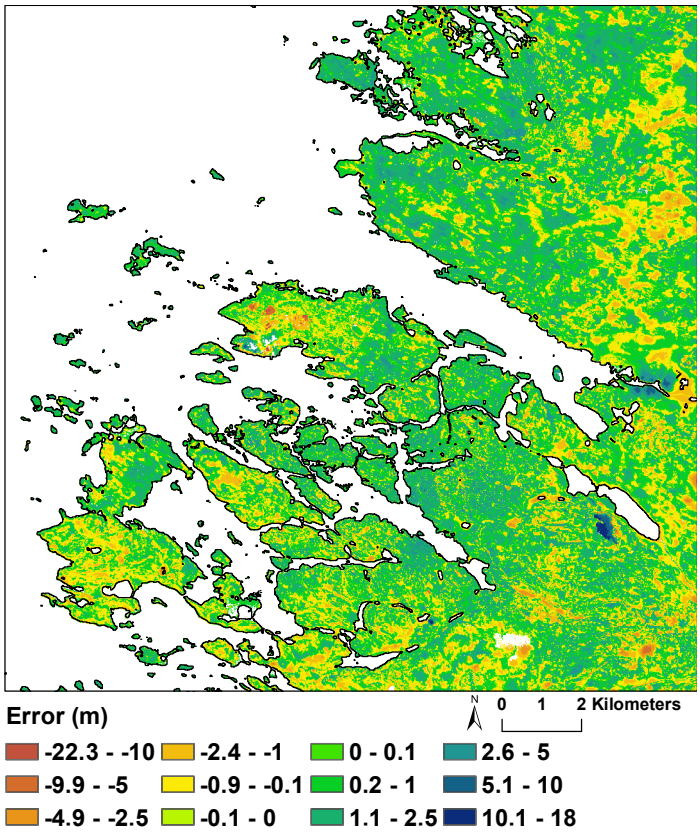

Figure 2.10: The error between the digital elevation model in Figure 2.6 and the LiDAR data by the NLS.

that no human action has been involved, these errors are due to the interpolation methodology.

When comparing the interpolation algorithms presented in section 2.2, the IDW is safe in the sense that the result never exceeds the range of values of the source data. However, the simulations showed that IDW and ordinary kriging did not yield as realistic terrain as the thin plate spline method. Selection of the interpolation method seems to be a compromise between preserving the visual properties of the terrain and not taking the risk of having relatively large errors in areas where source data are not available or is extremely unevenly distributed. Thorough analysis of the performance of the algorithms is difficult as the results depend significantly on the properties of the terrain and on the spatial distribution of the source data. In this thesis the usage of the thin plate spline method was justified as, firstly, to preserve

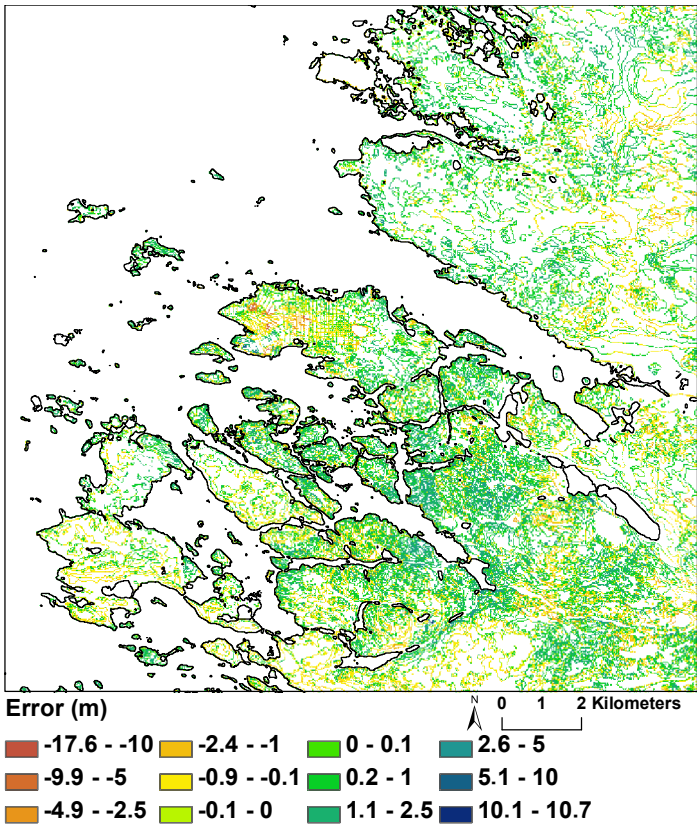

Figure 2.11: The error between the source data in Table 2.1 and the LiDAR data by the NLS.

the natural appearance of the terrain keeping in mind the next steps of the landscape developing modeling and, secondly, the realizations of the DEM drawn from the probabilistic model to be used in landscape development modeling were obtained in such a way that the most severe errors could be avoided. However, steep slopes and abruptly changing surface gradient of the landscape were challenging to model, due to the way how the thin plate spline method works. By carefully selecting the relaxation parameter p in the model this problem could be avoided in most cases. Landscape development modeling and the method of drawing realizations from the probabilistic DEM are described in chapter 4.

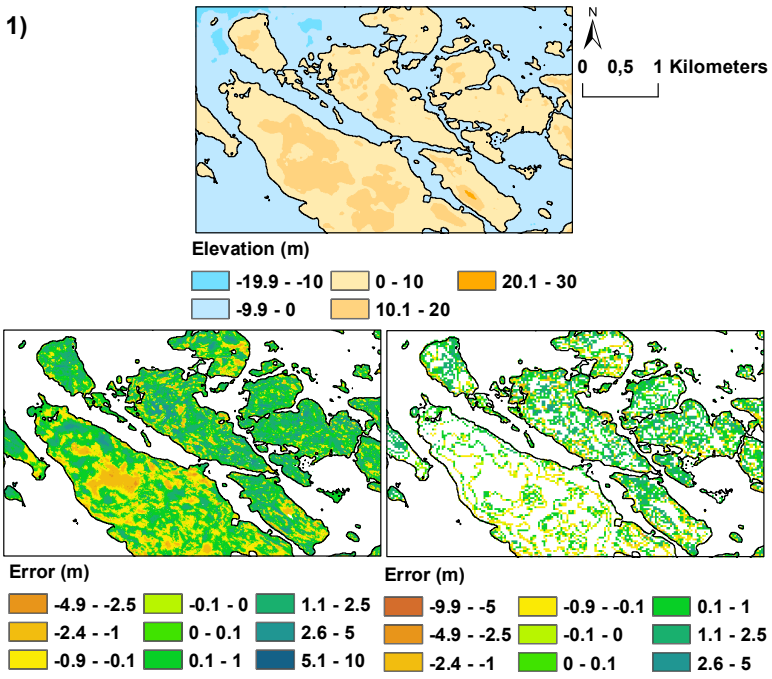

Figure 2.12: An enlargement of Figures 2.6, 2.10 and 2.11 from area 1 specified in Figure 2.6.

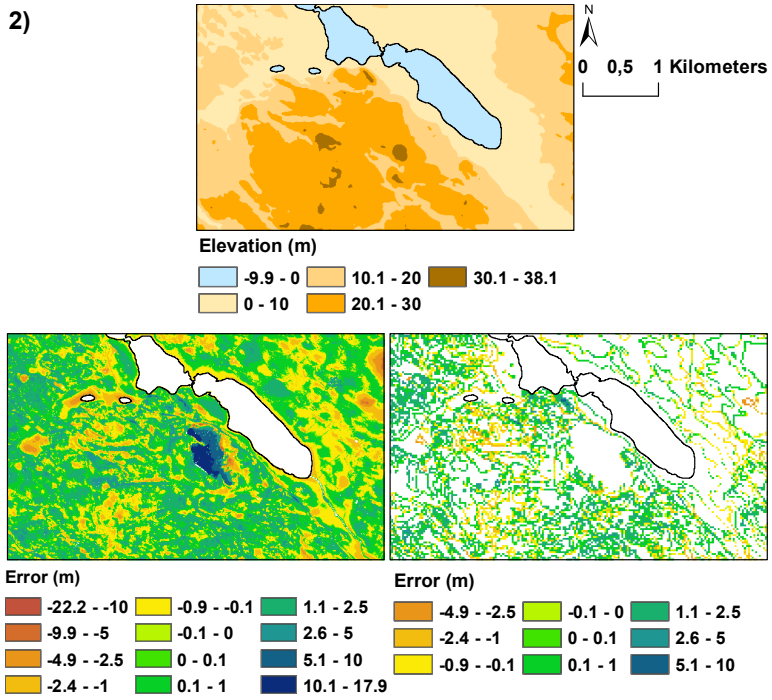

Figure 2.13: An enlargement of Figures 2.6, 2.10 and 2.11 from area 2 specified in Figure 2.6.

Chapter 3

Land uplift modeling

Post-glacial land uplift is a term referring to the rebound of the earth's surface after the melting of the ice formed during a glacial period. In the global world history the δ^{18}O studies from ice core samples and marine isotope records have shown several, almost periodic, cold temperature time sequences (Gibbard and Van Kolfschoten, 2004). Serbian geophysicist Milutin Milanković studied solar radiation and its effects on the earth's climate in the 1920's. He formulated a theory that there might have been a sequence of ice ages caused by eccentricity, axial tilt and precession in the earth's orbit (Milanković, 1998). His theory was proven in the 1970's when deep sea core sediment samples revealed non-uniform periodicity in δ^{18}O isotope concentration changes which correlate with climate temperature variations (Hays et al., 1976; Lisiecki and Raymo, 2005).

Periodical ice ages, occurring roughly every 100 000 years, pose a fundamental problem when modeling the post-glacial land uplift. The next ice age will destroy nearly all the signs of the previous ones. Also the remaining uplift rate of the previous ice ages will be unknown. When modeling the current uplift, the unknown effect of the previous ice ages can be thought as a cumulative convolution sum embedded into the current uplift. In Scandinavia, the thickness of the ice sheet during the latest ice age can be estimated from the dose of the ^{10}Be/^{26}Al isotope ratio affected by cosmic radiation. This method, where cosmogenic nuclides produced within rocks and minerals are studied, is based on the idea that cosmic radiation will hit the mountain

rocks uniformly causing nuclear reactions in certain atoms such as aluminium and beryllium. The cosmic radiation will cause a cumulative formation of isotopes but, at the same time, the decay of radionuclides will reduce the amount of isotopes. This process can be sufficiently modeled and the mathematical model allows the estimation of the beginning of the exposure period to cosmic radiation. The effect of the radiation is so weak that a one meter deep water container can stop it almost completely. This fact can be utilized in the estimation of Fennoscandian ice sheet thickness. There are several peaks in Norwegian mountains that are assumed to have been ice free during the Fennoscandian ice age. By taking samples from the Norwegian mountains and by determining the cumulative doses of ^{10}Be/^{26}Al isotopes the starting time of the melting process of the ice sheet from different heights can be estimated. In (Brook et al., 1996) the height of the latest Fennoscandian ice sheet is estimated to have been between $1400 - 1800$ meters above the sea level. As the half-life of ^{10}Be/^{26}Al is approximately 150 000 years, this method cannot reveal any information of the earlier ice ages (Gosse and Phillips, 2001).

The most recent ice age took place approximately from 115 000 to 10 000 years before present (BP). After that the surface of the earth has been slowly lifting up and the uplift is still in progress. Currently the maximum uplift rate in Fennoscandia is about 9 millimeters per year. Estimated annual land uplift rates are presented in Figure 3.1.

There are several land uplift models available. They can be divided into two categories:

- geodynamic models based on the earth's physical structure and equilibrium adjustment
- models based on fitting a mathematical function to existing data on shore level displacement.

The geodynamic models are derived from the physical characteristics of the land uplift while the curve-fitting models are data-driven. Each approach has its advantages and disadvantages. Geodynamic models are useful for gaining a better understanding of the properties of the earth's crust and its response to load. These models are usually developed for large scale modeling and in order to be solvable, they tend to

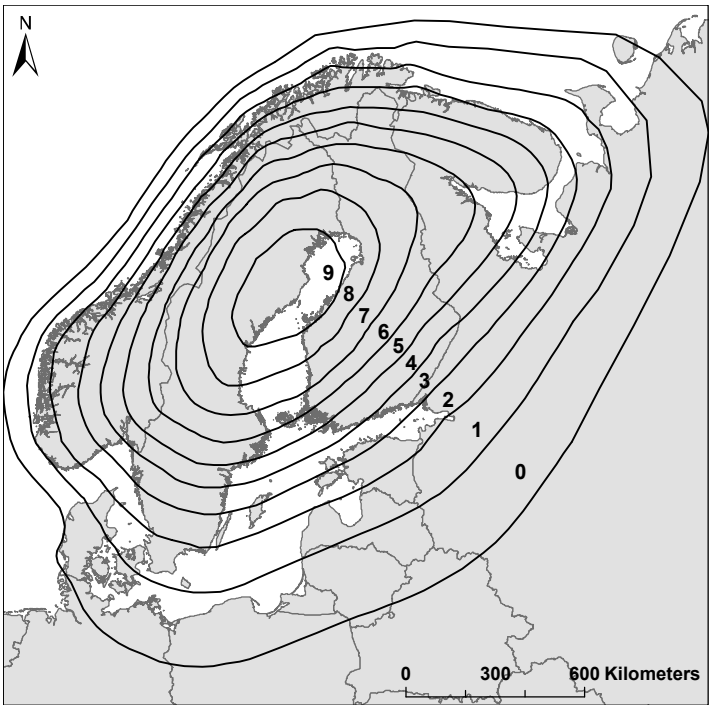

Figure 3.1: Absolute annual land uplift in millimeters in Fennoscandia. The figure includes edited material from (Poutanen, 2011).

make various simplifying assumptions. Due to the lack of detailed source information as well as the complexity of the geodynamic models, their usage for the prediction of future landscape development is limited. The curve-fitting models, on the other hand, have only remote connection to actual physical processes causing the land uplift and their accuracy is limited by the validity and accuracy of the underlying data.

In this thesis the main effort is put on the development and fine-tuning of Tore Påsse's land uplift model based on fitting an arctan-shaped curve to various types of data on past shoreline displacement. In the first part of the chapter, however, a short overview on geodynamic and other linear modeling methods is given.

3.1 Geodynamic land uplift models

Glacial Isostatic Adjustment (GIA) is a process where the earth's crust adjusts itself to a new state of equilibrium. The most recent ice age, the Weichselian, pressed

the surface of the earth down for 100 000 years' time period and the earth's crust reacted with elastic and viscous depression and displacement. Also, most of the sea-water was transformed into ice. In (Fairbanks, 1989), it is shown that the eustatic level was 100 meters below the current sea level in the pre-Holocene period. The water was transformed into ice increasing the load on the Northern hemisphere, and thus altered also the shape of the geoid. During Holocene the ice melted and the uplift process began in Fennoscandia. According to (Påsse, 2001) the elastic response of the earth's crust was fast and it was followed by a slowly evolving viscous process gradually going towards new equilibrium of balanced water and land masses. Geophysical models attempt to model the mentioned aspects as accurately as possible by taking into account such phenomena as gravitation, heat convection, viscosity, plate tectonics, bedrock properties and so on. The equilibrium in these cases is based on sea-level equations, where the physics of the earth's crust and various forces such as ice load/unload and the tidal forces, are combined. These equations are solved to find an equilibrium of the sea level and redistribution of masses. The equations can be solved either directly, which is a computer memory consuming operation, or by using finite element analysis (FEA).

In FEA the problem is solved iteratively. The computational structure is organized in a three dimensional mesh grid, where every node has a spatial connection to earth. The computational nodes are connected to the closest neighboring nodes and they exchange parameter values during computation epochs (Gerya, 2010). The computation can be done in time sequences so that the loads such as ice loading and unloading in the Northern hemisphere, for example, could be introduced at a given time to the model. FEA models are memory and computational capacity demanding and usually some compromises have to be made in order to maintain the computational time in acceptable limits. Known parameters are incorporated into the model and are computed using true physical equations while unknown elements in the grid are gradually updated to mimic the real values of the earth model (Sabadini and Vermeersen, 2004; Gerya, 2010).

The development of dynamic GIA models has started several decades ago. In (Peltier, 1976) the importance of global finite element model to solve the sea-level

equations was noticed first. The development of GIA models is an iterative and continuing effort: new physical features are gradually introduced to the models and initial values of the parameters are constantly updated according to the best available data and the iterative adjustment process of FEA analysis. The most common earth models in GIA analysis utilize a spherical geometry grid to represent the whole earth. These types of models usually consist of a lithosphere of constant thickness and a viscoelastic mantle divided into $1 - 20$ layers. This arrangement allows the full sea-level equation to be solved.

Richard Peltier (together with his colleagues) is one of the pioneers in defining differential equations for isostatic equilibrium computation (Peltier, 1976; Peltier and Andrews, 1976). FEA models were quickly adopted to the analysis (Peltier et al., 1978). The earth model consists of several uncertainties and assumptions and Peltier has also made major contributions to several areas that are closely related to earth modeling, for example, in (Peltier, 1981, 1984, 1986; Peltier and Tushingham, 1991; Mitrovica and Peltier, 1993). Also the ice models, describing the glacier size, shape and time dependent melting (and thus unloading) for the shore-level equilibrium model, have been a major part of Peltier's work. The models are called ICE-1G ... ICE-5G (Peltier, 1976; Tushingham and Peltier, 1992; Rostami et al., 2000; Peltier, 2004).

Another major contributor to earth modeling is Patrick Wu. His work has covered several fields of earth modeling, for example, in (Wu et al., 1999; Kaufmann et al., 2000; Wang et al., 2006; Steffen and Wu, 2011; Steffen et al., 2013). Geophysicist Kurt Lambeck working in the Australian National University has developed FEA modeling and function definition; his research group has developed the ANU ice model. His work has been published, for example, in (Lambeck, 1995, 1996; Lambeck et al., 1998; Johnston and Lambeck, 1999; Wu et al., 1999; Kaufmann and Lambeck, 2000; Lambeck et al., 2002, 2003).

Other researchers working on developing and refining GIA models are Jerry Mitrovica, Glenn Milne and Georg Kaufmann. In many cases the co-operation with other groups has given improved results when compared to earlier versions. These GIA models are usually global which means that other glaciers and global effects must be

included in the models. The distance between the nodes of the computational grid is usually hundreds of kilometers. Fortunately, Fennoscandian part of the global GIA model can be computed using a smaller and finer mesh version of the GIA model using carefully selected boundary conditions. However, even when using the fine mesh the local FEA is still sparse and the calculation procedure is a memory and computer power consuming process.

The physics related to the FEA models is well established but the underlying parameters such as the crustal rock density or the lithosphere thickness, for example, are presumed to be homogeneous over the globe. In real world, both of these parameters vary spatially. Some of the parameters such as the detailed crust density, for example, will remain unknown unless some non-invasive method for determining the deep rock density is developed. FEA models will be the future of the uplift analysis, but now even with generalizations of the parameters the computational time for fine mesh is very demanding in order to find out the local detailed uplift variations. A review of GIA models and a brief history of GIA modeling can be found in (Whitehouse, 2009).

3.2 Land uplift modeling based on linear extrapolation

Land uplift can also be modeled using linear extrapolation. The uplift can be assessed directly from short-term data sets, such as time series obtained from precise GPS-stations (Poutanen, 2011). (Lidberg et al., 2010) is a continuation of (Poutanen, 2011) and it introduces vertical components to the model solution. The paper uses a trigonometrical function based vertical velocity model for Fennoscandia. In (Lidberg et al., 2010) some parameters for FEA rheology models, such as upper and lower mantle viscosities and GPS station velocities, are revised from the data.

In (Vestøl, 2006) precise leveling, tide-gauge and GPS station data were fitted into an uplift model of Fennoscandia using a least squares solution. The period covered by these data sets is too short to make long-term extrapolations and in many cases the local deviations that can be seen in the data cannot be extrapolated to

follow the changes at the Fennoscandia scale. In (Scherneck et al., 2001) Scandinavian BIFROST (Baseline Inferences for Fennoscandian Rebound Observations Sea Level and Tectonics) GPS network was utilized to obtain land uplift time series for isostatic rebound model input. The model gave consistent results when compared to other similar models. However, the data collection had only lasted for just over four years and therefore, long-term assumptions cannot be made based on these measurements. In (Vermeer and Rahmstorf, 2009) BIFROST data was used for modeling both horizontal and vertical movements of the land uplift to obtain lithospheric thickness estimates. Combined gravimetric (from the GRACE satellite) and GPS network data were used for estimating the current uplift in Fennoscandia in (Timmen et al., 2004; Müller et al., 2012). In (Ågren and Svensson, 2007) several experiments were made by testing Vestøl's linear model with precision leveling data and by combining the models presented in (Lambeck, 1998) with the Vestøl model. However, when considering the long term lake isolation data it is revealed that the long-term Holocene uplift rate is not linear, as shown in (Eronen et al., 2001). Also, Nils-Axel Mörner has studied the land uplift in Fennoscandia, for example, in (Mörner, 1981).

3.3 Data-driven land uplift model by Tore Påsse

Tore Påsse has created a land uplift model based on shore level information. The basic formula for the shoreline displacement is presented as Equation 3.1:

$$S = U - E \tag{3.1}$$

In Equation 3.1 S is the shoreline displacement, U is the total glacio-isostatic uplift and E is the eustatic sea level rise (all in meters).

The first implementation of the model was presented in (Påsse, 1990) where the land uplift was studied in the area of lakes Fegen and Säven in southwestern Sweden. The uplift model was based on the lake-tilting method. The term lake-tilting refers to a situation where the uplift rate of the outlet of the lake differs from the uplift rate of the other parts of the lake. If the outlet has a faster uplift rate, the lake surface

is transgressed and vice versa. The model for the glacio-isostatic uplift U follows Equation 3.2:

$$U = -\frac{v_0}{2.25 \times 10^{-4}} + \frac{v_0}{2.25 \times 10^{-4}} e^{2.25 \times 10^{-4} \Delta t}, \tag{3.2}$$

where U is the land uplift (in meters), v_0 is the recent uplift rate (meters/year) and t is the time (in years BP) (Påsse, 1990).

The formula for the land uplift of Equation 3.2 was derived based on radiocarbon-dating of transgressed peat at different depths of the lakes. In (Påsse, 1990) the shoreline displacement S was derived from a previous study (Påsse, 1987) from the Sandsjöbacka area. The eustatic sea level rise was calculated based on S and U using Equation 3.1.

In the following model versions (Påsse, 1996, 1997, 2001; Påsse and Andersson, 2005) U is divided into two (slow and fast uplift) or three components (in addition to the previous two, fast subsidence) depending on the model version. In (Påsse, 1996) U is the combination of three components:

$$U = U_1 + U_2 + U_3 \tag{3.3}$$

and in (Påsse, 1997, 2001; Påsse and Andersson, 2005) U is divided into two components representing slow and fast uplift as follows:

$$U = U_s + U_f \tag{3.4}$$

U_s in Equation 3.4 is equivalent to U_1 in Equation 3.3. The fast subsidence U_2 and the fast uplift U_3 in Equation 3.3 have been merged in Equation 3.4 into fast uplift U_f. The notation of Equation 3.4 is used in the land uplift modeling effort presented in this thesis. Påsse also gives a formula for the eustatic sea level rise E.

3.3.1 Slow uplift

The formula for the slow uplift has basically stayed in the same form in all model versions (Påsse, 1996, 1997, 2001; Påsse and Andersson, 2005):

$$U_s = \frac{2}{\pi} A_s \left(\arctan\left(\frac{T_s}{B_s}\right) - \arctan\left(\frac{T_s - t}{B_s}\right)\right) \tag{3.5}$$

The meaning of the parameters and their effect on the land uplift curve is discussed in more detail in section 3.4. The values of the parameters for the Olkiluoto site in different model versions are given in Table 3.1.

Table 3.1: Slow uplift parameters for Olkiluoto

Version	A_s	B_s	T_s
1996	245	9 500	12 500
1997	265	8 600	12 500
2001	258	7 600	12 000
2005	240	9 000	12 000

3.3.2 Fast uplift and subsidence

Earth is usually modeled in GIA models as a visco-elastic system (Gerya, 2010) and there is also evidence supporting this idea. After the ice started to retreat and melt away, earth responded by elastic rebound (like rubber behaves in a quick pressure release) which can be considered as the fast uplift. After this elastic or fast uplift, the earth responded to the ice retreat with slow or viscous uplift which is a still ongoing process. The viscous uplift can be thought to be as a part of the equilibrium process of the earth's lithosphere.

In Fennoscandia, before the Weichselian ice started to finally melt, there is a short period called the Younger Dryas stadial, where the volume of the ice expanded. Before this time period, the ice sheet had already melted so that southern Finland and large parts of Sweden were free of ice. The Younger Dryas stadial has been dated in the literature to approximately $13\,000 - 11\,500$ calibrated years BP (Björck, 1995; Kneller and Peteet, 1999; Peteet, 2000; Yu and Eicher, 2001; Köhler et al., 2011). After this period, the temperature rose and ice started to retreat and melt. The crustal subsidence stopped and turned into uplift process of the crust. Both events are connected with the Younger Dryas cold period and both effects can be seen

best from geological studies near the outer edges of the glacier extent during that time, described, for example, in (Thomsen, 1981; Kaland et al., 1984; Krzywinski and Stabell, 1984; Svendsen and Mangerud, 1990; Björck and Digerfeldt, 1991; Helle et al., 1997). Also in (Påsse, 1997) the uplift curves of Hardanger fjord (Norway) and Great Belt/Fakse Bugt (Denmark) show the effect of the subsidence and the following uplift. Majority of Finland and northern Sweden were under the glacier during this time period so the effects of the subsidence and uplift cannot be seen from the Finnish and nearby uplift data.

Påsse combined the Younger Dryas crust subsidence and uplift and Weichselian ice cover retreat and its elastic response to a single fast uplift component in his model. This seems reasonable, because the elastic and viscous responses of earth are difficult to separate from archaeological and geological data. The error caused by Påsse's fast uplift model is also minimized by combining it with the slow uplift component model.

The formulas of the fast uplift and subsidence have appeared in several different forms in (Påsse, 1996), (Påsse, 1997), (Påsse, 2001) and (Påsse and Andersson, 2005). In (Påsse, 1996) the formula for the fast uplift is given as:

$$U_{23} = \sum_{i=2}^{3} \frac{2}{\pi} A_i \left(\arctan\left(\frac{T_i}{B_i}\right) - \arctan\left(\frac{T_i - t}{B_i}\right)\right) \tag{3.6}$$

In (Påsse, 1997) the fast uplift and subsidence were combined into a single function:

$$U_f = A_f e^{-0.5\left(\frac{t-T_f}{B_f}\right)^2} \tag{3.7}$$

In Equation 3.7 A_f is the total subsidence (in meters), B_f is the inertia factor (year^{-1}), T_f is the time for the turning point from subsidence to uplift (i.e. the symmetry point of the function; in years) and t is time (in years). This formula was also used in (Påsse, 2001).

The formula for the fast uplift was changed again in (Påsse and Andersson, 2005) into the form:

$$U_f = \frac{2}{\pi} A_f \left(\arctan\left(\frac{T_f}{B_f}\right) - \arctan\left(\frac{T_f - t}{B_f}\right)\right) \tag{3.8}$$

In Equation 3.8 B_f can be written as a function of A_f as follows:

$$B_f = 6.6 \times A_f + 335 \tag{3.9}$$

The parameter values for the Olkiluoto site in various model versions (except in (Påsse, 1996), where the values were not given) are presented in Table 3.2.

Table 3.2: Fast uplift parameters for Olkiluoto

Version	A_f	B_f	T_f
1997	90	900	11 500
2001	90	850	11 600
2005	70	800	10 650

3.3.3 Eustatic sea level rise

The formula for the eustatic sea level rise E was given in (Påsse, 1996, 1997) as:

$$E = \frac{2}{\pi} \times 50 \left(\arctan\left(\frac{9350}{1375}\right) - \arctan\left(\frac{9350 - t}{1375}\right)\right) \tag{3.10}$$

In (Påsse, 2001) the formula was changed into the form:

$$E = \frac{2}{\pi} \times 56 \left(\arctan\left(\frac{9500}{1350}\right) - \arctan\left(\frac{9500 - t}{1350}\right)\right) \tag{3.11}$$

In (Påsse and Andersson, 2005) the eustatic sea level rise was expressed as a sum of three arctan based terms:

$$\begin{aligned} E = & \frac{2}{\pi} \times 61 \left(\arctan\left(\frac{9600}{1500}\right) - \arctan\left(\frac{9600 - t}{1500}\right)\right) \\ & - \frac{2}{\pi} \times 7 \left(\arctan\left(\frac{11500}{350}\right) - \arctan\left(\frac{11500 - t}{350}\right)\right) \\ & + \frac{2}{\pi} \times 8 \left(\arctan\left(\frac{12500}{350}\right) - \arctan\left(\frac{12500 - t}{350}\right)\right) \end{aligned} \tag{3.12}$$

In Equations 3.10, 3.11 and 3.12 t is the time in years. In Figure 3.2 the different versions of the eustatic sea level rise model are presented.

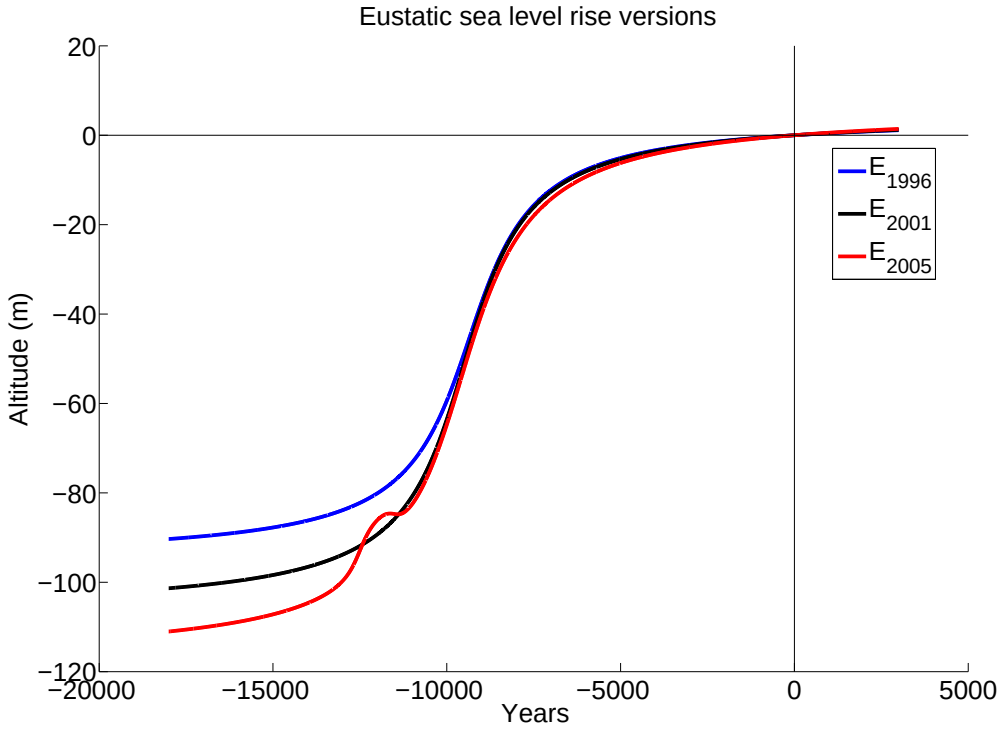

Figure 3.2: The eustatic sea level rise curves used in Påsse's land uplift models.

3.4 Data-driven land uplift model parameter details

The reasons for selecting the data-driven land uplift model by Påsse (2001) to be used in this thesis can be summarized as:

- implementation of the model is a simple process in majority of programming languages
- the model covers the whole Fennoscandia
- the model has a linkage to physical properties of the land uplift.

Also, in (Lindborg and Rubio Lind, 2006) it is stated that Posiva Oy and Swedish Nuclear Fuel and Waste Management Co have decided to use the model version described in (Påsse, 2001). The formulas underlying the land uplift modeling effort considered in the remaining part of the thesis are summarized below; the model for

the eustatic sea level rise E is discussed separately in section 3.5.2, however, as this was modified considerably from the model used by Påsse based on findings in the literature.

The shore level displacement is expressed as:

$$S = U - E \tag{3.13}$$

$$U = U_s + U_f, \tag{3.14}$$

where U is the total glacio-isostatic uplift, U_s is the slow component of the glacio-isostatic uplift, U_f is the fast component of the glacio-isostatic uplift, and E is the eustatic sea level rise (all in meters). The slow uplift is modeled using a linear combination of two arc tangent functions (Påsse, 2001):

$$U_s = \frac{2}{\pi} A_s \left(\arctan\left(\frac{T_s}{B_s}\right) - \arctan\left(\frac{T_s - t}{B_s}\right)\right), \tag{3.15}$$

where A_s is the download factor (in meters), T_s is the time for maximal uplift rate (i.e. the symmetry point of the arc tangent function, in years), t is the time (in years) and B_s is the inertia factor (year^{-1}). The fast uplift component is expressed as:

$$U_f = A_f e^{-0.5\left(\frac{t-T_f}{B_f}\right)^2}, \tag{3.16}$$

where A_f is the total subsidence (in meters), B_f is the inertia factor (year^{-1}), T_f is the time for the turning point from subsidence to uplift and t is time (in years). The components of the model are presented in Figure 3.3. In the figure the altitudes corresponding to the components of the model are shown instead of the rate of change. This can be done by choosing a certain reference level. The figure follows the convention used in (Påsse, 2001) by setting the reference point at the altitude of the sea level in AD 1950, common also in carbon dating (e.g. before/after 'present', BP/AP).

The focus in this thesis is on the parameters of the slow uplift U_s. The fast uplift took place over 10 000 years ago, so its impact on the source data points, described in section 3.6 is only marginal. The slow uplift formula contains three parameters: A_s, B_s and T_s. The influence of the B_s and A_s parameters on the slow uplift model U_s

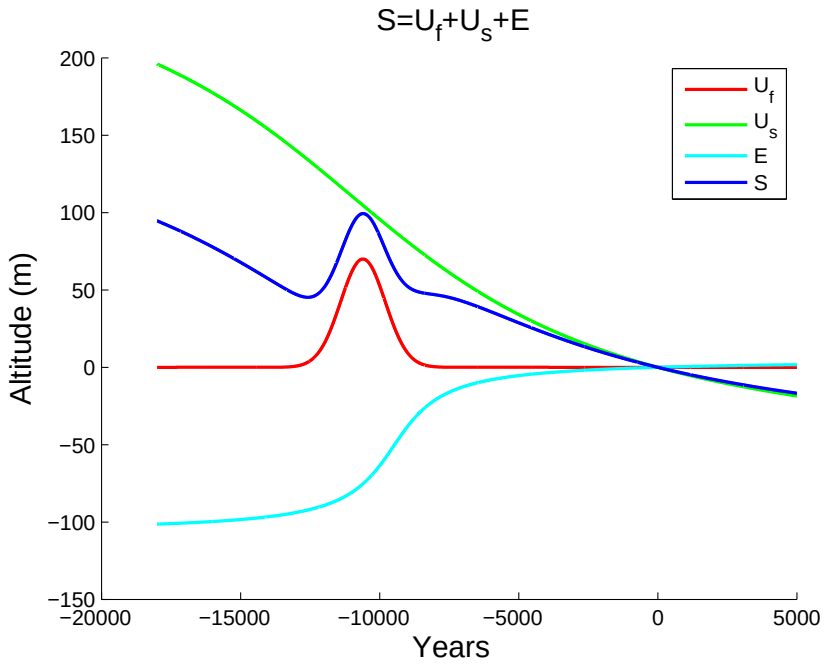

Figure 3.3: An example of shore level displacement, slow and fast uplift and eustatic sea level rise given by Påsse (2001).

is presented in Figures 3.4 and 3.5, respectively. The B_s parameter has an effect on the steepness of the slow uplift model U_s. The A_s parameter (the download factor) affects the amplitude of U_s and it indicates the half of the total slow uplift according to (Påsse, 2001). These parameters were the target of the optimization procedure described in section 3.6.4. The T_s parameter describes the time of the maximal uplift rate and is determined based on the ice retreat data as described in section 3.5.1 (Vuorela et al., 2009).

3.5 Updating the components of the land uplift model

The effort of improving the land uplift model presented in (Påsse, 2001) involves two steps. In the first step the components and parameters of the model are modified or constrained based on what is known about the respective processes based on the

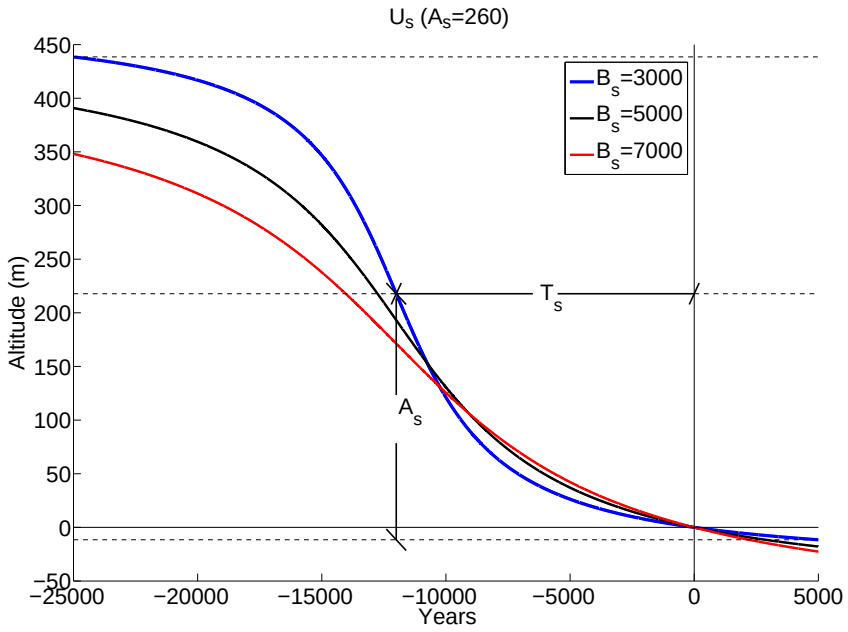

Figure 3.4: The effect of the value of the B_s parameter on the slow uplift curve U_s.

literature. This includes

- determining the value of the T_s parameter based on what is known about the ice retreat process
- modifying the eustatic sea level rise curve according to the evidence on the local sea level changes in the Baltic Sea
- constraining the value of the B_s paramater according to what is known about the physical properties of the earth's crust.

In the second step the A_s and B_s parameter values are optimized based on various source data on the shoreline displacement in the past. This step is described in section 3.6.

3.5.1 Ice retreat estimation

In Påsse's uplift model the T_s parameter is related only to the retreat of the ice sheet at a certain time. In other words, a reconstruction of the extent of the ice sheet as a function of time is required to define the value of this parameter. Ice retreat

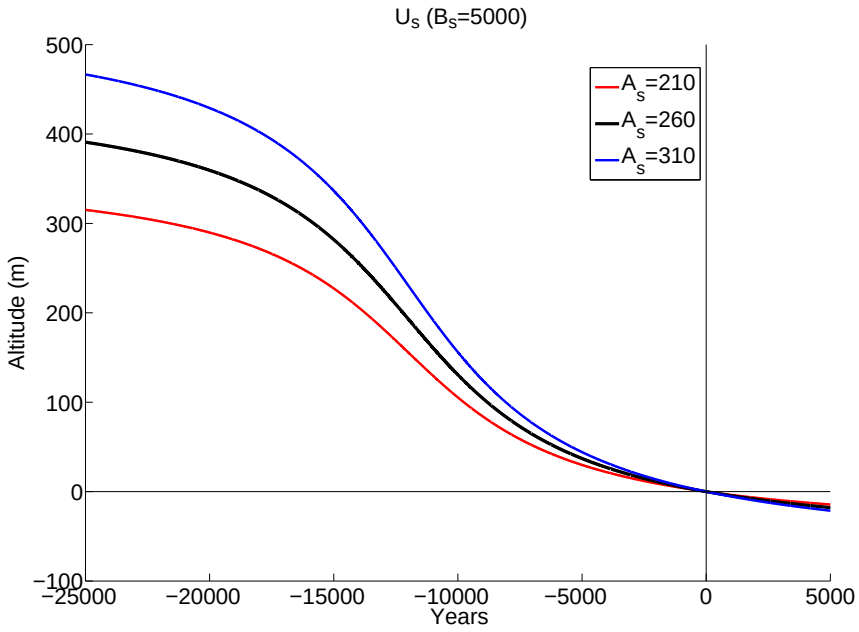

Figure 3.5: The effect of the value of the A_s parameter on the slow uplift curve U_s.

and subsidence in Fennoscandia have been linked to certain land formations in some studies and these formations have been dated. For example, in (Björck, 1995), the detailed analysis of the southern Baltic sea history and ice retreat from 13 000 to 8 000 BP is covered. In (Lokrantz and Sohlenius, 2006) and (Lunkka and Erikkilä, 2012) the ice retreat is studied by observing bedrock scratches and marks, post-glacial ridge formations, till and pollen analysis, GIS and geophysical analysis methods as well as data obtained from other indirect sources. In (Lokrantz and Sohlenius, 2006) an ice sheet reconstruction for Fennoscandia and in (Lunkka and Erikkilä, 2012) especially for Finland are presented. In this thesis the ice retreat model is obtained from (Geological Survey of Sweden, 2013), which has a consensus about the ice extent with (Björck, 1995) and (Lokrantz and Sohlenius, 2006). In Figure 3.6 some phases of ice retreat according to (Geological Survey of Sweden, 2013) are presented.

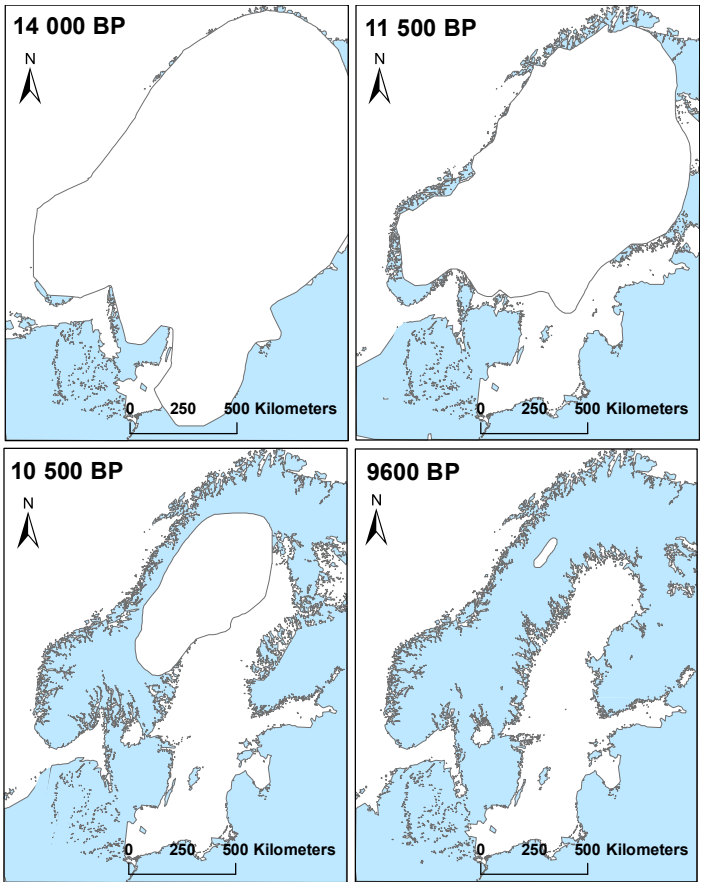

Figure 3.6: Ice retreat at 14 000 BP, 11 500 BP, 10 500 BP and 9 600 BP.

3.5.2 Eustatic model estimation

The eustatic model was presented in (Påsse, 2001) as:

$$E = \frac{2}{\pi} 56 \left(\arctan\left(\frac{9500}{1350}\right) - \arctan\left(\frac{9500 - t}{1350}\right)\right). \tag{3.17}$$

The arctan function in Equation 3.17 was derived using an iterative process, where the difference between the hypothetical uplift curves and empirical shore level curves was calculated (Påsse, 2001). In this thesis an alternative eustatic model is used in addition to the eustatic model of Equation 3.17. The alternative model is based on water level data from several sources. The main component of the model for the last 10 000 years is the eustatic curve by Punning (1987), where the water level

changes in the Baltic Sea area have been described. Radiocarbon-dated coral data collected by Fairbanks (1989), Chappell and Polach (1991) and Bard et al. (1996) and information about the past lake phases in the Baltic Sea area by Björck (2008) are used to extend the model beyond 10 000 BP. It is known that during the past 15 000 years there have been two periods when the Baltic Sea has actually formed a lake being separated from the oceans. These periods are referred as lake phases: the Baltic Ice Lake ($16\,000 - 11\,600$ BP) and the Ancylus Lake ($10\,700 - 10\,200$ BP) (Björck, 2008). Påsse (2001) discussed the effects of the lake phases on the parameters of the shore level displacement model and concluded that the evidence is insufficient and that the influence of these lake phases might be negligible in long-term studies. This is true if only the future land uplift is of interest and the parameter values are fully known. However, in order to use the source data from the lake periods in land uplift parameter optimization, the lake phases should be taken into account.

The eustasy in the Baltic Sea has a correlation with the eustasy in the North Sea (Madsen et al., 2007). The level of the Baltic Sea follows the level of the North Sea that is 20 cm (long-term average) higher than the global mean sea level (Meehl and Stocker, 2007). The narrow straits connecting the Baltic Sea to the Atlantic referred as The Danish Straits, and the long-term water balance have also an influence on the Baltic Sea level (Brydsten et al., 2009). According to the resolution achieved by the land uplift models, their effects are not significant. In this study the lake phases, i.e., the duration and the estimates of the altitude of the lake levels, were taken from (Björck, 2008), and the water level changes from (Punning, 1987). Two curves, one presenting the model suggested by Påsse (2001) and another obtained by approximating the coral data from the three mentioned sources and taking into account the effects of the lake phases, are presented in Figure 3.7. The approximation was done using a polynomial function where the segments of the two lake phases and water level changes were taken from (Björck, 2008) and (Punning, 1987), respectively. In this thesis the alternative eustatic model by Punning (1987) is referred as Punning et al.'s eustatic model. It can be seen from Figure 3.7 that during the lake phases the water level remained significantly higher compared to the global sea level represented by Påsse's curve until the connection opened again.

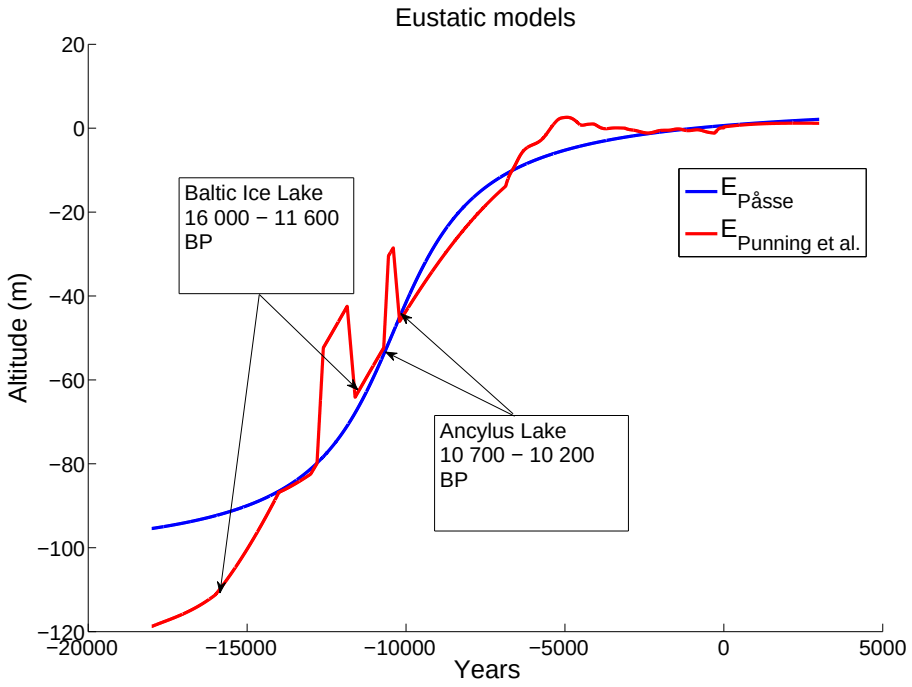

Figure 3.7: Sea and lake level estimates. The blue curve is the eustatic rise according to (Påsse, 2001). The red curve has been compiled from the data presented by Punning (1987), Fairbanks (1989), Chappell and Polach (1991), Bard et al. (1996) and Björck (2008).

3.5.3 Inertia factor estimation

Påsse has used crust parameters and their variations in his models to resemble fast (elastic response) uplift and slow (viscous response) uplift. In (Påsse, 1996), Påsse formulated the uplift model using three crustal uplift parameters $B_1 \ldots B_3$, without a clear connection to crustal or lithosphere properties. In (Påsse, 1997) the dependence between the inertia or slow uplift parameter B_s and the empirical data of Mohorovičić discontinuity map was established and it can be written as:

$$B_s = 302e^{0.067ct} \tag{3.18}$$

In Equation 3.18 ct is the crustal thickness of the earth. Påsse used the Moho map by Kinck et al. (1993) which is quite similar to the latest more detailed Moho map

presented in (Grad and Tiira, 2009).

In his later revisions of the model, Pårsse changed the B_s reference from the Moho map to lithosphere thickness (Pårsse, 2001) in order to find a better estimate for the inertia parameter. In this assumption, either the depth of the Moho discontinuity or the lithosphere thickness must correlate directly with regression or uplift speed. Pårsse has taken the lithosphere thickness data from (Ansorge et al., 1992), where the map data has been taken from (Calcagnile, 1982) and (Panza, 1985). In these analyses the local maximum of lithosphere thickness resides near the Gulf of Bothnia, which is the location of the fastest slow uplift at present. Babuška et al. (1988) estimated that the local maximum in Bothnian Bay might be $160-180$ km. However, Calcagnile (1982) was criticized by Kukkonen and Peltonen (1999) because the surface wave data was not able to detect a low-velocity asthenospheric layer under the thickest lithosphere area in Fennoscandia. Sacks et al. (1979) presented that the lithosphere-asthenosphere layer might be at 250 km depth as estimated by the body wave data. Kukkonen and Peltonen (1999) also found that the lithosphere thickness (i.e., the depth of the lithosphere-asthenosphere border) might be $160-250$ km in the Fennoscandian area as assessed by several different analysis methods (e.g. seismic, petrological and temperature). They also concluded that the lithosphere thickness is petrologically at least 240 km in eastern Finland. This supports also the latest studies (Conrad and Lithgow-Bertelloni, 2006; Artemieva and Thybo, 2008), where the 'local' lithosphere thickness is found to be around $200-250$ km and the nearest local maximum is near Moscow, Russia. From this point of view the lithosphere thickness, a variable underlying the B_s parameter, does not explain properly the inertia properties of Equation 3.18 if the latest data is considered.

Temporary subsidence followed by fast or elastic uplift is estimated by Pårsse (1997, 2001) based on shore level curves from Norway and from the northern parts of Swedish west coast. In (Pårsse, 1997), for example, the shore level uplift curves of Hardanger fjord (Norway) and Great Belt/Fakse Bugt (Denmark) show the effect of late Younger Dryas subsidence and uplift following it. Pårsse made an empirical fit of the fast uplift parameters to these curves.

Due to the dissenting opinions about the lithosphere thickness, the estimation of

the inertia factor B_s was decided to be based on a Moho map of Europe by Grad and Tiira (2009) presented in Figure 3.8. The Moho map describes the depth of the boundary between the earth's crust and the mantle (Mohorovičić discontinuity). Based on this fact, the Moho depth can be regarded as the crustal thickness of the earth and the inertia factor B_s can be calculated using Equation 3.18.

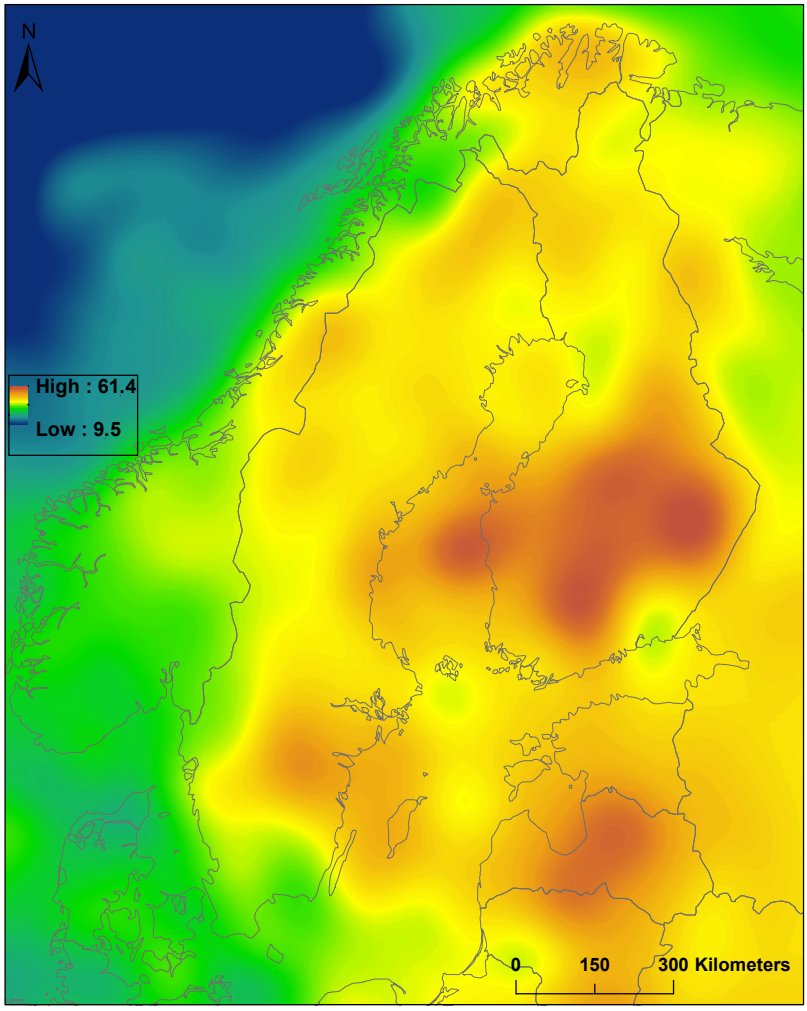

Figure 3.8: The Moho depth (in kilometers) in Fennoscandia according to (Grad and Tiira, 2009).

3.6 Land uplift model parameter refinement

In this section the optimization procedure of the parameters of the slow uplift component based on the source data on past shoreline displacement is described. The final result of the model parameter refinement is the probabilistic land uplift model to be used in the landscape development modeling described in chapter 4.

The main reasons for updating the parameters of Påsse's land uplift model were:

- to incorporate data sets and types of data previously unavailable or not taken into account
- to make use of more accurate eustatic models and crust thickness estimates
- to develop a statistical model, i.e., to compute also the confidence limits of the model parameters.

In the following the available source data is presented first after which the parameter optimization procedure is described.

Two kinds of input data were available for the land uplift model: one collected from lake basins, indicating the age of the sediment level where the environment changes from brackish water to fresh water, and the other collected from archaeological sites of prehistoric human activity, indicating the time when the particular location definitely represented dry land. Observations from the precise levellings or from GPS measurements were not used since they cover, at the best, only some decades.

3.6.1 Source data from lake basins

This data set consists of 133 points that were taken from (Vuorela et al., 2009). 94 of the points are from Finland and 39 points are from Sweden. The majority of the Finnish data points are originally from (Eronen et al., 1995), where the isolation time of several lake basins in Finland due to the land uplift was studied. The isolation time from the Baltic Sea was based on drilled core samples taken from the bottom of the basins. The layer where the freshwater algae have replaced the saltwater algae was radiocarbon dated. Also, the estimate of the water level was determined based on observations from the surrounding landscape. The Finnish data points were selected

so that only lakes and mires that had clear outlets were included. The location of the points most relevant for the Olkiluoto region is shown in Figure 3.9.

3.6.2 Archaeological data

This data set consists of 258 data points taken from (Tallavaara et al., 2010). The data set includes house and village sites, graves, ancient fireplaces etc.; for further description (Pesonen et al., 2011) can be referred. The archaeological findings have been radiocarbon dated. The archaeological data points represent the upper limit for the water level. The location of the points most relevant for the Olkiluoto region is shown in Figure 3.9.

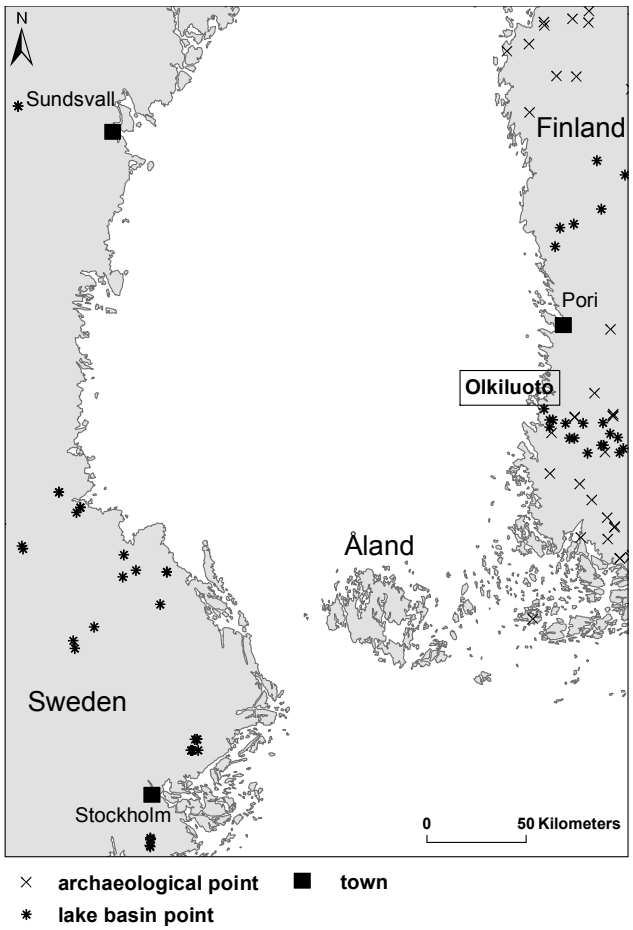

Figure 3.9: The location of the most relevant data points for the Olkiluoto modeling area.

Both data sets involved the usage of the ^{14}C radiocarbon dating procedure. The OxCal software (Bronk Ramsey, 2009) was used to convert the ^{14}C radiocarbon dating results into calendar year taking into account the underlying uncertainties. OxCal uses Bayesian analysis to get a calibration curve for the conversion (see also Section 3.6.3 for principles of radiocarbon dating). In Figure 3.10 an example of the calibration and conversion procedure of the data point from Lake Vähäjärvi in Eura is presented. The dating procedure yields quite a complex-shaped error distribution for the age of each data point.

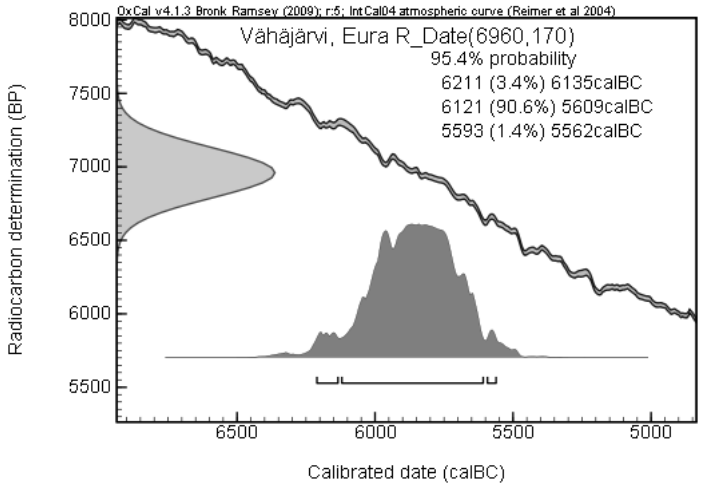

Figure 3.10: Screen capture from the OxCal program. The ^{14}C age (6960) and its uncertainty (170) are the inputs. The line indicates the calibration curve while the error distribution of the calendar age (95.4 % confidence) is shown in dark gray

3.6.3 Radiocarbon dating

The idea of using ^{14}C radiocarbon dating for determining the ages of carbonaceous materials, such as charcoal, bone, etc., was introduced in (Anderson et al., 1947). In (Libby et al., 1949) the ^{14}C radiocarbon dating was tested for determining the age of known samples. The three principal isotopes of carbon which occur naturally are listed in Table 3.3:

The radiocarbon dating is based on the rate of decay of the carbon isotope ^{14}C. It is formed in the upper atmosphere through the effect of cosmic ray neutrons upon

Table 3.3: Carbon isotopes

Carbon isotope	Status	Amount (%)
^{12}C	stable	98.89
^{13}C	stable	1.11
^{14}C	unstable or radioactive	0.00000000010

^{14}N. The reaction can be expressed as (Bronk Ramsey, 2008):

$$n + {}^{14}_{7}\mathrm{N} \rightarrow {}^{14}_{6}\mathrm{C} + p, \tag{3.19}$$

where n is a neutron and p is a proton.

After ^{14}C has been produced in the upper atmosphere, it is eventually oxidized to $^{14}CO^2$. The ^{14}C enters the plants and animals through photosynthesis and the food chain. After a plant or an animal dies, the function of carbon uptake is ceased and the radioactive carbon starts decaying. The two best known values for the decay rate (the half-life of ^{14}C) are 5568 ± 30 (Anderson and Libby, 1951) and 5730 ± 40 (Godwin, 1962). The decay process in which the ^{14}C decays back to ^{14}N is described by Bronk Ramsey (2008):

$$ {}^{14}_{6}\mathrm{C} \rightarrow {}^{14}_{7}\mathrm{N} + e^{-}\overline{v}_e, \tag{3.20}$$

where e is an electron and $\overline{v}_e$ is an electron antineutrino.

3.6.4 Parameter optimization

In addition to the dating, another source of uncertainty is the elevation value of the data points. This uncertainty was taken into account by applying Gaussian distribution (standard deviation of 3 m was considered sufficient to count for the uncertainty due to, e.g., erosion related to lake tilting) to each elevation datum in the data sets. Monte Carlo simulation involving 1 000 realizations was then used to obtain the probabilistic estimates of the A_s and B_s parameter values of Påsse's

shoreline displacement model. The estimation of model parameters proceeded as follows (see the flow chart in Figure 3.11).

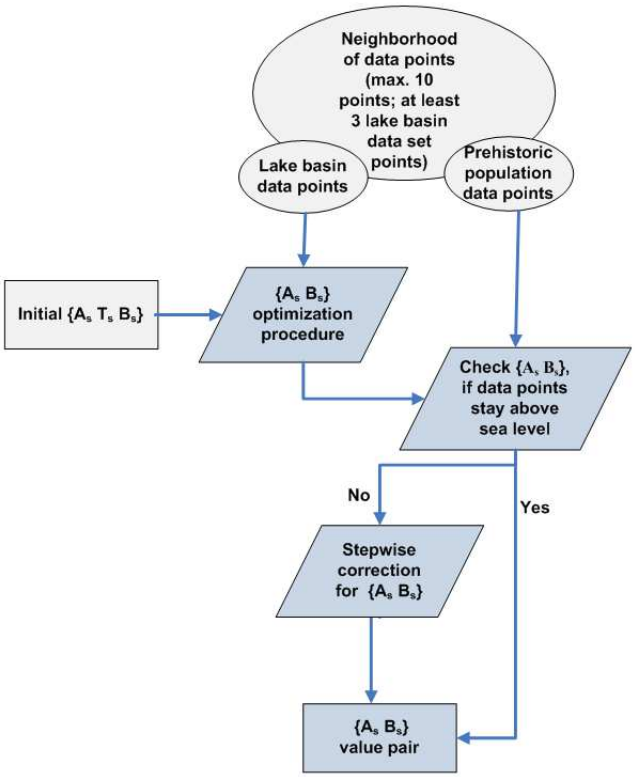

Figure 3.11: Flow chart of the land uplift parameter refinement algorithm.

The first task was to find the neighboring points for the particular data point and calculate the A_s and B_s parameters. A set of 10 points was selected including the point in question and at least 3 points from the lake basin data were required. As a starting point, a $\{A_s\ B_s\}$ parameter value pair was selected according to (Påsse, 2001) and (Grad and Tiira, 2009). The value of the T_s parameter was taken from (Geological Survey of Sweden, 2013), discussed in section 3.5.1.

The optimization procedure for estimating the A_s and B_s parameters was carried out using an orthogonal least squares optimization method. A region in the $\{A_s\ B_s\}$ parameter space was defined where the true parameter values were supposed to lie according to the data. This region was assigned a cost function: the less probable the obtained parameter values were, the higher was the cost. The minimum value of the

cost function was dependent on the value of the A_s parameter given in (Påsse, 2001) and the value of the B_s parameter calculated based on the Moho map (see Figure 3.8) using Equation 3.18 for the particular site. It was assumed that the estimate given in (Påsse, 2001) is at least approximately right in the wider scale. An optimization procedure was then initiated and performed to produce all the parameter value pairs corresponding to the minimum values of cost functions. The curve fitting was done in the MatLab computation environment using the `fminsearch` function, which is based on the Nelder-Mead method presented in (Nelder and Mead, 1965).

As the prehistoric population data set presents archaeological evidence on human residence, the corresponding sites should locate above the sea level at the particular time. If the parameter values $\{A_s\ B_s\}$ from the previous step indicated the opposite, the parameter values were changed step-by-step until the resulting land uplift curve remained below the elevation obtained based on the selected neighboring data points from the archaeological data set. Thus, an adjusted parameter value pair was obtained as the result. If no correction was needed, i.e. the elevation of the prehistoric population data was higher than the sea level at the particular time, this data set was ignored.

The statistical estimation of parameters was performed using Monte Carlo simulation (Mosegaard and Sambridge, 2002). In this way, the resulting parameters were actually represented by probability distributions. The probability distributions were smoothed with kernel density estimation in order to get more reliable estimates for the parameter values. The calculation space was defined for each data point so that the particular data point occurred in the center of the space. Thus, the resulting probabilistic parameter value pair was assigned to the location of the data point around which the space was located.

During the estimation process it became clear that the download factor A_s, the ice recession parameter T_s and the inertia factor B_s in Equation 3.15 are highly dependent on one another. To study the dependencies, error surfaces were created between the elevation values of the actual source data points and the elevation values predicted by the land uplift model for various parameter sets $\{T_s\ A_s\ B_s\}$. An example of such an error surface for the case where the B_s parameter is fixed at 6 000 year^{-1} is shown

in Figure 3.12. The figure indicates that the relationship between the T_s and A_s parameters is almost linear. There is no clear minimum in the error surface; various different *download factor / ice recession time* pairs give approximately equally low error.

As discussed earlier, the parameters T_s and B_s can be constrained based on what is known about the ice recession process and the Moho depth, respectively. In Figure 3.13 another error surface is shown where this kind of constraint has been introduced. As can be seen, constraining the T_s parameter reshapes the error surface so that a more distinct minimum can be found. Also, the numeric value of the error is decreased. However, the analysis shows that land uplift modeling based on curve fitting using the formulas proposed by Påsse has the serious drawback of ambiguity with respect to the model parameters.

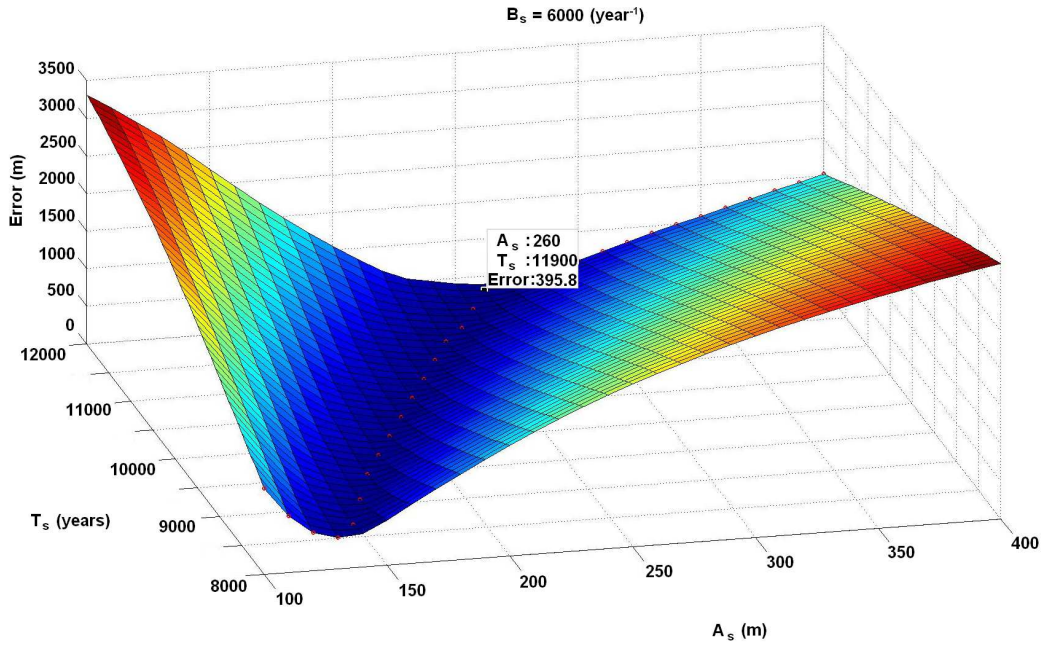

Figure 3.12: An error surface describing the behavior of the model error with respect to A_s and T_s with B_s fixed.

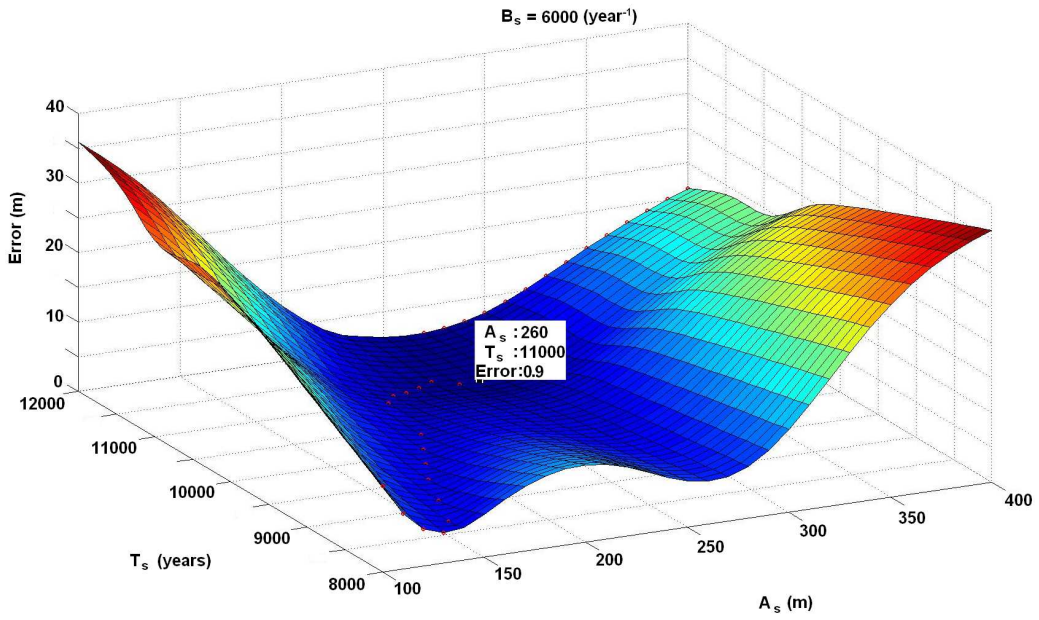

Figure 3.13: An error surface obtained taking into account a priori knowledge.

3.7 Analysis of the effects of model parameter refinement

The resulting spatial distributions of the A_s and B_s parameters for the Olkiluoto modeling area are presented in Figures 3.14 and 3.15, respectively. The parameter optimization was performed for the cases of two different eustatic curves, one presented by Påsse (2001) and the other constructed as described in section 3.5.2. For comparison, the deterministic A_s and B_s grids presented in (Vuorela et al., 2009) are shown in the figures. All the surfaces are used in the surface water body modeling described in chapter 4.

Figure 3.14 shows that the Vuorela et al. (2009)'s land uplift model version gives much higher download factor (i.e., the A_s parameter value) estimates compared to the two probabilistic model versions. The Vuorela et al. (2009)'s model version can be considered less reliable, however, as it extrapolates past and future land uplift solely based on the current uplift rate and is thus highly dependent on the shape of the U_s

function. The shape of the U_s function is not based on any geophysical model but is rather an educated guess. Figure 3.14 also indicates that the three models differ in spatial variability of the download factor. The difference of the download factor (and thus the past land uplift rate) between the eastern and western parts of the modeling area is highest with the model version based on the Punning et al.'s eustatic curve. Also, the distribution of the download factor within the modeling area differs among the three model versions.

As indicated in Figure 3.4, the B_s parameter affects the land uplift curve in an opposite manner compared to the A_s parameter: the lower the B_s parameter value (the inertia factor) the steeper the land uplift curve. Figure 3.15 indicates that the B_s parameter value is the lowest for the Vuorela et al. (2009)'s land uplift model version. This adds up with the effect of the A_s parameter yielding higher land uplift rates for the Vuorela et al. (2009)'s model in the past as well as in the future. The spatial distribution of the B_s parameter value is quite similar for all the three model versions.

The resulting A_s and B_s surfaces for the area of Finland are presented in Figure 3.16. Both the A_s and B_s surfaces calculated with two different eustatic curves have only minor differences between them in larger scale. When comparing the A_s surfaces with (Påsse, 2001), it can be noticed that the area of maximum A_s values has been slightly shifted towards Central Finland. This might be linked to the behavior of the land uplift model discussed earlier at the end of section 3.6.4. The B_s surfaces correlate with the Moho map in Figure 3.8.

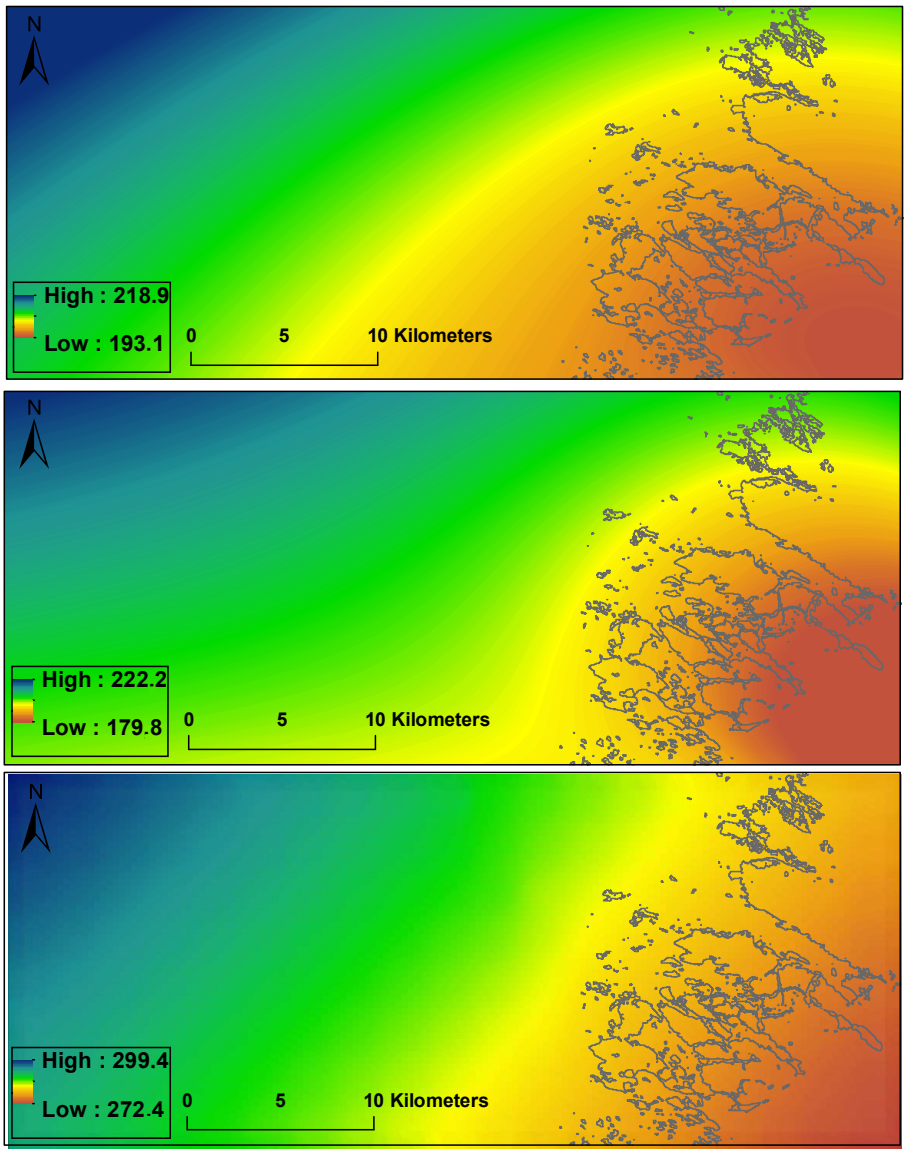

Figure 3.14: Spatial distribution of the A_s parameter value (in meters) for the Olkiluoto area created using Påsse's (top subfigure) and Punning et al.'s. (middle subfigure) eustatic curves. The reference A_s grid calculated as proposed by Vuorela et al. (2009) is shown in the bottom subfigure. In the case of the probabilistic models the parameter values of highest probability are presented. Note the different scaling indicated at the left side of the subfigures.

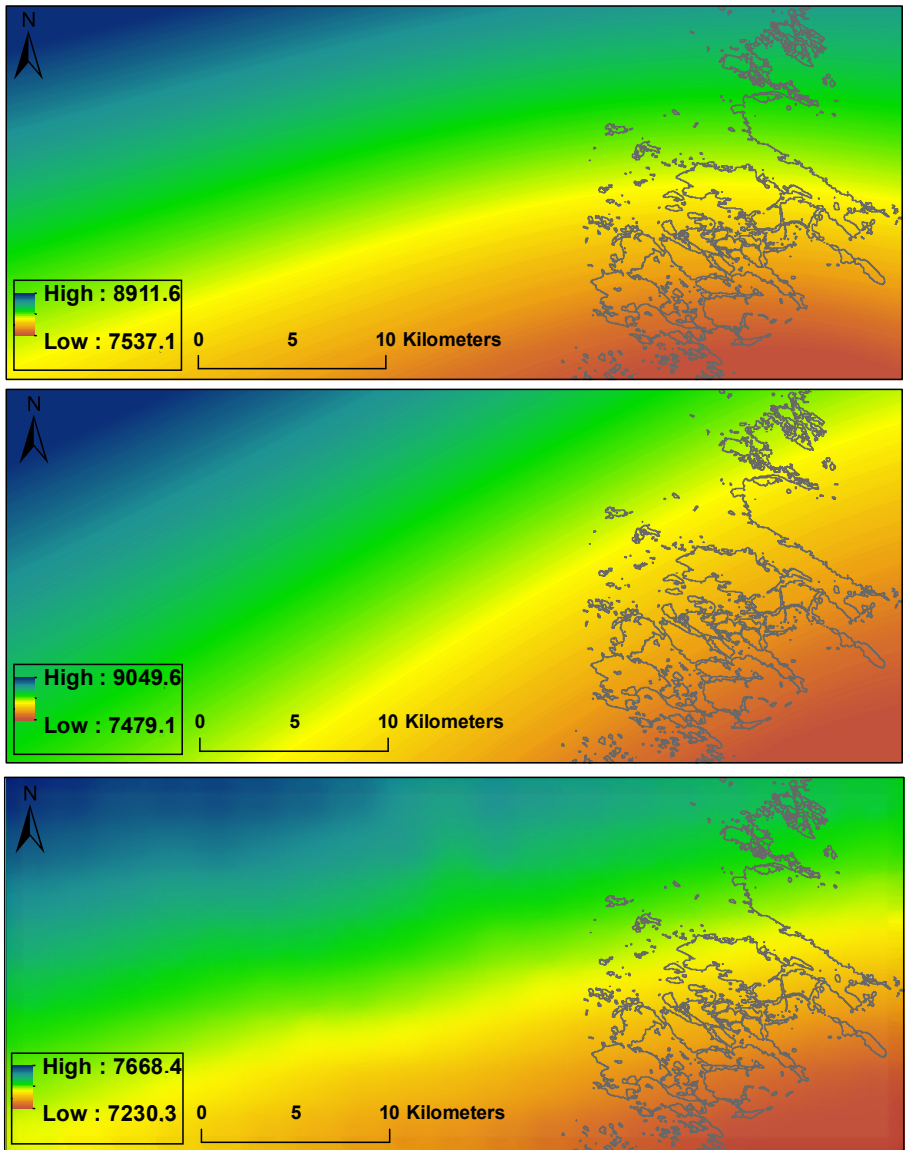

Figure 3.15: Spatial distribution of the B_s parameter value (in year^{-1}) for the Olkiluoto area created using Påsse's (top subfigure) and Punning et al.'s. (middle subfigure) eustatic curves. The reference B_s grid calculated as proposed by Vuorela et al. (2009) is shown in the bottom subfigure. In the case of the probabilistic models the parameter values of highest probability are presented. Note the different scaling indicated at the left side of the subfigures.

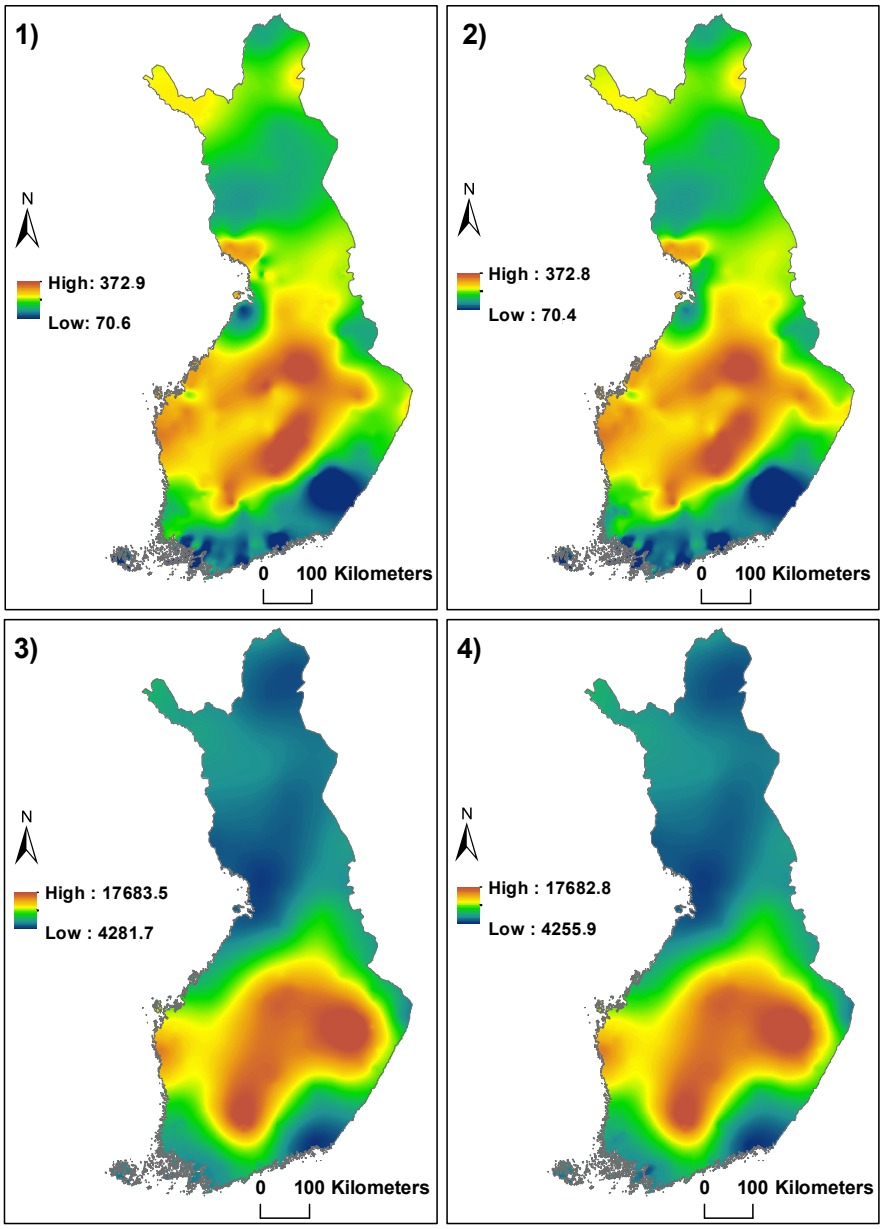

Figure 3.16: Spatial distribution of the A_s parameter value (in meters) for the area of Finland created using (1) Påsse's eustatic curve and (2) Punning et al.'s. eustatic curve; Spatial distribution of the B_s parameter value (in year^{-1}) for the area of Finland created using (3) Påsse's eustatic curve and (4) Punning et al.'s. eustatic curve.

Chapter 4

Probabilistic modeling of biosphere development in Olkiluoto

In this chapter the results of DEM generation and land uplift modeling, described in previous chapters, are used to predict the future geomorphic landscape development in the Olkiluoto area. Geomorphic landscape development and water body formation form a part of wider biosphere development modeling effort required for the safety assessment of the spent nuclear fuel repository.

A short overview on the research related to biosphere modeling is given first. After that, the geomorphic landscape development modeling procedure and the considered scenarios are presented. Finally the results of the development of the areas and volumes of four main future lakes to be formed in the vicinity of the Olkiluoto Island are presented.

4.1 Biosphere modeling

Ambitious purpose of biosphere modeling is to model earth's biological, geological and chemical processes and their interactions as accurately as possible. When thinking about the sheer size of the model and the number of parameters affecting the outcome, the modeling task seems to be impossible. The whole process involves sun radiation, its effects on earth's heat, atmospheric and oceanic circulation and

finally on the different biological processes and interactions. Earth's geological properties such as land uplift, crust movements, erosion and sedimentation are constantly reforming the surface of the Earth thus opening new habitable areas to biological processes and destroying the old ones. Geology and geological processes, in general, form an important part of biosphere development modeling.

It is obvious that the computer capacity today is not sufficient for global biosphere modeling. Also, the simulation of the overall global biosphere process requires the understanding on how the different sub-processes will interact with each other. Two approaches can be taken: biosphere development can either be modeled locally, or global modeling may be performed using only a few parameters with a computationally sparse grid.

One of the first attempts to model plant formations with climatic data is presented in (Holdridge, 1947). In this model, the plant species were classified using elevation, moisture and temperature data. A 'Simple biosphere model' was presented in (Sellers et al., 1986; Sato et al., 1989) and its purpose was to model the most important parameters concerning vegetation growth and combine the system with general circulation models. During the past two decades various biosphere models have been proposed, each of which models the biosphere using different parameter configurations. For example in (Foley et al., 1996) a hierarchical computation of carbon balance, vegetation dynamics and land surface dynamics is presented. In (Friend et al., 1997) a hybrid biosphere model combining several research efforts is proposed. The results obtained by individual research groups are incorporated into the hybrid model as separate modules and complex interactions are suggested between these modules when computing the overall result. Many models concentrate on carbon and carbon dioxide (CO_2) cycle in the context of global circulation (Kowalczyk et al., 2006; Keenan et al., 2012; Richardson et al., 2012; Pestunov et al., 2014; Yates et al., 2000; Meyer et al., 1999; Migliavacca et al., 2012; Medvigy and Moorcroft, 2012; Lüdeke et al., 1994). Biosphere models have been used also for identifying the past and predicting the future. The Middle Miocene period (15 million years ago) was simulated using a coupled atmosphere-ocean-biosphere model in (Krapp and Jungclaus, 2011). In (Franck and Bounama, 2006), global carbon cycle model is introduced and

carbon-based life form survival predictions are made up to 1.6×10^9 years ahead.

Long-term safety of the nuclear waste disposal is connected closely to biosphere modeling. IAEA has set guidelines for radionuclide transportation prediction and modeling in the BIOMASS program (BIOsphere Modeling and ASSessment) in (IAEA, 2003). It defines the necessary biosphere model components and their characteristics, radionuclide transportation options and assessment guidelines for the modeling procedure. Local nuclear waste companies and organizations have made several reports on radionuclide transportation and biosphere modeling. For example the Swedish Nuclear Fuel and Waste Management Co has summarized their work in (SKB, 2011a,b). Consequently, Posiva has made similar analysis and summarized it in (Posiva Oy, 2013b). Several initial documents concerning the Yucca mountain nuclear waste repository have been produced. For example in (Inhofe, 2006) the repository research and long-term safety requirements have been specified for consideration by the U.S senate. Also, the IAEA has made initial biosphere assessment program for the Yucca mountain in (IAEA, 2001) and the performance of the Yucca mountain biosphere models has been assessed, for example, in (Tappen et al., 2001).

Nuclear safety assessment is usually local and the models and the boundary conditions can be defined and computed locally very precisely. The nuclear safety area is relatively small when compared to global models, but it must cover the whole area possibly affected by imaginary repository disaster as well as cumulative areas such as those affected by rivers and other water bodies in the region. This thesis concentrates mainly on modeling land uplift and water body formation in the Olkiluoto area.

4.2 Modeling the formation of future water bodies in Olkiluoto

The probabilistic digital elevation model (see chapter 2) and the locally adjusted land uplift model (chapter 3) were used to acquire a probabilistic overview on the locations and dimensions of the lakes projected to form at the Olkiluoto modeling area.

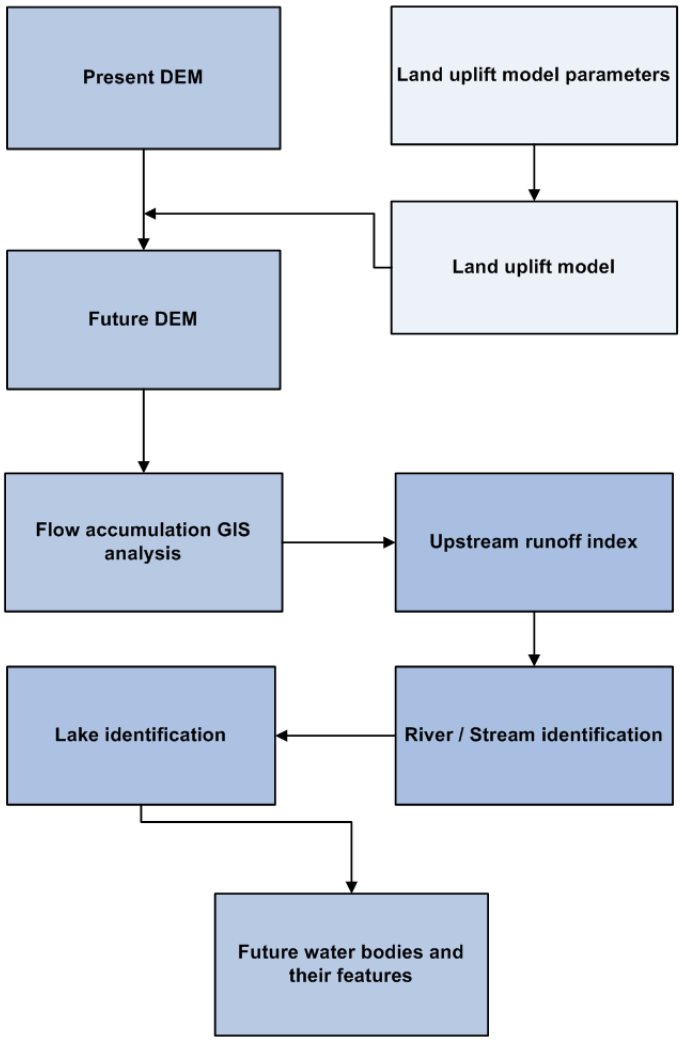

Figure 4.1: Flow chart of the of the simulation procedure for lake projection.

The modeling was carried out by applying conventional GIS analysis of flow accumulation to identify future lakes and streams. For each cell of the digital elevation model the number of upstream cells is calculated indicating the extent of the area, in grid cell units, from which the water is accumulated to the particular cell by surface runoff. The cells having a large accumulation value are combined into streams and rivers. Cells where the flow accumulation value is larger than in any of the surrounding cells are bottoms of depressions (sink points), aggregations of which are identified as lakes. These depressions are filled until the water pours out of the depression,

i.e., to the lowest point still having flow direction towards the depression. This is, however, slightly lower than the actual water level of the lake since in reality the size of the outlet is limiting the outflow and the water level would raise until a sufficient outlet cross-section area has been achieved (Ikonen et al., 2010). Basins that fill up to a smaller size than a specified area and mean depth are not considered lakes but are identified as peat bogs. The water body development simulation procedure did not contain any sedimentation or erosion processes. The simulation procedure is illustrated in Figure 4.1 and it was carried out using the ArcGIS-based toolbox UNTAMO (Arbonaut Ltd.). UNTAMO is a set of tools with which the future properties of geomorphic landscape, human settlement, land use etc. can be estimated.

4.3 Geomorphic landscape development scenarios and general features of the future geomorphic landscape

One of the main study questions addressed in this thesis is related to the influence of the uncertainties in the elevation and land uplift models on the future geomorphic landscape development. The uncertainties in the elevation are considered by drawing a number of realizations from the probabilistic DEM presented in chapter 2. In land uplift modeling, however, various choices, such as the form of the eustatic curve or the premises for parameter optimization (either based on shoreline displacement data or precise values of the present uplift rate), can be made. Therefore, three different land uplift models were used in the simulations, two of which are based on the probabilistic land uplift parameter grids presented in chapter 3 and the third one is based on the deterministic land uplift model optimized according to the present land uplift rate and proposed by Vuorela et al. (2009). The two probabilistic land uplift models differ from each other in the shape of the eustatic curve: one model version is based on Påsse's and the other on Punning et al.'s eustatic model (see section 3.5.2). In both cases 10 realizations of the spatial distribution of the A_s parameter value were created

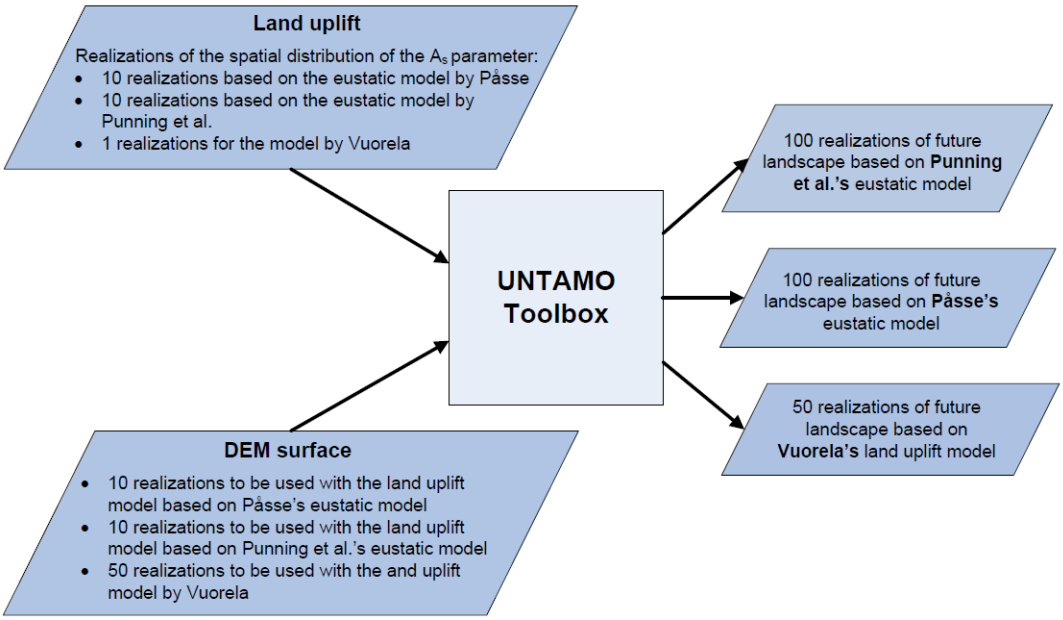

Figure 4.2: Three scenarios considered in the geomorphic landscape development modeling.

inside the predefined confidence limits.

As a result, the following three probabilistic future geomorphic landscape development scenarios were obtained (see Figure 4.2):

- 100 realizations (10 A_s distribution realizations times 10 DEM realizations) of the geomorphic landscape projection based on Påsse's eustatic model
- 100 realizations (10 A_s distribution realizations times 10 DEM realizations) of the geomorphic landscape projections based on Punning et al.'s eustatic model
- 50 realizations (A_s distribution as in (Vuorela et al., 2009) and 50 DEM realizations) of the geomorphic landscape projections based on Vuorela et al. (2009)'s land uplift model.

4.3.1 Drawing realizations from the probabilistic DEM and land uplift models

In order to maintain natural geomorphic landscape forms such as hills and depressions, at their right locations and, at the same time, keep all the realizations within the computed error limits of the DEM, the following scheme was developed. The modeling area was divided into 2 km × 2 km area blocks as shown in Figure 4.3. Each block contained 800×800 grid points of the probabilistic DEM. A random location within each block was then drawn and random numbers between $1 \ldots 100$ to represent the indexes into the histograms of the elevation values at these locations were generated. Thin plate spline interpolation was applied subsequently to the indexes to determine the index values of the elevation histograms at all the grid points of the DEM. This ensures that the values of the DEM realizations will change spatially smoothly within the individual DEM point error tolerance. As the interpolation process yields fractional numbers, the values had to be rounded to get valid indexes. The elevation of the particular DEM realization was obtained by looking up the elevation values from the histograms of all the grid points according to the interpolated and rounded histogram indexes. To obtain 50 DEM realizations the procedure was repeated 50 times, i.e., within each 2 km × 2 km block 50 different locations with corresponding random bin numbers were drawn as the starting points for DEM generation.

To obtain 10 realizations of both probabilistic versions (one based on Påsse's and the other based on Punning et al.'s eustatic curve) of the land uplift model, the most probable value for the B_s parameter was selected and 10 estimates of the A_s parameter grids were calculated using A_s histograms in the same manner as for the random DEM surfaces. The number of realizations in each model was a compromise between the computation time of UNTAMO simulations and statistical confidence.

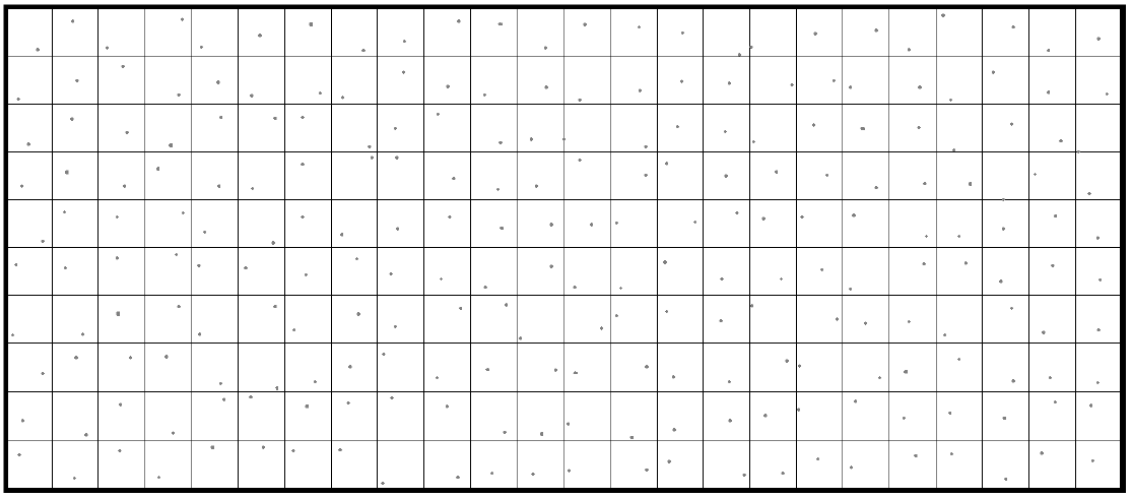

Figure 4.3: The modeling area divided into 2 km × 2 km blocks with random locations drawn within each block.

4.4 Simulation results

In this section the results of geomorphic landscape development and surface water body formation modeling are presented. The future shoreline displacement is discussed first and then the volumes and surface areas of the most prominent future lakes near the present Olkiluoto Island are analyzed.

4.4.1 General features of the projected geomorphic landscape

Figure 4.4 shows the most probable shoreline locations at 10 000 AP as predicted by the three scenarios presented in Figure 4.2. Most probable lake and river formations produced by the UNTAMO toolbox are also shown. The upper subfigure in Figure 4.4 is generated with Påsse's eustatic curve, the middle subfigure with Punning et al.'s eustatic curve and the lower subfigure has been created using the land uplift model version by Vuorela et al. (2009) based on current land uplift rate and computed with Påsse's eustatic curve. Current shoreline is marked with a black line. In Figure 4.5 the proportional shares of dry land, lakes and sea in the modeling area are presented at present day situation and at 10 000 AP as predicted by the three scenarios.

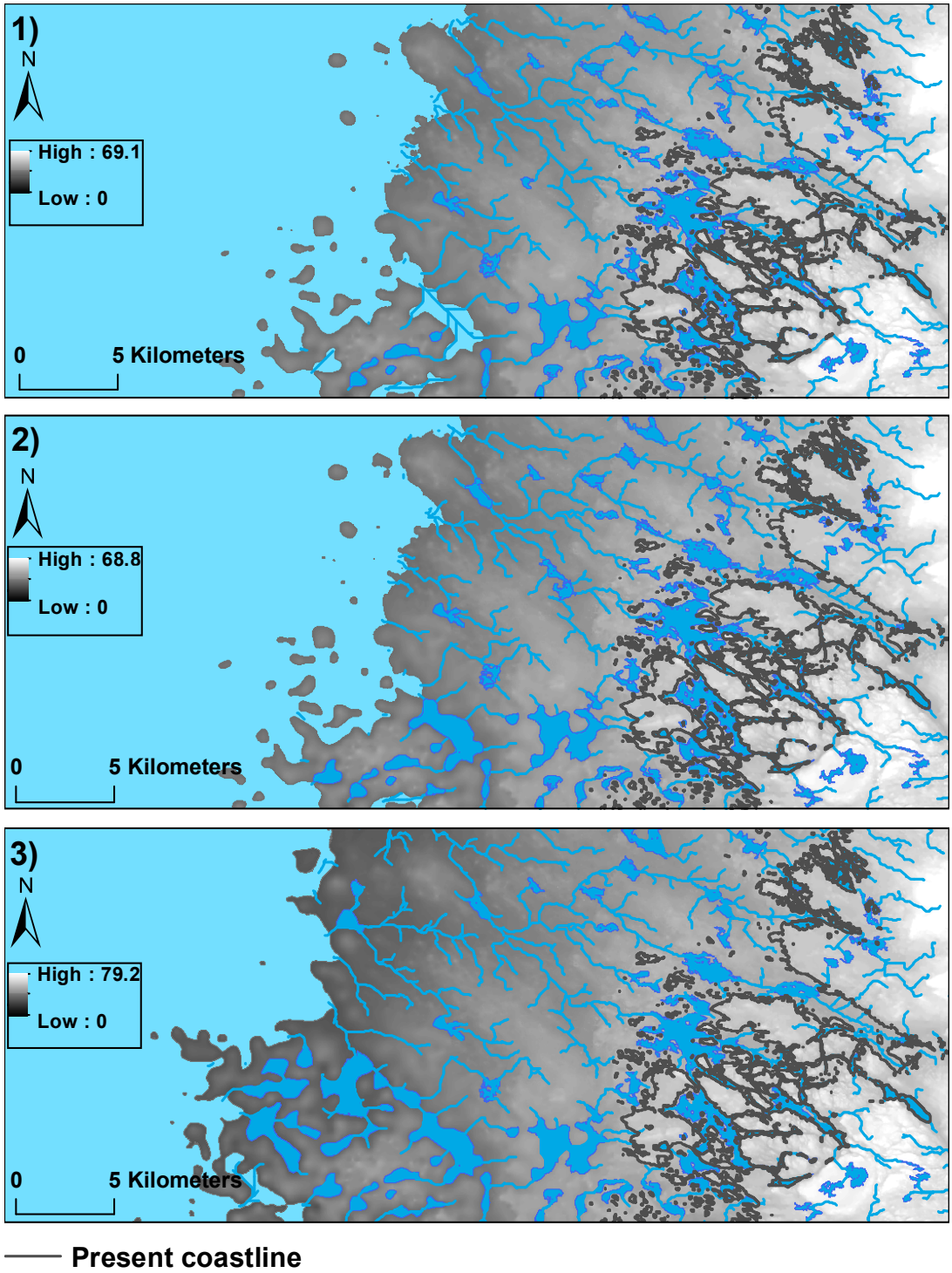

Figure 4.4: General features of the geomorphic landscape at 10 000 AP as predicted by the land uplift model version based on 1) Påsse's eustatic curve, 2) Punning et al.'s eustatic curve, 3) Vuorela et al. (2009).

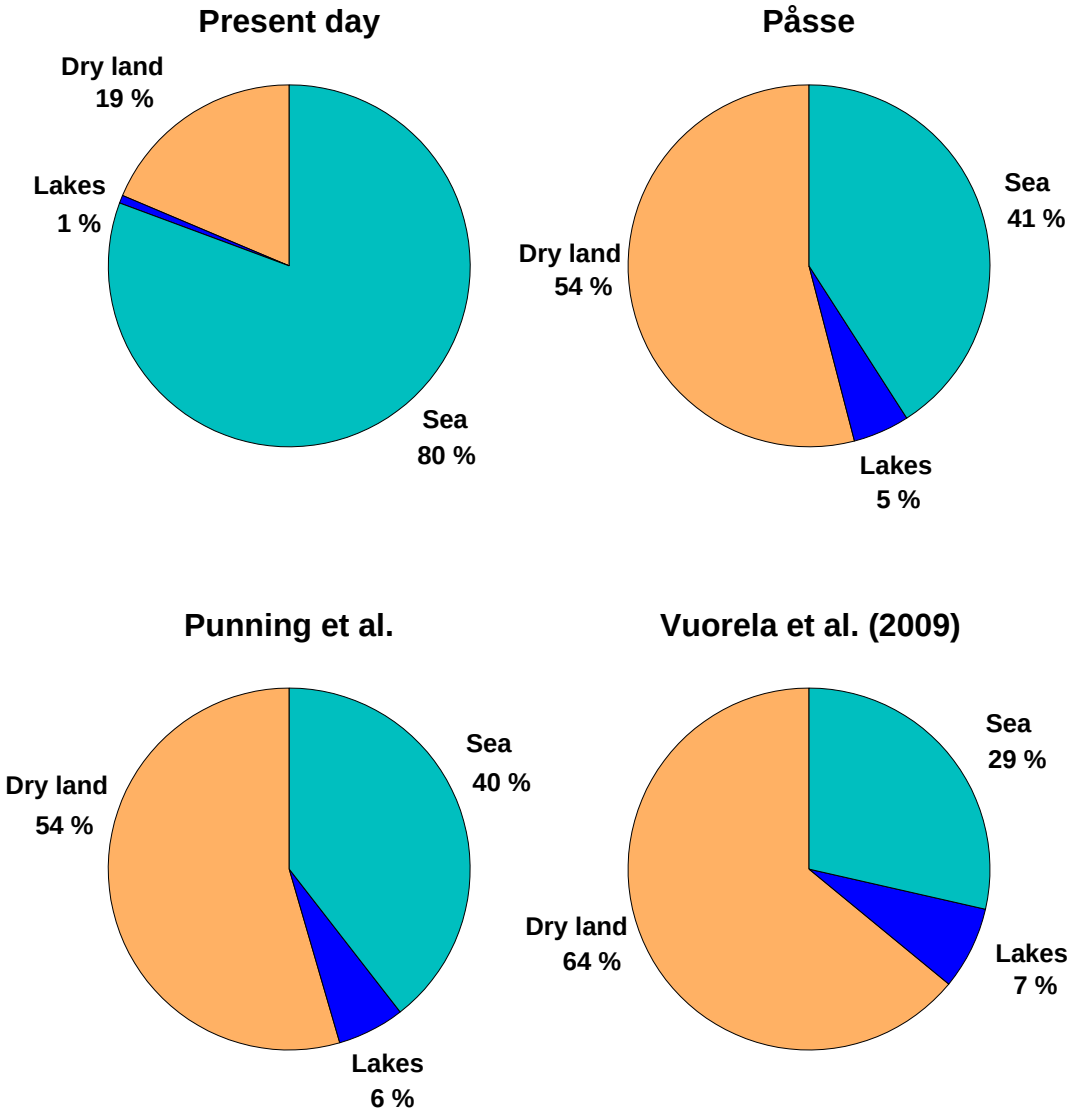

Figure 4.5: Proportional areal share of dry land, lakes and sea at present day and 10 000 AP as predicted by the land uplift model version based on 1) Påsse's eustatic curve, 2) Punning et al.'s eustatic curve, 3) Vuorela et al. (2009) in Figure 4.4.

The figures indicate that the land uplift model version based on (Vuorela et al., 2009) predicts significantly faster shore level displacement compared to the two probabilistic model versions. This is in concordance with Figure 3.14 where it is illustrated that Vuorela et al. (2009)'s model version yields higher A_s parameter values and thus a higher download factor. It is important to note, however, that despite of this difference in the model versions, the main surface water bodies are projected in a similar way by all the three model versions.

4.4.2 Shoreline location probability

As geomorphic landscape development is viewed as a statistical process, it is also important to assess the uncertainty of the shoreline displacement estimation. In Figures 4.6...4.9 this uncertainty is presented in the form of the probability that a certain location is covered by sea at 1 000 AP, 4 000 AP, 7 000 and 10 000 AP, respectively. The areas covered by sea with 100 % probability at certain time instant in the future are colored blue and the areas definitely forming dry land are colored red. The region where the shoreline will reside with some probability between 0 and 100 are colored according to the probability scale indicated in each table below the maps.

As may be expected the uncertainty of the shoreline location becomes slightly higher when predicting further into the future. Also, the confidence limits of the current probabilistic DEM are wider further away from the current coastline as the available data are less reliable there. Flatness of the seabed also affects the width of the area where the shoreline is predicted to reside.

Another observation is that the land uplift model version based on (Vuorela et al., 2009) yields shoreline displacement estimates of less uncertainty compared to the probabilistic land uplift model versions. This is probably due to the fact that in the Vuorela et al. (2009)'s model only the DEM was probabilistic while land uplift was considered to be deterministic. Although 50 realizations of the DEM were used with this scenario (compared to 10 with the other two scenarios), this does probably not increase significantly the variability of the probabilistic DEM while the additional

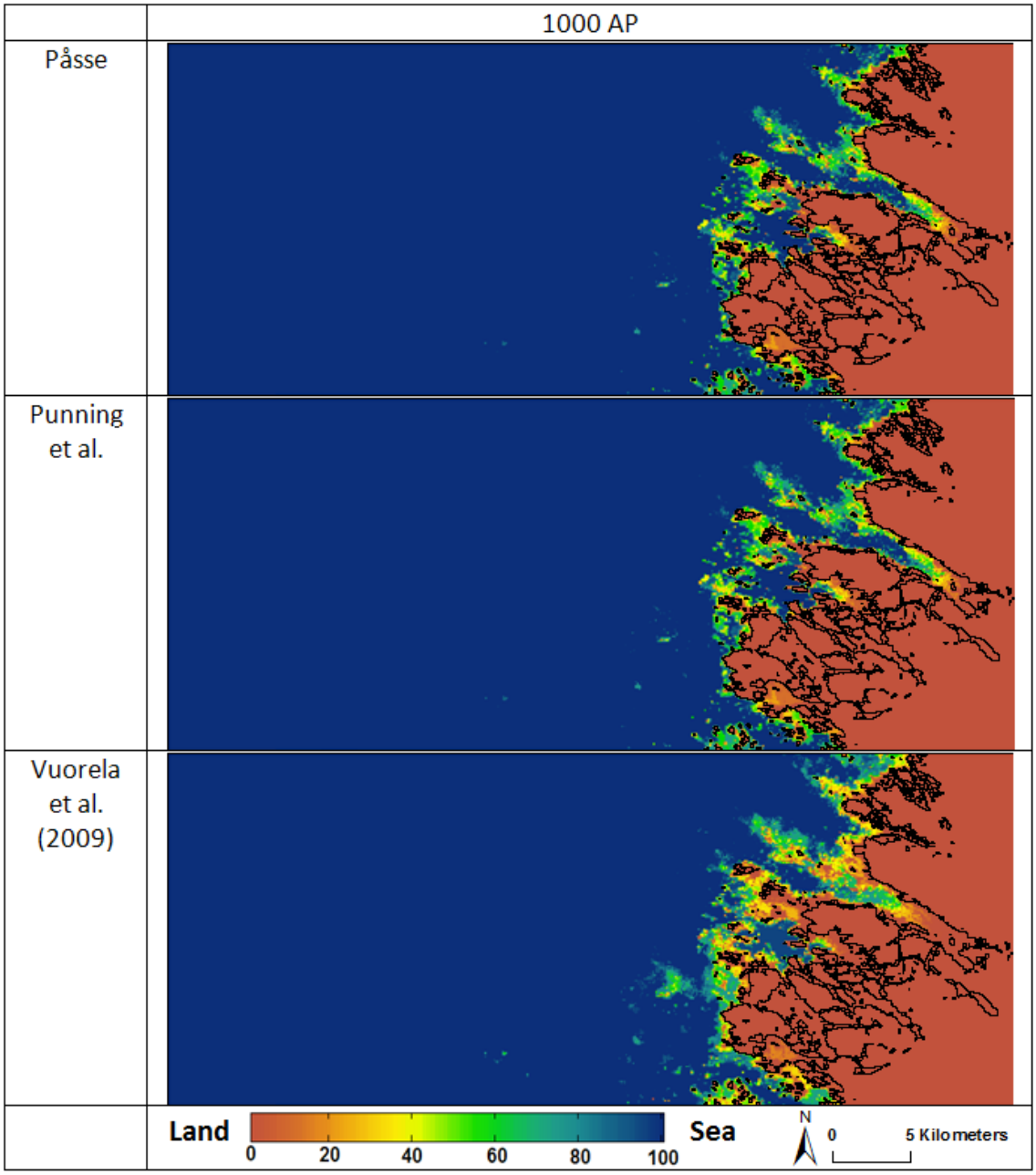

Figure 4.6: Sea extent probability at 1 000 AP.

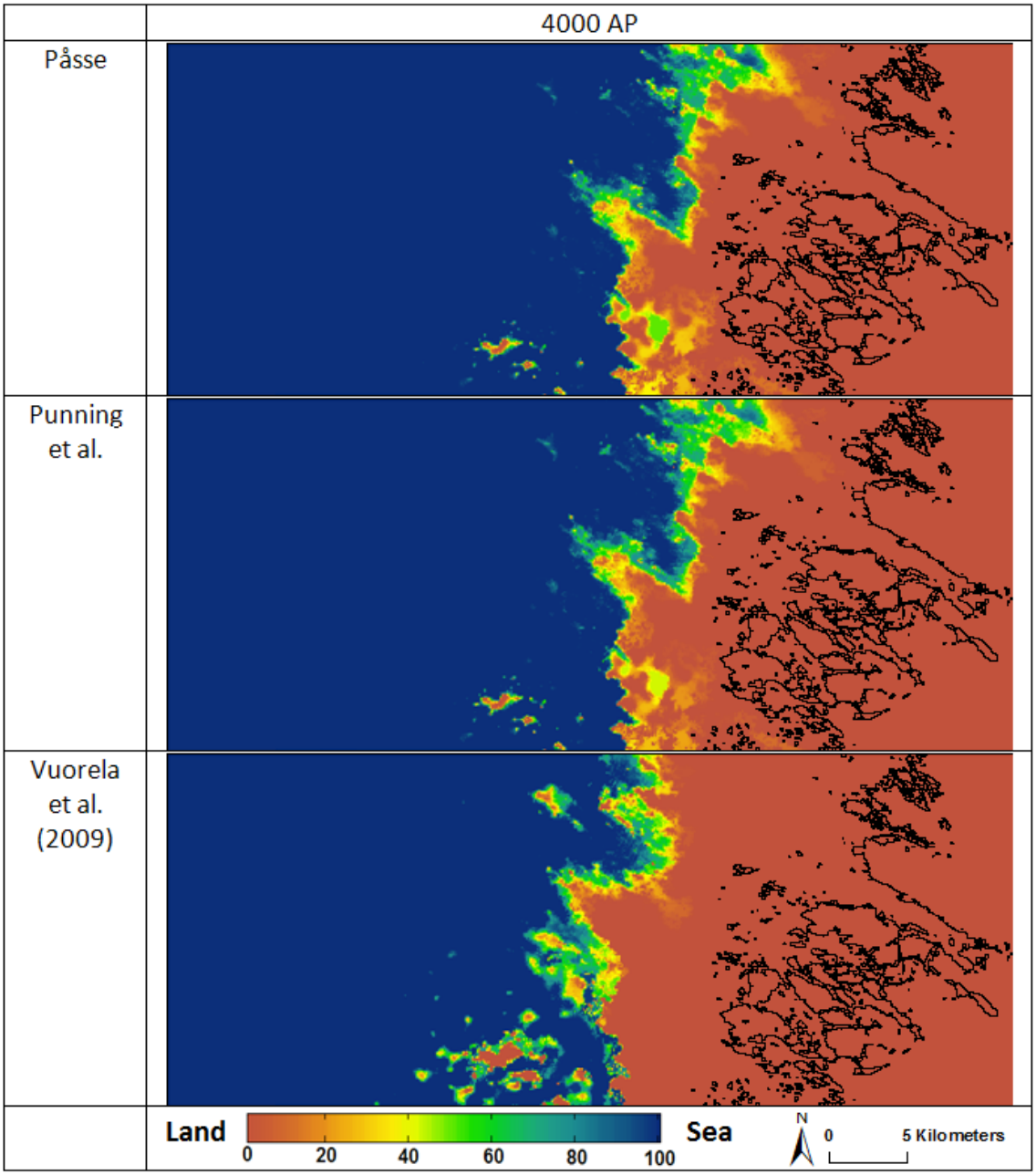

Figure 4.7: Sea extent probability at 4 000 AP.

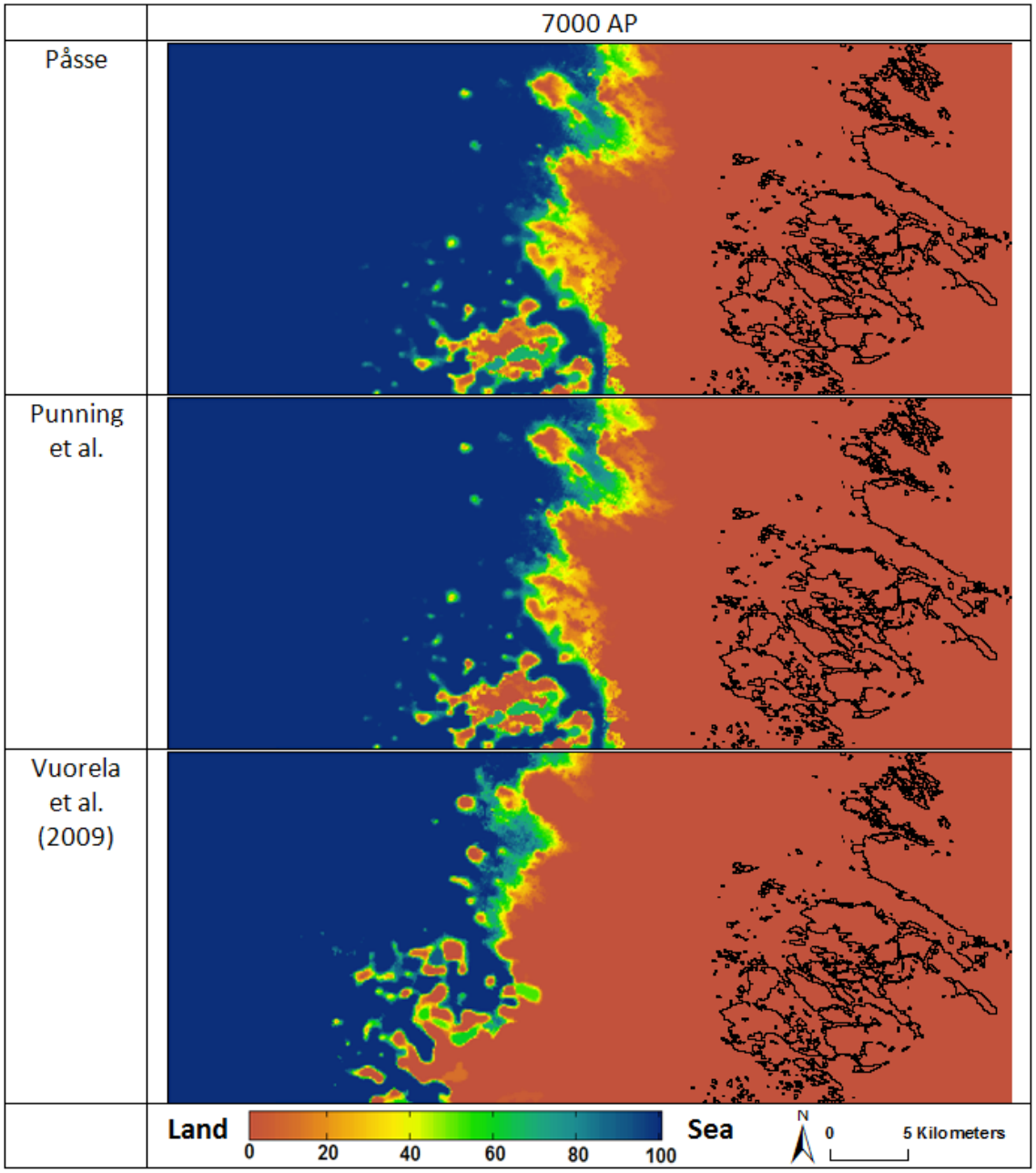

Figure 4.8: Sea extent probability at 7 000 AP.

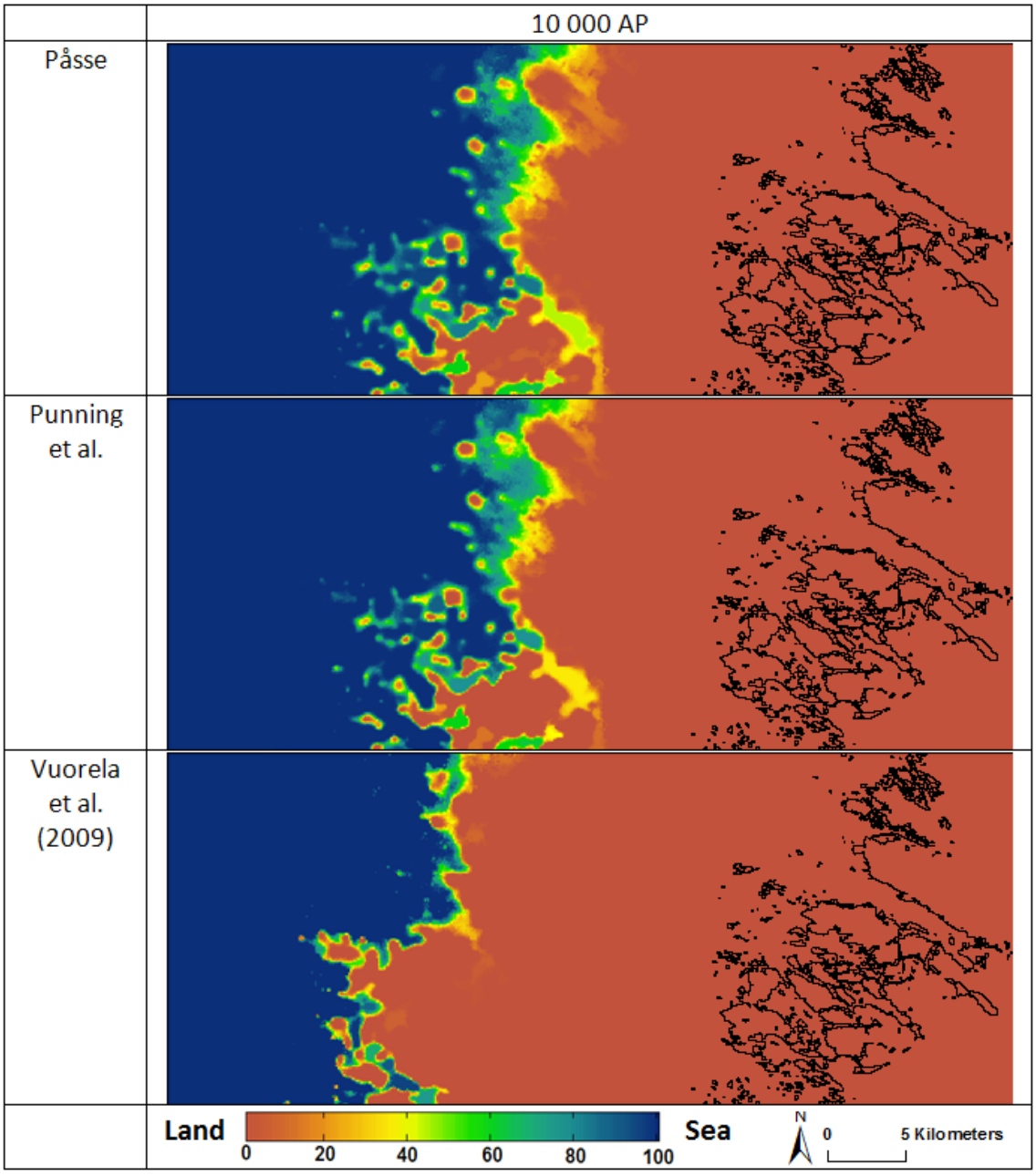

Figure 4.9: Sea extent probability at 10 000 AP.

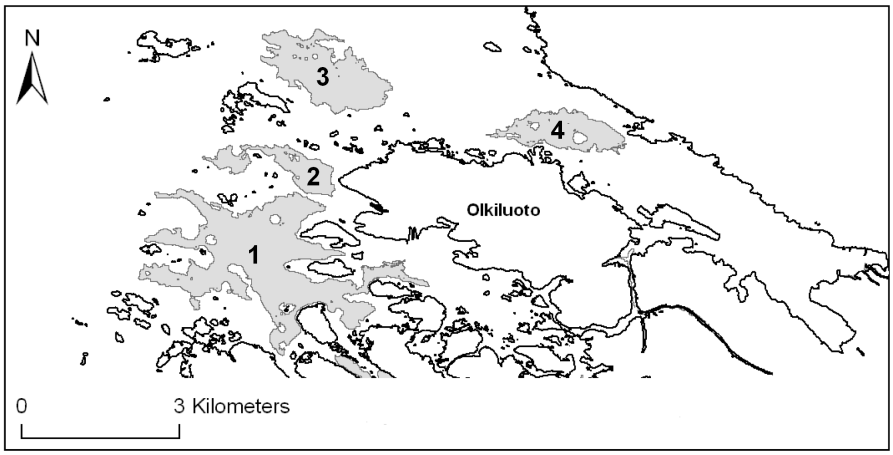

Figure 4.10: The location of the four lakes projected to form at the Olkiluoto repository site at 10 000 AP. The numbering of the lakes indicated in the figure is used in further discussion and figures.

uncertainty added by the probabilistic land uplift model clearly has an effect on the results. As the data used in the land uplift modeling have several sources of errors, it is suggested that the scenarios involving a probabilistic land uplift model enable to assess the future geomorphic landscape development in a more realistic manner and are thus more useful in modeling the surface water body formation and, eventually, the assessment of possible doses of radionuclides.

4.4.3 Lake area and volume probabilities

All the three scenarios of geomorphic landscape projections of the Olkiluoto modeling area indicated formation of four lakes in the vicinity of the present Olkiluoto Island. The location of these lakes in the case of the most probable DEM realization and the land uplift model by Vuorela et al. (2009) is shown in Figure 4.10. These lakes are referred later in the text by their corresponding numbers indicated in Figure 4.10.

The formation of the future water bodies is studied in this section by presenting and discussing the simulation results on lake area and volume probabilities. In Figures 4.11...4.14 a 3D surface view of the lake formation probability of Lake 2 is presented at years 1 000 AP, 4 000 AP, 7 000 AP and 10 000 AP, respectively; the triplets of

subfigures are obtained for Påsse's, Punning et al.'s and Vuorela et al. (2009)'s geomorphic landscape development scenarios (see Figure 4.2). As the area of the other three lakes is much larger, it was not feasible to present their formation probability as a 3D cross sectional view. In Figure 4.15 the 1 %, 50 % and 100 % probability curves are presented for the crossection used in 3D visualizations of Figure 4.14.

Due to the higher download factor and thus higher land uplift rates predicted by Vuorela et al. (2009)'s scenario, Lake 2 forms more rapidly according to this scenario. At 1 000 AP this lake will already be formed with high probability by this scenario while at the same time the other two scenarios consider the formation of Lake 2 improbable. At later time instants, however, the 50 % probable lake bottom of Lake 2 follows approximately the same surface by all the three scenarios although there is some probability that the lake is significantly deeper and covers a larger area by the scenario based on (Vuorela et al., 2009).

The probability of the future surface area of all the four lakes is illustrated in Figures 4.16...4.19 at 1 000 AP, 4 000 AP, 7 000 AP and 10 000 AP, respectively. The minimum (Min), maximum (Max), median (Med) and standard deviation (Std dev) values for the surface areas are listed in Tables 4.1...4.4, respectively. In these tables the proportional differences in lake area estimates are also presented. The Punning et al. and the Vuorela et al. (2009) scenario values are compared to the Påsse scenario values. Similar conclusion as from the 3D cross section visualizations can also be drawn from the lake surface area simulations. At 1 000 AP the geomorphic landscape development scenario based on (Vuorela et al., 2009) predicts larger lake surface area especially for Lake 1 and much higher lake formation probability for Lake 2. By 10 000 AP, however, the surface area of highly probable lake formations is similar for all three scenarios. There are even some regions where lake probability is higher for the Påsse and Punning et al. scenarios than for the Vuorela et al. (2009) scenario (the western branch of Lake 1, for example). This can be explained by possible outflow and drying up of some regions as the land uplift exceeds some critical threshold.

The lake volume probabilities for lakes 1...4 are shown in Figures 4.20...4.23, respectively. The volume probabilities are calculated in 1 000 years' time step (horizontal axis of the subfigures) and the values are scaled so that they add up to

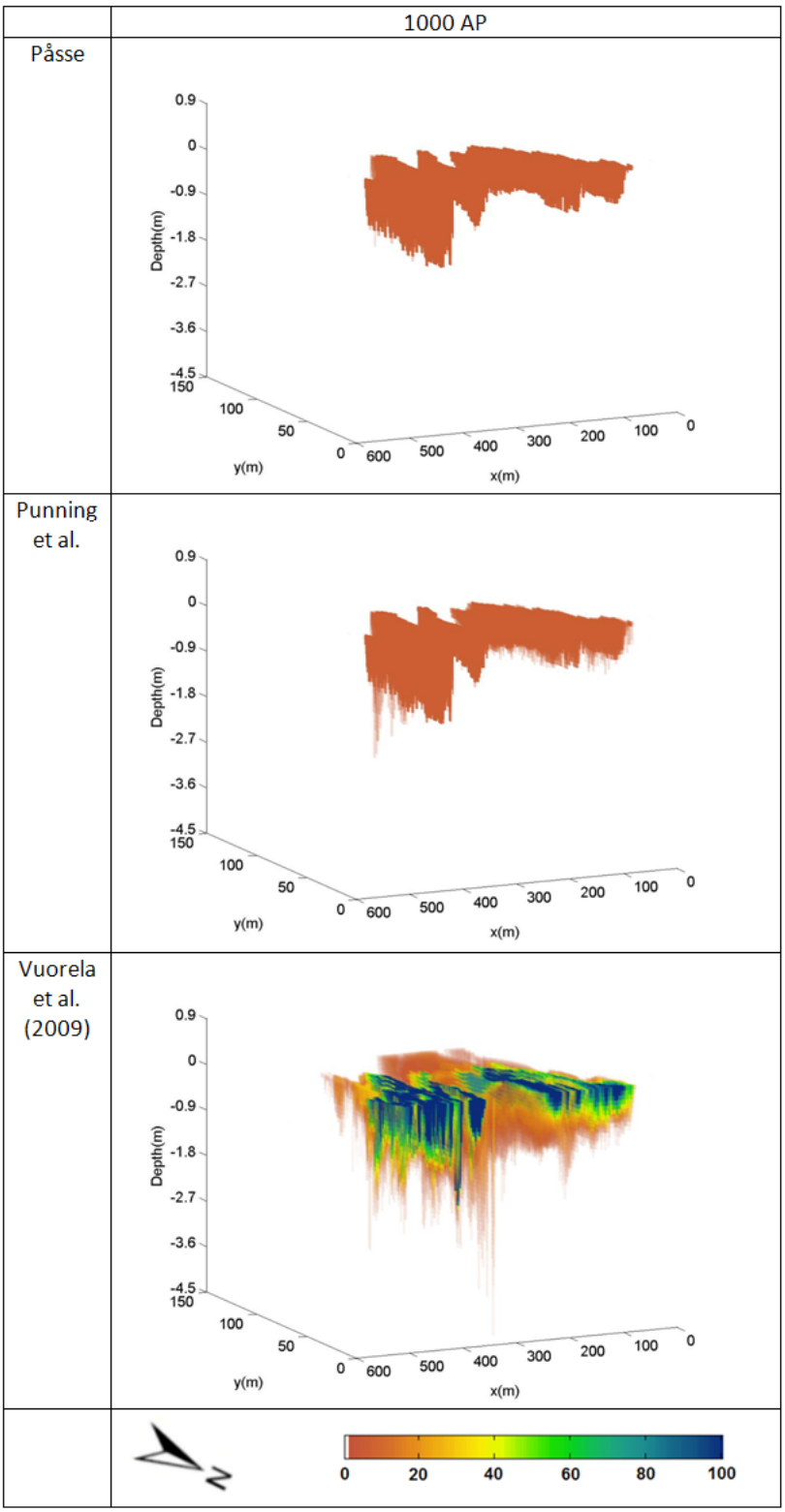

Figure 4.11: 3D surface of the formation probability of Lake 2 at 1 000 AP.

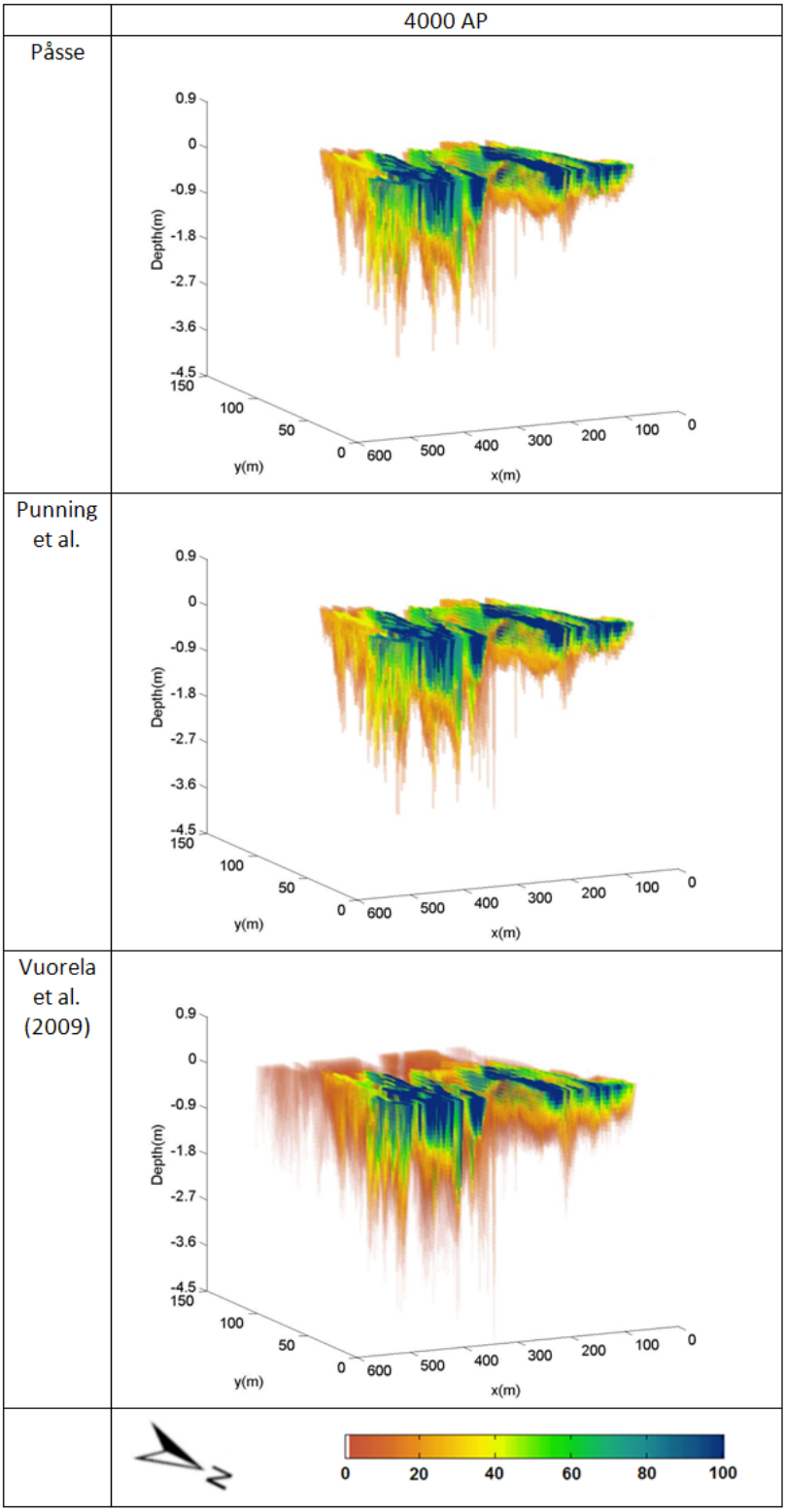

Figure 4.12: 3D surface of the formation probability of Lake 2 at 4 000 AP.

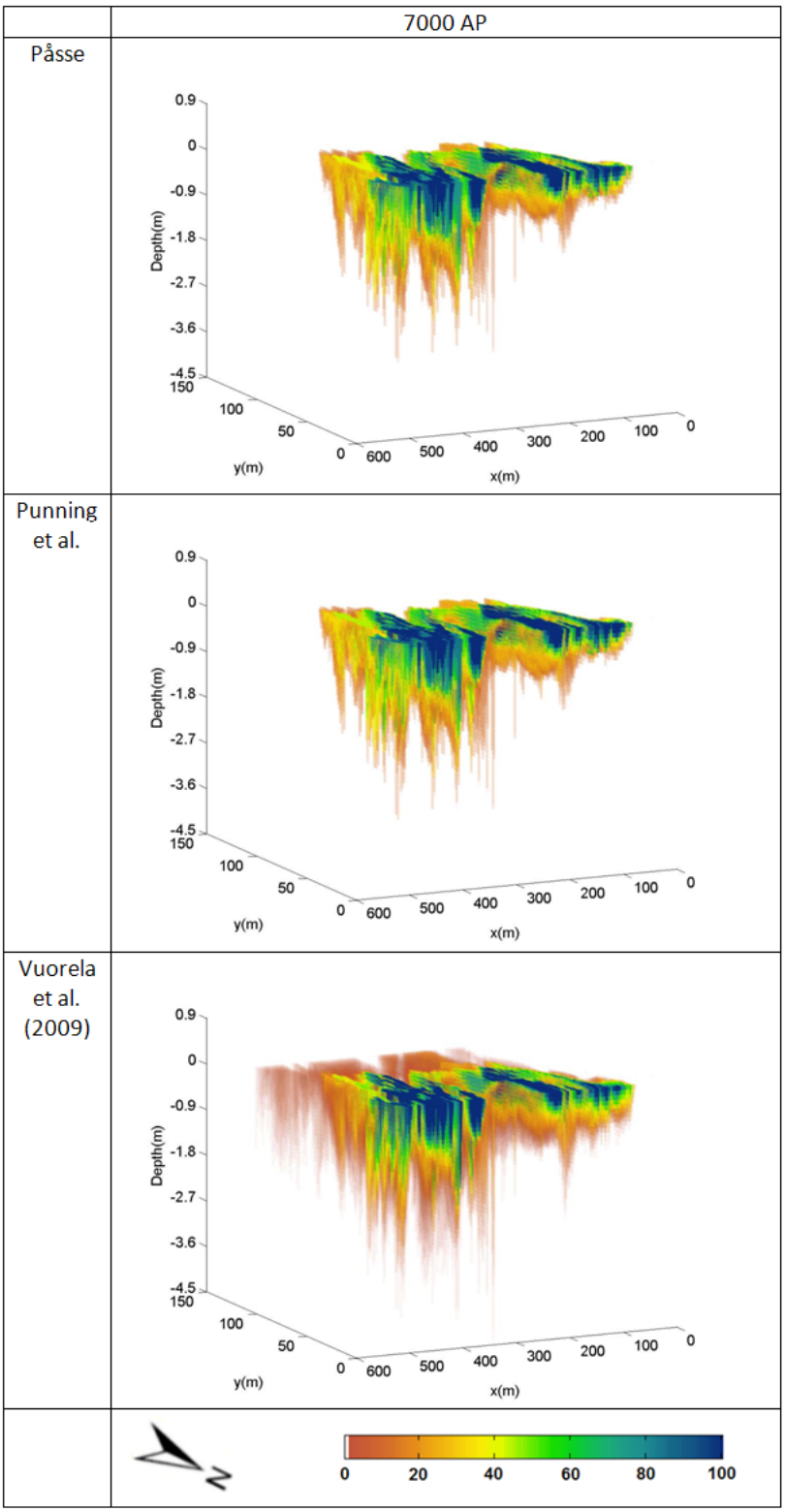

Figure 4.13: 3D surface of the formation probability of Lake 2 at 7 000 AP.

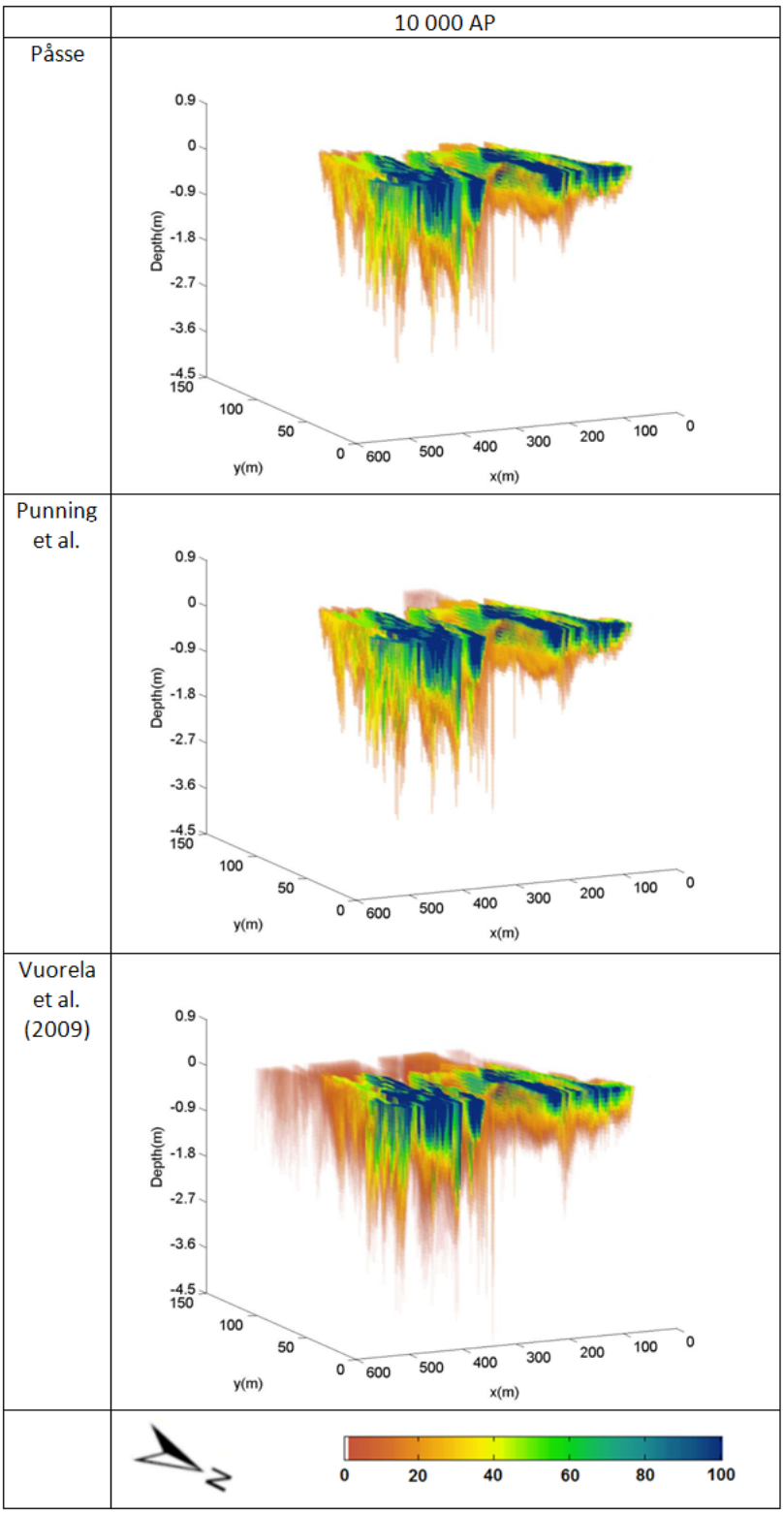

Figure 4.14: 3D surface of the formation probability of Lake 2 at 10 000 AP.

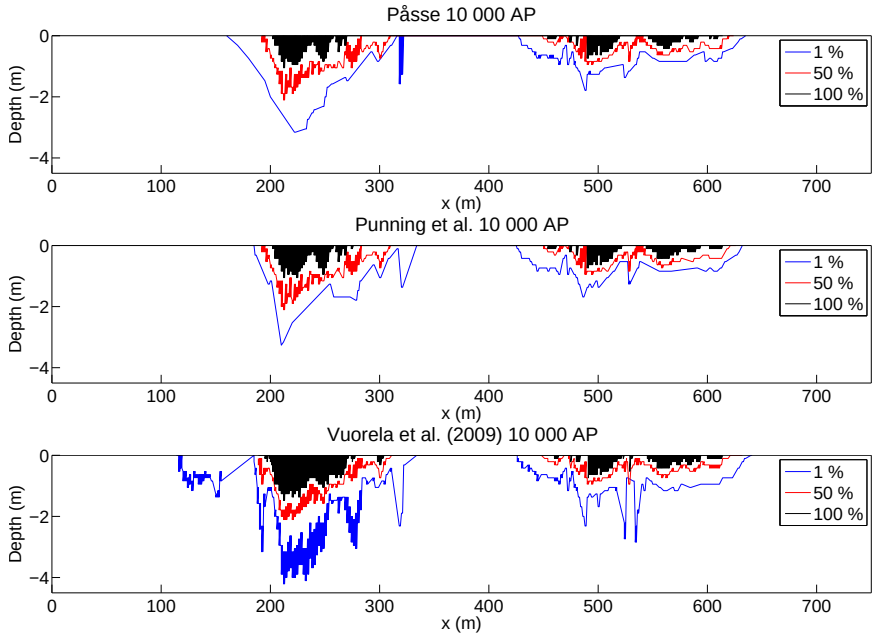

Figure 4.15: The formation probability of Lake 2 at 10 000 AP.

100 % along the vertical lines corresponding to a particular time instant. It can be seen from the figures that the lakes start to form at about 2 000 . . . 3 000 AP as there is a sudden step in predicted lake volumes at this time period. Especially in the case of lakes 2. . .4 the model version by Vuorela et al. (2009) predicts earlier lake formation compared to the two probabilistic model versions. A general observation from Figures 4.20. . .4.23 is that while the two probabilistic land uplift model versions yield quite similar and consistent lake volume development estimates with clear probability peaks at certain values, the Vuorela et al. (2009)'s model yields a more disorganized picture. For Lake 2, for example, Vuorela et al. (2009)'s model predicts – with some small probability – much higher lake volumes than the other two model versions. This might be partly due to the fact that in (Vuorela et al., 2009)'s model only the DEM is probabilistic and therefore the probability is distributed more evenly along the lake volume scale. The probabilistic land uplift component in the other two models may be responsible for the discriminative effect in the lake volume distribution. In the development of Lake 1, for example, two clearly different scenarios with almost equally high probability can be observed.

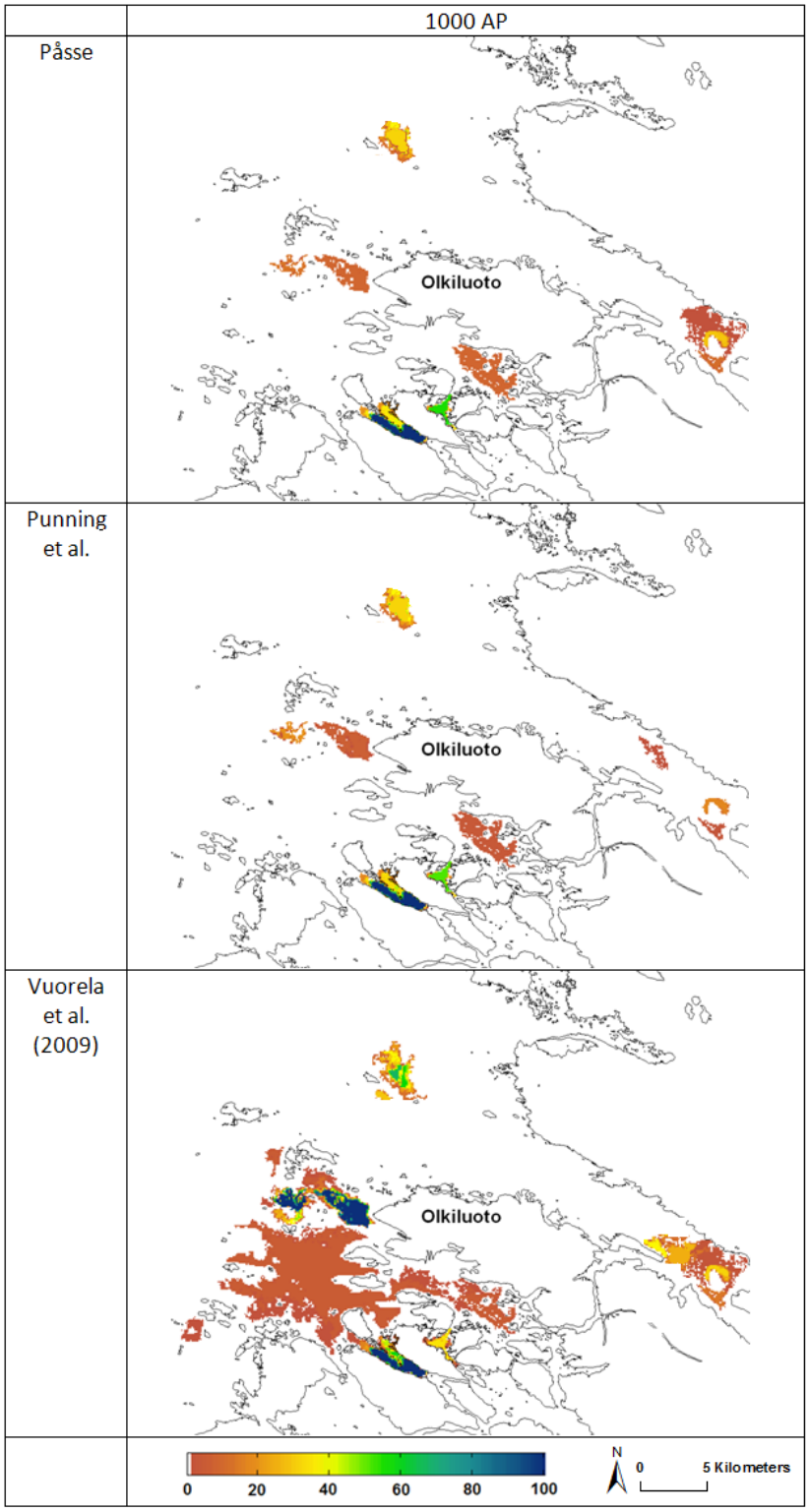

Figure 4.16: The probability of lake surface area at 1 000 AP.

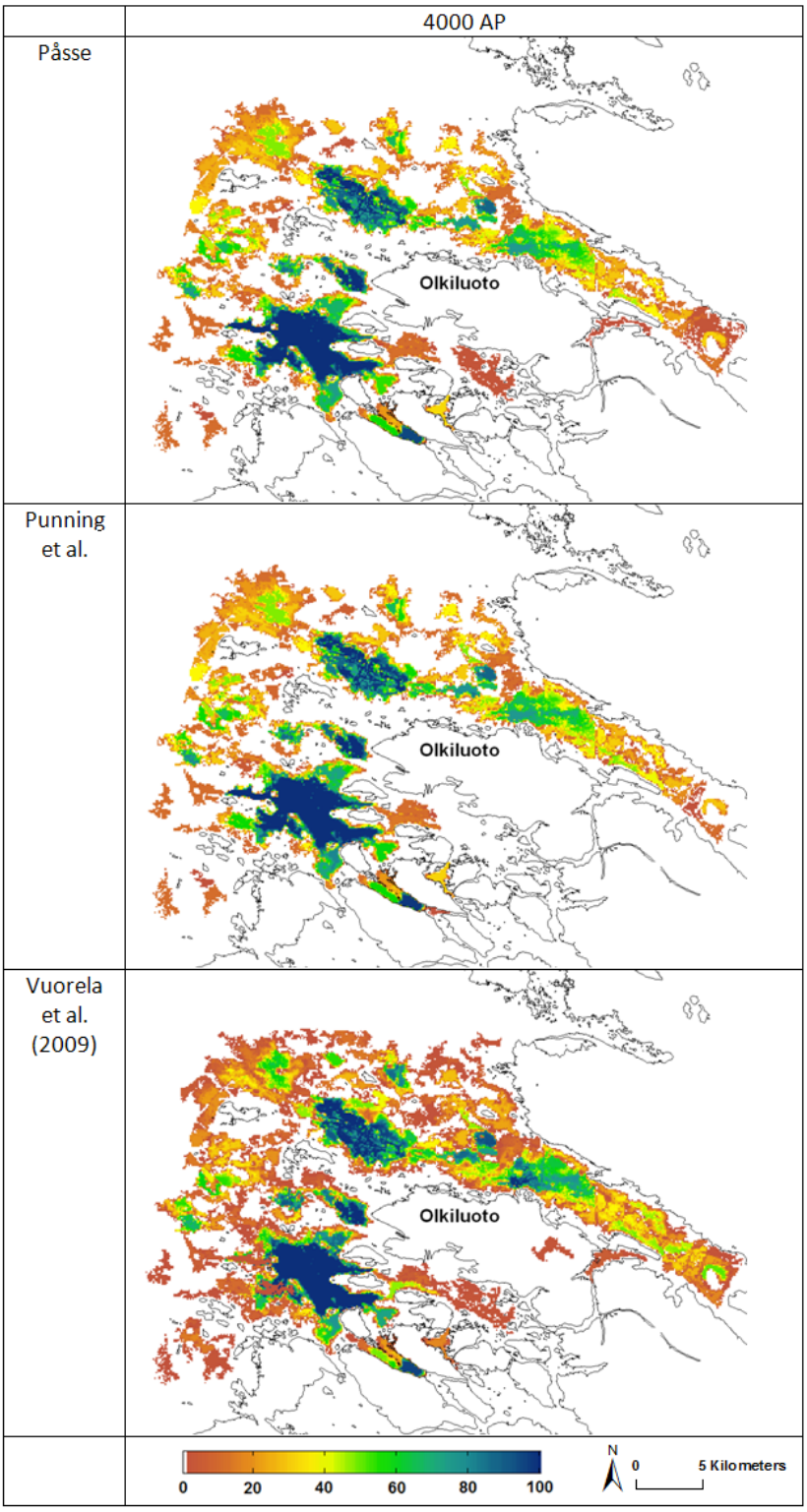

Figure 4.17: The probability of lake surface area at 4 000 AP.

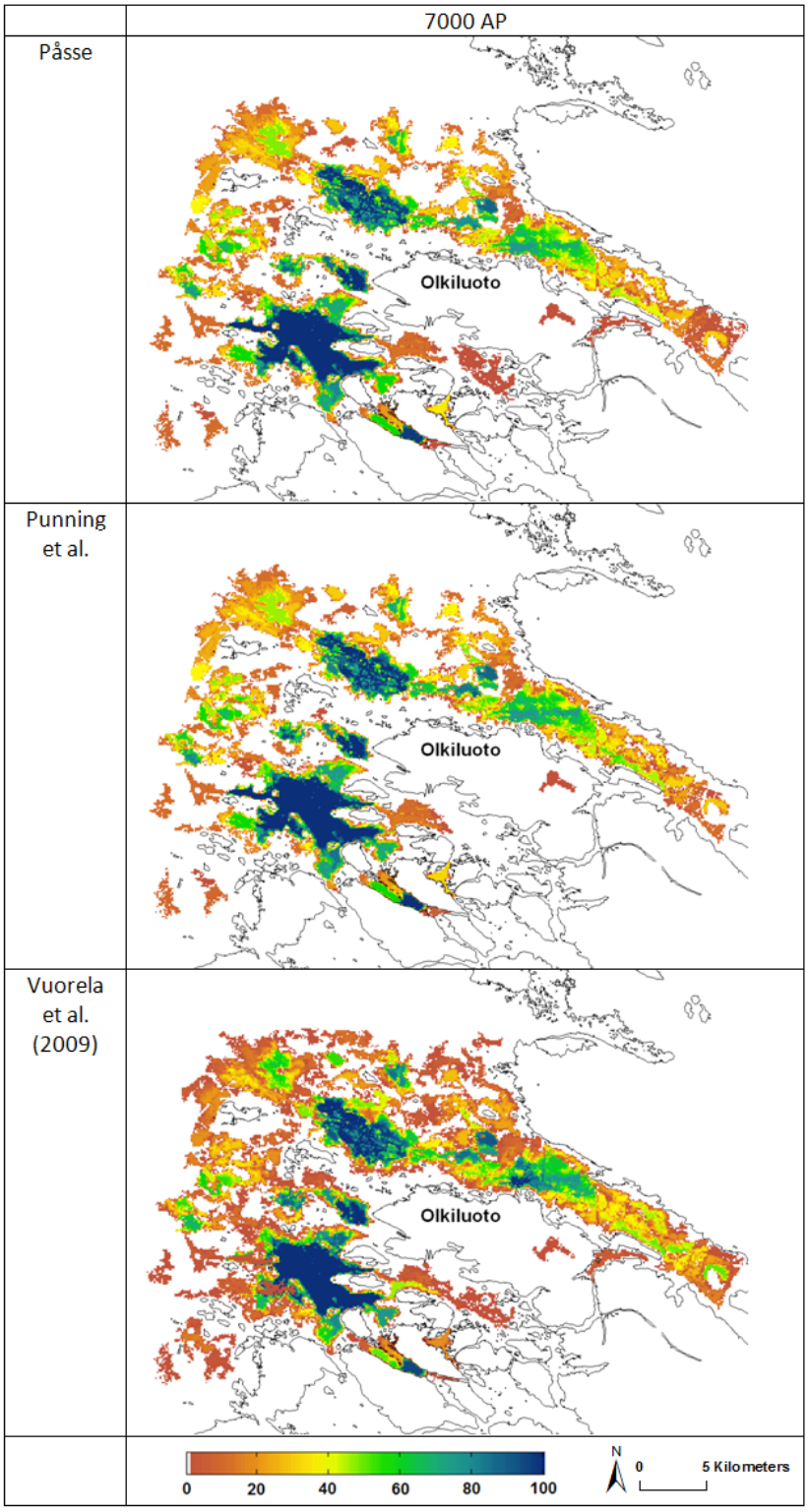

Figure 4.18: The probability of lake surface area at 7 000 AP.

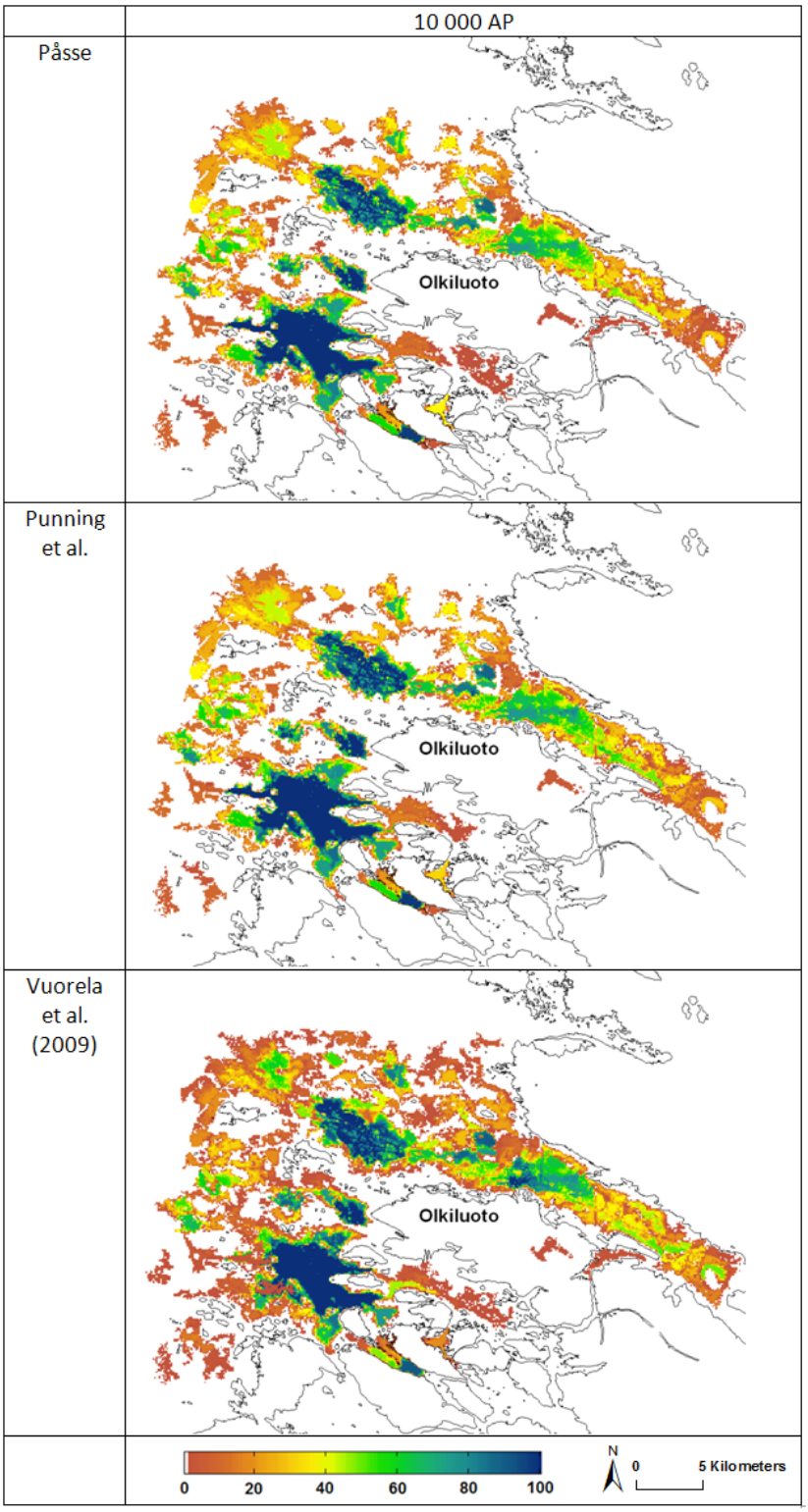

Figure 4.19: The probability of lake surface area at 10 000 AP.

Table 4.1: Projected areal estimates for Lake 1 (10^3 m^2).

		1 000 AP	4 000 AP	7 000 AP	10 000 AP
Påsse	Min	0	2 585	2 575	2 570
	Max	761	6 260	6 493	6 717
	Med	281	4 603	4 665	4 754
	Std dev	194	968	999	1 012
Punning	Min	0 (0.0 %)	2 614 (1.1 %)	2 614 (1.5 %)	2 624 (2.1 %)
	Max	758 (−0.4 %)	6 318 (0.9 %)	6 604 (1.7 %)	7 024 (4.6 %)
	Med	281 (0.0 %)	4 698 (2.1 %)	4 799 (2.9 %)	4 930 (3.7 %)
	Std dev	182 (−6.2 %)	985 (1.8 %)	1 027 (2.8 %)	1 047 (3.5 %)
Vuorela et al. (2009)	Min	0 (0.0 %)	2 374 (−8.1 %)	2 527 (−1.9 %)	2 565(-0.2%)
	Max	6 598 (767.0 %)	6 823 (9.0 %)	6 959 (7.2 %)	7 089 (5.5 %)
	Med	282 (0.4 %)	4 244 (−7.8 %)	4 305 (−7.7 %)	4 386 (−7.7 %)
	Std dev	1 141 (488.1 %)	988 (2.1 %)	1 000 (0.1 %)	1 024 (1.1 %)

Table 4.2: Projected areal estimates for Lake 2 (10^3 m^2).

		1 000 AP	4 000 AP	7 000 AP	10 000 AP
Påsse	Min	0	349	347	347
	Max	522	1 102	1 146	1 175
	Med	0	514	510	506
	Std dev	121	159	156	163
Punning	Min	0 (0.0 %)	362 (3.7 %)	359 (3.5 %)	351 (1.2 %)
	Max	544 (4.2 %)	1 118 (1.5 %)	1 169 (2.0 %)	1 204 (2.5 %)
	Med	0 (0.0 %)	517 (0.6 %)	513 (0.6 %)	512 (1.2 %)
	Std dev	114 (−5.8 %)	167 (5.0 %)	198 (26.9 %)	195 (19.6 %)
Vuorela et al. (2009)	Min	0 (0.0 %)	282 (−19.2 %)	286 (−17.6 %)	290 (−16.4 %)
	Max	1 316 (152.1 %)	1 830 (66.1 %)	1 857 (62.0 %)	1 828 (55.6 %)
	Med	0 (0.0 %)	514 (0.0 %)	514 (0.8 %)	514 (1.6 %)
	Std dev	325 (168.6 %)	280 (76.1 %)	282 (80.8 %)	279 (71.1 %)

Table 4.3: Projected areal estimates for Lake 3 (10^3 m^2).

		1 000 AP	4 000 AP	7 000 AP	10 000 AP
Pårsse	Min	0	535	513	506
	Max	522	4 850	5 894	6 343
	Med	0	2 218	2 232	2 245
	Std dev	138	886	968	1 052
Punning	Min	0 (0.0 %)	527 (−1.5 %)	512 (−0.2 %)	503 (−0.6 %)
	Max	544 (4.2 %)	5 155 (6.3 %)	5 809 (−1.4 %)	6 172 (−2.7 %)
	Med	0 (0.0 %)	2 240 (1.0 %)	2 269 (1.6 %)	2 229 (−0.7 %)
	Std dev	133 (−3.6 %)	886 (0.0 %)	1 056 (9.1 %)	1 143 (8.7 %)
Vuorela et al. (2009)	Min	0 (0.0 %)	555 (3.7 %)	532 (3.7 %)	530 (4.7 %)
	Max	1 316 (152.1 %)	6 518 (34.4 %)	6 575 (11.6 %)	6 616 (4.3 %)
	Med	0 (0.0 %)	2 455 (10.7 %)	2 464 (10.4 %)	2 511 (11.8 %)
	Std dev	302 (118.8 %)	1 124 (26.9 %)	1 180 (21.9 %)	1 218 (15.8 %)

Table 4.4: Projected areal estimates for Lake 4 (10^3 m^2).

		1 000 AP	4 000 AP	7 000 AP	10 000 AP
Pårsse	Min	0	179	177	172
	Max	1 130	3 721	4 302	5 552
	Med	190	1 076	1 131	1 155
	Std dev	197	967	1 079	1 183
Punning	Min	0 (0.0 %)	177 (−1.1 %)	170 (−3.9 %)	218 (26.7 %)
	Max	507 (−55.5 %)	4 237 (13.9 %)	5 787 (34.5 %)	6 889 (24.1 %)
	Med	190 (0.0 %)	1 118 (3.9 %)	1 239 (9.5 %)	1 264 (9.4 %)
	Std dev	173 (−12.2 %)	1 053 (8.9 %)	1 265 (17.2 %)	1 366 (15.5 %)
Vuorela et al. (2009)	Min	0 (0.0 %)	250 (39.7 %)	250 (41.2 %)	177 (2.9 %)
	Max	4 911 (334.6 %)	4 967 (33.5 %)	5 120 (19.0 %)	5 197 (−6.4 %)
	Med	562 (195.8 %)	1 601 (48.8 %)	1 670 (47.7 %)	1 686 (46.0 %)
	Std dev	1 093 (454.8 %)	1 066 (10.2 %)	1 088 (0.8 %)	1 132 (−4.3 %)

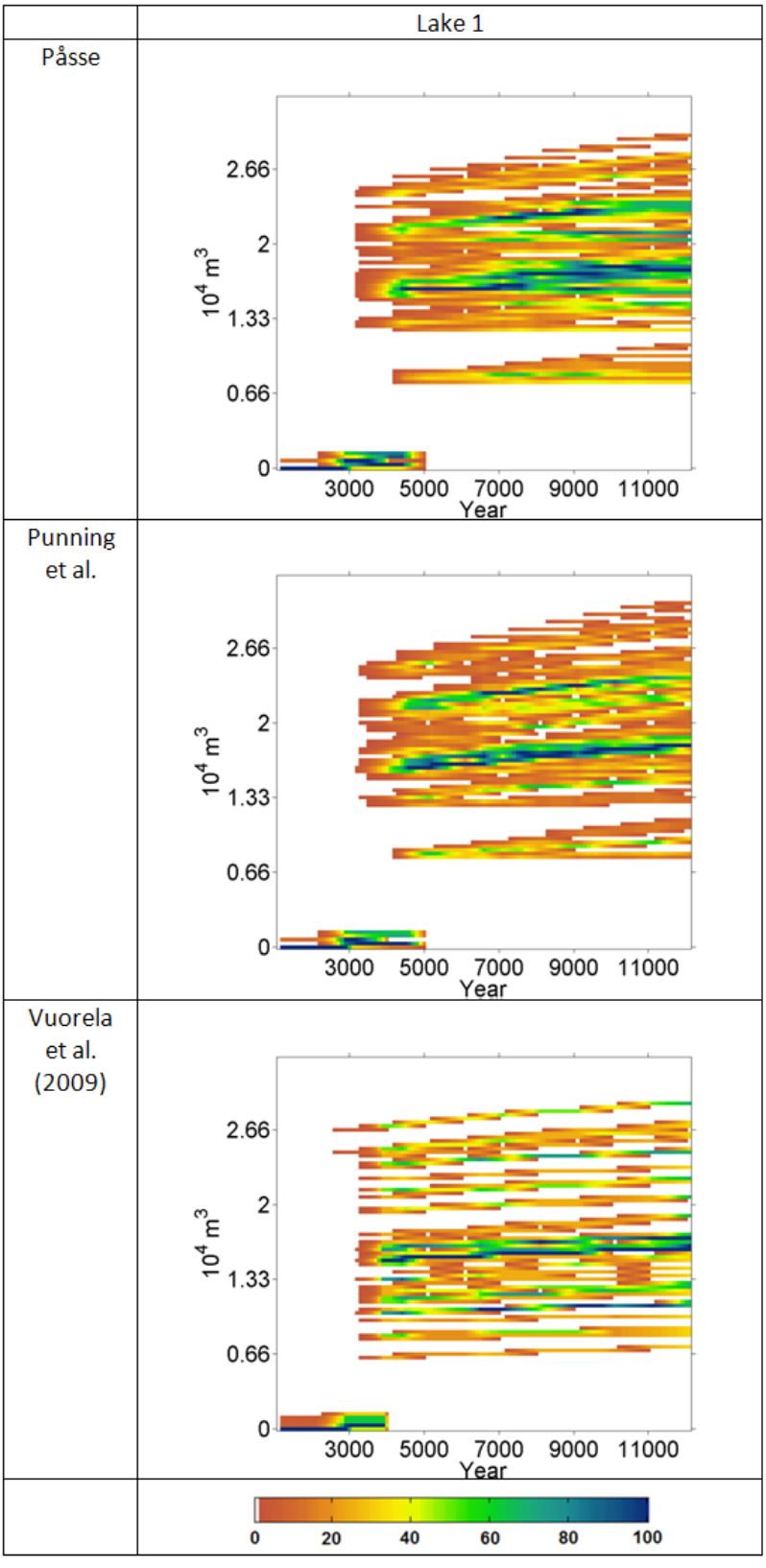

Figure 4.20: The probability of the volume of Lake 1 (% of the realizations).

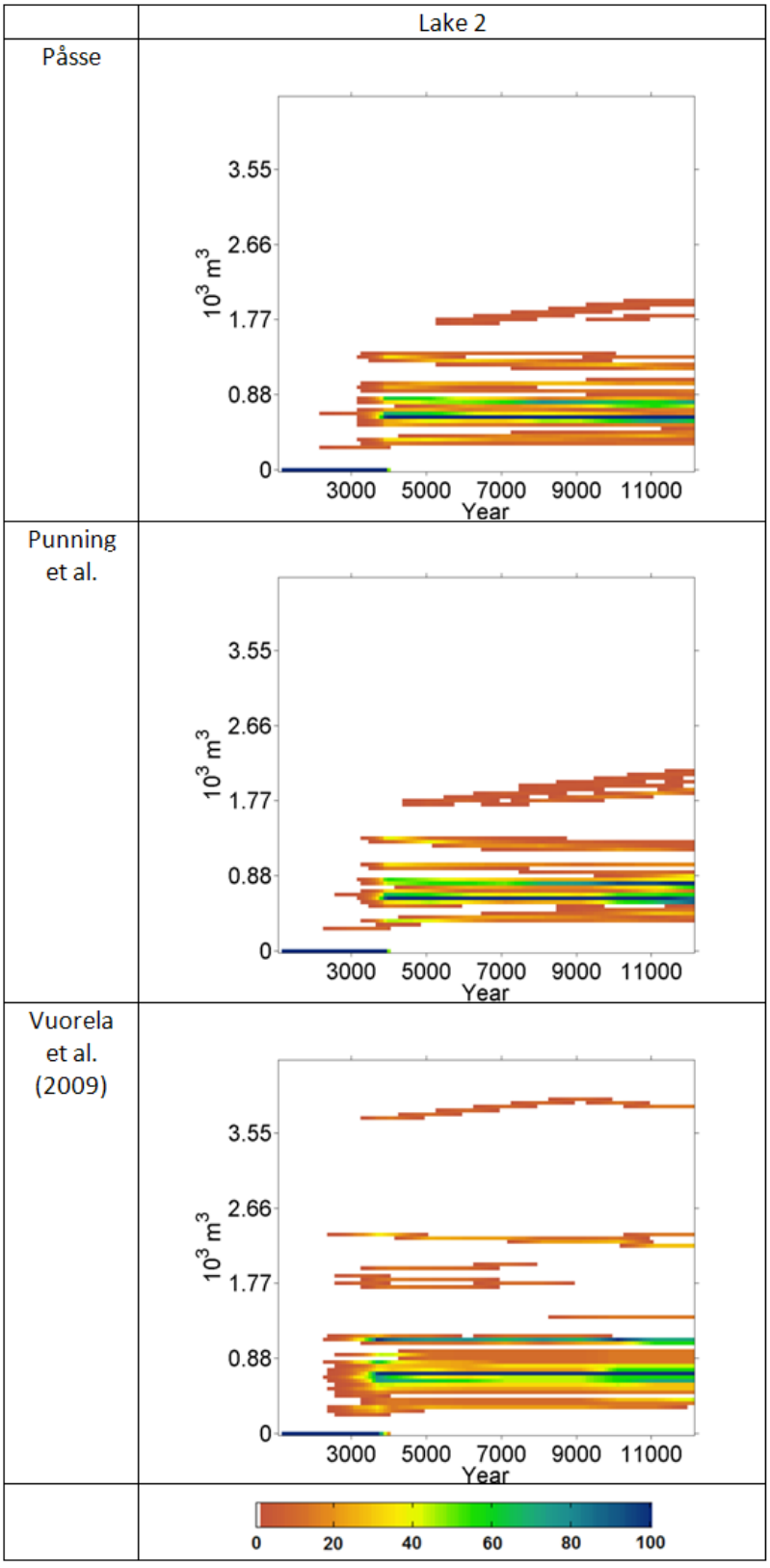

Figure 4.21: The probability of the volume of Lake 2 (% of the realizations).

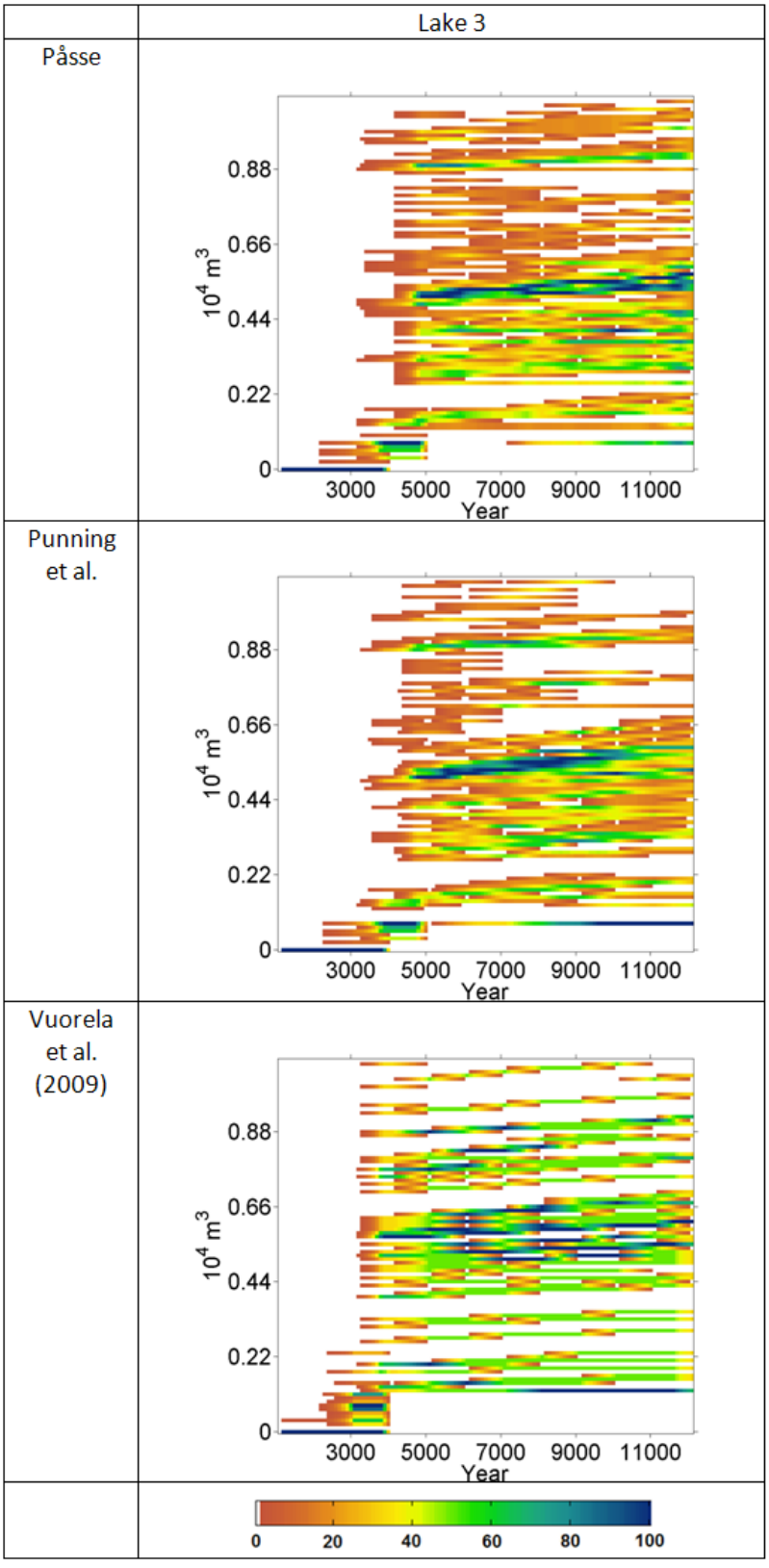

Figure 4.22: The probability of the volume of Lake 3 (% of the realizations).

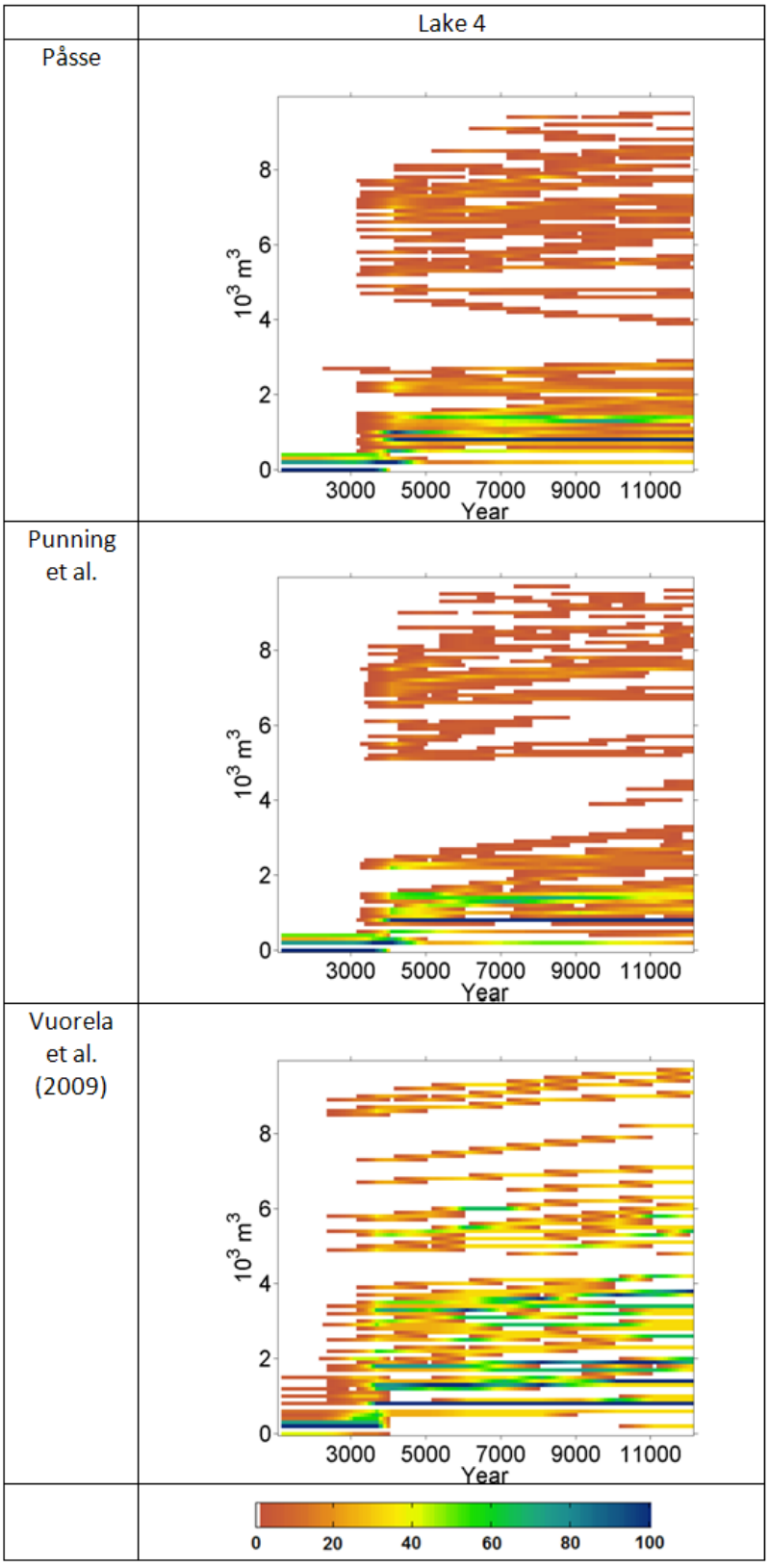

Figure 4.23: The probability of the volume of Lake 4 (% of the realizations).

Chapter 5

Discussion and conclusions

As stated in section 1.1, the Finnish Nuclear Energy Act provides a basis for this thesis. The work described here will be used as a part of the biosphere modeling effort to assess the doses and risks of radionuclides to humans in the worst case scenario, i.e., a leakage from a nuclear waste copper capsule into the groundwater. In biosphere modeling and dose assessments for the safety analysis of the deep spent nuclear fuel repository the volume of the surface water bodies regulates - together with the surface water discharge - the mixing volume encountered by the radionuclides and thus affects the degree of exposure of people and biota directly or, e.g., via drawing irrigation water. Also, in the case of direct releases to the perimeter of the lake, there is a usually clear effect to the doses whether the area is underwater or terrestrial. Overall, the geomorphic landscape dynamics plays an important role in the dose assessment of the Olkiluoto site.

The post-glacial land uplift rate in Olkiluoto is approximately 6 mm/year at the moment. The shoreline is continuously shifting westwards and the groundwater is seeking new pathways and storage basins following the geomorphic dynamics. In this thesis geomorphic landscape projections of the Olkiluoto spent nuclear fuel repository site in Finland are estimated, based on combinations of a probabilistic digital elevation model and a probabilistic land uplift model, in 10 000 years' time scope. The aim of the thesis was to assess the influence of various uncertainties in the source data and the modeling methods on the prediction results of the formation of surface water

bodies in the study area. The work contained three clearly distinguishable subtasks:

- generating probabilistic digital elevation model for the study area based on various source data
- refinement of the arctangent based land uplift model taking into account various sources of uncertainties
- simulating the future development of the geomorphic landscape in the study area with the main emphasis on surface water body formation.

For each subtask a survey of the related scientific background knowledge was performed together with a comparison of corresponding methodology to find the most suitable solution. Therefore, each subtask also contributed its own findings and conclusions. The conclusions drawn from the final subtask - simulation of the future geomorphic landscape development for three different scenarios - can be considered as the overall conclusions of the whole thesis. In the following, each of these subtasks is discussed separately.

Creating a high resolution digital elevation model based on sparse and highly irregular source data involves determination of the neighborhood and selection of the interpolation method. No methodology exists for finding a generally optimal solution as the results are highly dependent on the properties of the underlying terrain and the evaluation criteria depend on the application the DEM is created for. The following conclusions can be drawn from the work on DEM generation performed in this thesis:

1. The thin plate spline interpolation algorithm produces more realistic terrain, compared to algorithms based on calculation of the weighted sum of the neighboring source data values, at the expense of having the risk of large errors in the areas where data is missing. The relaxation parameter of the thin plate spline algorithm can be adapted according to the variability of the elevation values.
2. Selection of the interpolation neighborhood is crucial, especially when using the thin plate spline interpolation algorithm; source data values from all directions are required to avoid large errors.
3. The uncertainties of the source data values can be taken into account by assigning probability distributions to each data set and using the Monte Carlo simulation.

Development of the LiDAR technology has changed the practice of DEM generation making it easier to acquire an accurate high resolution DEM efficiently. However, interpolation based on sparse and highly irregular source data is still relevant if the seabed is considered. The elevation model of the seabed can be refined in the future as the measurement methodology develops and new data become available.

Modeling the post-glacial land uplift can be done using either geodynamical modeling or by fitting a mathematical model to the source data on past shoreline displacement. The latter approach based on the mathematical model developed by Tore Påsse was selected in this thesis for modeling the geomorphic landscape development in the Olkiluoto area. The model parameters were optimized according to the source data from lake basins and archaeological findings. Two different eustatic curves were used. The model was compared to the version presented by Vuorela et al. (2009), where the model parameters were determined based on present land uplift rate. The following conclusions can be drawn from the land uplift modeling effort:

1. Refinement of the eustatic curve did not change the land uplift model parameters (and thus the land uplift process as described by the model) significantly. On the other hand, significantly higher download factor and lower inertia factor were obtained, if the model parameters were optimized according to the present uplift rate only (the Vuorela et al. (2009) model).
2. The mathematical land uplift model proposed by Tore Påsse has the serious drawback of not being specific with respect to the model parameters, i.e., the error surface indicating the optimization error is fairly flat. Constraining the parameters according to geodynamical reference data (the Moho map, the timing of the ice recession process, etc.) helps to better confine the parameter values.
3. In the future, geodynamical modeling combined with source data extrapolation would be a promising approach in local geomorphic landscape development modeling tasks.

Land uplift modeling, similarly to the DEM modeling, was performed in a probabilistic manner to take into account the various uncertainties in the source data.

There is an ongoing debate on the validity of land uplift modeling based on fitting

a mathematical function to source data on past shoreline displacement. For example, Lambeck (2006) argues that this kind of modeling does not lead to better understanding of the actual physical process underlying the uplift of the Earth's crust but is rather a computational exercise. On the other hand, geodynamical modeling has not yet the required spatial resolution and complexity to be used for this kind of a task. Combining the two might be the solution to be considered in the future.

Geomorphic landscape development and surface water body formation was simulated for three scenarios: two scenarios involving model parameter optimization based on source data on past shoreline displacement differed from each other by the eustatic curve used in the parameter optimization procedure; the third scenario followed the model proposed by Vuorela et al. (2009). In this subtask the results of the DEM modeling and land uplift modeling efforts were employed, therefore, these results can be considered as overall results for the whole thesis. The main conclusions can be listed as:

1. Optimizing the land uplift model parameters based on current uplift rate (the Vuorela et al. (2009) model) overestimates the speed of the land uplift process. This model also gives more definite location of the future shoreline (sharper transition from water (blue) to land (red) in Figure 4.9). The reduced uncertainty does not take into account the uncertainties in land uplift modeling and is therefore less realistic compared to the scenarios where the land uplift model parameters were optimized based on the source data in a probabilistic manner.
2. All three scenarios predict four main lakes in the vicinity of the Olkiluoto Island to be isolated from the Baltic Sea most probably between 1 000 to 2 000 years from now. In some less probable projections the lakes 1 and 2 (see Figure 4.10) will eventually be connected while in other projections Lake 1 will be split into several smaller lakes. The Vuorela et al. (2009) scenario predicts faster isolation and more rapid spread of the lakes, however, after about 4 000 years AP the most probable realization of the lakes' volume is not necessarily larger for this scenario compared to the two other scenarios.
3. The simulation results clearly converge to one or two probable tracks of lake volume projections into the future indicating robustness of geomorphic landscape

development modeling (convergence is not so clear in the case of the Vuorela et al. (2009) model scenario though). The results also point out some quite different but highly improbable development tracks, which would be relevant to consider in the further safety analysis for the spent nuclear fuel repository site.

Perhaps the most critical open question when modeling surface water body formation is the effect of the sedimentation and erosion processes. The four lakes predicted and modeled in this thesis form part of the Eurajoki and Lapijoki river systems. Eurajoki and Lapijoki rivers flow through agricultural areas carrying mineral and agricultural sediments all the time. According to Posiva Oy (2014), average discharges in Eurajoki and Lapijoki rivers are 8.3 m^3/s and 3.3 m^3/s, respectively, and average suspended sediment loads are 6.81 x 10^6 kg/year and 1.28 x 10^6 kg/year dry matter, respectively. Lakes 1 and 2 will be part of the future Lapijoki river and lakes 3 and 4 will be a part of the Eurajoki river system. Although the discharge in Eurajoki river is 2.5-fold when compared to Lapijoki river, the sediment load is over 5-fold.

Although the sedimentation and erosion processes were not in the scope of this thesis, some assumptions can be made according to (Posiva Oy, 2014). In (Posiva Oy, 2014) the sedimentation model created by Brydsten (2004, 2006) and later adjusted for the Olkiluoto site has been considered. According to the model a lake is first assumed to be filled up to a fraction of 4 % of the initial volume by silty sand. After this, the sedimentation process continues with fine-grained sediments until about 18 % of the remaining volume of the lake is filled up. For modeling further sedimentation a site-specific rate of fine-grained sedimentation evaluated, for example, based on empirical studies, is needed.

In the case of the four lakes discussed in this thesis, it can be assumed that the volumes of the lakes will decrease in time due to sedimentation but the overall rate is dependent on various additional factors such as reed bed growth, peat accumulation and water flow. Common reed will occupy the newborn lake shores almost immediately, depending on the growing conditions such as water depth and wind. The peat accumulation will follow after the dead reeds start to decompose. Peat accumulation in swamp areas is 0.5 mm/year (tolerance $0.2 - 4.0$ mm/year), according to (Turveteollisuusliitto, 2014). Sedimentation together with the reed growth form an iterative

cycle. Sedimentation lowers the depth of the lakes, the common reed settles down in new areas and also slows down the water speed causing increasing sedimentation in the area. Eventually, the formed lake will find an equilibrium where the water flow, peat accumulation and sedimentation rates are in balance. Alternatively, the lake may be totally filled up.

Erosion of the studied lakes can be estimated by taking into consideration the dominant soil type in the area. When comparing the lake positions in Figure 4.10 with the soil type map in Figure 1.2, it can be noticed that three of the four estimated lakes (1, 3 and 4) will be formed in 'Gyttja mud' or 'Litorina clay' areas. The only exception is lake 2, which will be formed in 'Compact till' area. It can be assumed that the threshold levels of lakes 1, 3 and 4 will erode more rapidly than in lake 2 causing a slower reduction in volume in lakes 1, 3 and 4.

Global sea level development is an important topic when assessing the land uplift in the future. In this thesis a mild increase in the sea level after the present day has been included in the eustatic models (Figure 3.7). In majority of the future sea level estimates, for example in (Meehl and Stocker, 2007), it is predicted that the sea level is rising slightly in the future. The future development of the sea level at the Olkiluoto site has been discussed in (Posiva Oy, 2014). In (Posiva Oy, 2014) two kinds of climate simulations are considered. According to moderate scenarios the sea level will rise up to about half a meter in the next 500 years, after which it starts to gradually decrease. According to these scenarios the sea level near the Olkiuluoto island will be 2.8 . . . 6.3 meters lower at 10 020 years AP compared to the present level. In addition, a less probable scenario is considered according to which the sea level rises nearly 4.5 meters in the next 500 years and then starts gradually decreasing, being at 2.2 meters above the current level by 10 020 AP. These assessments indicate that the future development of the sea level is difficult to take into account and that even very improbable scenarios would not predict long-term dramatic sea level rise. If the above mentioned less probable scenario for the sea level rise would be taken into notice in this thesis, the geomorphic landscape evolvement process would be slower as the sea level rise would counteract the effect of the land uplift.

Despite the above mentioned open questions the work presented in this thesis

shows that the proposed and developed methods for future geomorphic landscape development are feasible and produce useful results. The presented geomorphic landscape development model and its components are currently used by Posiva Oy for simulating also other aspects (besides surface water body formation) of biosphere development in the Olkiluoto area.

Bibliography

Ågren, J. and Svensson, R. (2007). System Definition and Postglacial Land Uplift Model for the New Swedish Height System RH 2000. LMV-Rapport 2007:4, Lantmäteriet, Gävle.

Airborne Hydrography AB (2014). HawkEye II. "http://www.airbornehydro.com/hawkeyeii".

Anderson, E. and Libby, W. F. (1951). World-wide distribution of natural radiocarbon. *Physical Review*, 81(1):64–69.

Anderson, E. C., Libby, W. F., Weinhouse, S., Reid, A. F., Kirshenbaum, A. D., and Grosse, A. V. (1947). Radiocarbon From Cosmic Radiation. *Science (New York, N.Y.)*, 105:576–7.

Ansorge, J., Blundell, D., and Mueller, S. (1992). Europe's lithosphere - seismic structure. In Blundell, D., Freeman, R., and Mueller, S., editors, *A continent revealed. The European Geotraverse*, pages 33–69. Cambridge University Press, Cambridge.

Artemieva, I. and Thybo, H. (2008). Deep Norden: highlights of the lithospheric structure of Northern Europe, Iceland, and Greenland. *Episodes*, 31(1):98–106.

Babuška, V., Plomerova, J., and Pajdušák, P. (1988). Seismologically determined deep lithosphere structure in Fennoscandia. *GFF*, 110:380–382.

Bard, E., Hamelin, B., Arnold, M., Montaggioni, L., Cabioch, G., Faure, G., and Rougerie, F. (1996). Deglacial sea-level record from Tahiti corals and the timing of global meltwater discharge. *Nature*, 382:241–244.

Björck, S. (1995). A review of the history of the Baltic Sea, 13.0-8.0 ka BP. *Quaternary International*, 27:19–40.

Björck, S. (2008). *The late quaternary development of the Baltic Sea Basin*, chapter A.2, pages 398–407. Springer-Verlag, Berlin-Heidelberg.

Björck, S. and Digerfeldt, G. (1991). Allerød-Younger Dryas sea level changes in southwestern Sweden and their relation to the Baltic Ice Lake development. *Boreas*, 20:115–133.

Bronk Ramsey, C. (2008). Radiocarbon dating: revolutions in understanding. *Archaeometry*, 50(2):249–275.

Bronk Ramsey, C. (2009). Bayesian analysis of radiocarbon dates. *Radiocarbon*, 51(1):337–360.

Brook, E., Nesje, A., and Lehman, S. (1996). Cosmogenic nuclide exposure ages along a vertical transect in western Norway: Implications for the height of the Fennoscandian ice sheet. *Geology*, 24(3):207–210.

Brydsten, L. (2004). A mathematical model for llake ontogeny in terms of filling with sediments and macrophyte vegetation. Technical Report TR-04-09, Swedish Nuclear Fuel and Waste Management Co, Stockholm.

Brydsten, L. (2006). A model for landscape development in terms of shoreline displacement, sediment dynamics, lake formation, and lake choke-up processes. Technical Report TR-06-40, Swedish Nuclear Fuel and Waste Management Co, Stockholm.

Brydsten, L., Engqvist, A., Näslund, J.-O., and Lindborg, T. (2009). Expected extreme sea levels at Forsmark and Laxemar-Simpevarp up until year 2100. Technical Report TR-09-21, Swedish Nuclear Fuel and Waste Management Co, Stockholm.

Calcagnile, G. (1982). The lithosphere-astenosphere system in Fennoscandia. *Tectonophysics*, 90:19–35.

Chappell, J. and Polach, H. (1991). Post-glacial sea-level rise from a coral record at Huon Peninsula, Papua New Guinea. *Nature*, 349:147–149.

Conrad, C. and Lithgow-Bertelloni, C. (2006). Influence of continental roots and asthenosphere on plate-mantle coupling. *Geophysical Research Letters*, 33.

Cressie, N. A. C. (1993). *Statistics for Spatial Data*. John Wiley & Sons, Ltd.

de Berg, M., Cheong, O., van Kreveld, M., and Overmars, M. (2008). *Computational Geometry: Algorithms and Applications*. Springer-Verlag, Berlin.

de Smith, M. J., Goodchild, M. F., and Longley, P. A. (2007). *Geospatial Analysis - A comprehensive guide*. Matador, Leicester, 2nd edition.

Delaunay, B. (1934). Sur la sphère vide. A la mémoire de Georges Voronoï. *Bulletin of Academy of Sciences of the USSR*, 6:793–800.

Donato, G. and Belongie, S. (2002). Approximate Thin Plate Spline Mappings. In Heyden, A., Sparr, G., Nielsen, M., and Johansen, P., editors, *Lecture Notes in Computer Science*, volume 2352, pages 21–31. Springer, Berlin.

Duchon, J. (1977). Splines minimizing rotation invariant seminorms in sobolev spaces, constructive theory of functions of several variables. *Lecture Notes in Mathematics*, 571:85–100.

Eronen, M., Glückert, G., Hatakka, L., van de Plassche, O., van der Plicht, J., and Rantala, P. (2001). Rates of Holocene isostatic uplift and relative sea-level lowering of the Baltic in SW Finland based on studies of isolation contacts. *Boreas*, 30(1):17–30.

Eronen, M., Gunnar, G., van de Plassche, O., van der Plicht, J., and Rantala, P. (1995). Land uplift in the Olkiluoto-Pyhäjärvi area, Southwestern Finland, during the last 8000 years. Report YJT-95-17, Nuclear Waste Commission of Finnish Power Companies, Olkiluoto.

Fairbanks, R. G. (1989). A 17,000-year glacio-eustatic sea level record: influence of glacial melting rates on the Younger Dryas event and deep-ocean circulation. *Nature*, 342:637–642.

Foley, J. A., Prentice, I. C., Ramankutty, N., Levis, S., Pollard, D., Sitch, S., and Haxeltine, A. (1996). An integrated biosphere model of land surface processes, terrestrial carbon balance, and vegetation dynamics. *Global Biogeochemical Cycles*, 10(4):603–628.

Franck, S. and Bounama, C. (2006). Causes and timing of future biosphere extinctions. *Biogeosciences*, 3:85–92.

Friend, A. D., Stevens, A. K., Knox, R. G., and Cannell, M. G. R. (1997). A process-based, terrestrial biosphere model of ecosystem dynamics (Hybrid v3.0). *Ecological Modelling*, 95(2-3):249–287.

Geological Survey of Sweden (2013). Kartgenerator. "`http://maps2.sgu.se/kartgenerator/sv/maporder.html`".

Gerya, T. (2010). *Introduction to Numerical Geodynamic Modelling*. Cambridge University Press.

Gibbard, P. and Van Kolfschoten, T. (2004). The pleistocene and holocene epochs. In Gradstein, F. M., Ogg, J. G., and Smith, A. G., editors, *A Geologic Time Scale 2004*, pages 441–452. Cambridge University Press.

Godwin, H. (1962). Half-life of radiocarbon. *Nature*, 195:984.

Gosse, J. C. and Phillips, F. M. (2001). Terrestrial in situ cosmogenic nuclides: theory and application. *Quaternary Science Reviews*, 20(14):1475–1560.

Grad, M. and Tiira, T. (2009). The Moho depth map of the European Plate. *Geophysical Journal International*, 176(1):279–292.

Hays, J., Imbrie, J., and Shackleton, N. (1976). Variations in the Earth's orbit: Pacemaker of the ice ages. *Science*, 194(4270):1121–1132.

Helle, S. K., Anundsen, K., Solveig, A., and Haflidason, H. (1997). Indications of a Younger Dryas marine transgression in inner Hardanger, West Norway. *Norsk Geologisk Tidskrift*, 77:101–117.

Holdridge, L. R. (1947). Determination of world plant formations from simple climatic data. *Science*, 105(2727):367–368.

IAEA (2001). An International Peer Review of the Biosphere Modelling Programme of the US Department of Energy's Yucca Mountain Site. Report of the IAEA International Review Team 5, IAEA.

IAEA (2003). "Reference Biospheres" for solid radioactive waste disposal. Report IAEA-BIOMASS-6, IAEA.

IAEA (2011). *Disposal of Radioactive Waste: Specific Safety Requirements*. International Atomic Energy Agency, Vienna.

Ikonen, A. T. K., Aro, L., Haapanen, R., Helin, J., Hjerpe, T., Kirkkala, T., Koivunen, S., Lahdenperä, A.-M., Puhakka, L., and Salo, T. (2010). Site and Regional Data for Biosphere Assessment BSA-2009 Supplement to Olkiluoto Biosphere Description 2009. Working Report 2010-36, Posiva Oy, Olkiluoto.

Inhofe, J. M. (2006). Yucca Mountain: The Most Studied Real Estate on the Planet. Report March, U.S. Senate Committee on Environment and Public Works.

Johnston, P. and Lambeck, K. (1999). Postglacial rebound and sea level contributions to changes in the geoid and the Earth's rotation axis. *Geophysical Journal International*, 136(3):537–558.

Jones, D., Schonlau, M., and Welch, W. (1998). Efficient Global Optimization of Expensive Black-Box Functions. *Journal of Global optimization*, 13:455–492.

Kaland, P. E., Krzywinski, K., and Stabell, B. (1984). Radiocarbon-dating of transitions between marine and lacustrine sediments and their relation to the development of lakes. *Boreas*, 13:243–258.

Kaufmann, G. and Lambeck, K. (2000). Mantle dynamics, postglacial rebound and the radial viscosity profile. *Physics of the Earth and Planetary Interiors*, 121(3-4):301–324.

Kaufmann, G., Wu, P., and Li, G. (2000). Glacial isostatic adjustment in Fennoscandia for a laterally heterogeneous earth. *Geophysical Journal International*, 143(1):262–273.

Keenan, T. F., Baker, I., Barr, A., Ciais, P., Davis, K., Dietze, M., Dragoni, D., Gough, C. M., Grant, R., Hollinger, D., Hufkens, K., Poulter, B., McCaughey, H., Raczka, B., Ryu, Y., Schaefer, K., Tian, H., Verbeeck, H., Zhao, M., and Richardson, A. D. (2012). Terrestrial biosphere model performance for inter-annual variability of land-atmosphere CO^2 exchange. *Global Change Biology*, 18(6):1971–1987.

Kinck, J., Husebye, E., and Larsson, F. (1993). The Moho depth distribution in Fennoscandia and the regional tectonic evolution from Archean to Permian times. *Precambrian Research*, 64:23–51.

Kneller, M. and Peteet, D. (1999). Late-Glacial to Early Holocene Climate Changes from a Central Appalachian Pollen and Macrofossil Record. *Quaternary Research*, 51(2):133–147.

Köhler, P., Knorr, G., Buiron, D., Lourantou, A., and Chappellaz, J. (2011). Abrupt rise in atmospheric $^{14}CO^2$ at the onset of the Bølling/Allerød: in-situ ice core data versus true atmospheric signals. *Climate of the Past*, 7(2):473–486.

Korhonen, K., Kuivamäki, A., Paananen, M., and Paulamäki, S. (2005). Lineament interpretation of the Olkiluoto area. Working Report 2005-34, Posiva Oy, Olkiluoto.

Kowalczyk, E. A., Wang, Y. P., Law, R. M., Davies, H. L., Mcgregor, J. L., and Abramowitz, G. (2006). The CSIRO Atmosphere Biosphere Land Exchange (CABLE) model for use in climate models and as an offline model. Technical Report November, CSIRO.

Krapp, M. and Jungclaus, J. H. (2011). The Middle Miocene climate as modelled in an atmosphere-ocean-biosphere model. *Climate of the Past*, 7(4):1169–1188.

Krzywinski, K. and Stabell, B. (1984). Late Weichselian sea level changes at Sotra, Hordaland, western Norway. *Boreas*, 13:159–202.

Kukkonen, I. and Peltonen, P. (1999). Xenolith-controlled geotherm for the central Fennoscandian Shield: implications for lithosphere-asthenosphere relations. *Tectonophysics*, 304(4):301–315.

Lambeck, K. (1995). Constraints on the Late Weichselian ice sheet over the Barents Sea from observations of raised shorelines. *Quaternary Science Reviews*, 14:1–16.

Lambeck, K. (1996). Limits on the areal extent of the Barents Sea ice sheet in Late Weichselian time. *Global and Planetary Change*, 12(1-4):41–51.

Lambeck, K. (1998). Sea-level change, glacial rebound and mantle viscosity for northern Europe. *Geophysical Journal International*, 134:102–144.

Lambeck, K. (2006). Hyperbolic tangents are no substitute for simple classic physics. *GFF*, 128:349–350.

Lambeck, K., Purcell, A., Johnston, P., Nakada, M., and Yokoyama, Y. (2003). Water-load definition in the glacio-hydro-isostatic sea-level equation. *Quaternary Science Reviews*, 22(2-4):309–318.

Lambeck, K., Smither, C., and Ekman, M. (1998). Tests of glacial rebound models for Fennoscandinavia based on instrumented sea- and lake-level records. *Geophysical Journal International*, 135(2):375–387.

Lambeck, K., Yokoyama, Y., and Purcell, T. (2002). Into and out of the Last Glacial Maximum: sea-level change during Oxygen Isotope Stages 3 and 2. *Quaternary Science Reviews*, 21(1-3):343–360.

Lehtimäki, T. (2003). Supplementary Interpretation of Seismic Refraction Data at Olkiluoto. Working Report 2003-63, Posiva Oy, Olkiluoto.

Leino, J. (2001). Maatutkaluotaukset Eurajoen Olkiluodon Olkiluodonjärven tutkimusalueella 2001. Working Report 2001-27, Posiva Oy, Olkiluoto.

LeMay, N. E. (1995). *Variogram Modeling and Estimation.* M.sc thesis, University of Colorado.

Li, Z., Zhu, Q., and Gold, C. (2005). *Digital Terrain Modeling: Principles and Methodology.* CRC Press, Boca Raton, Fl.

Libby, W. F., Anderson, E. C., and Arnold, J. R. (1949). Age Determination by Radiocarbon Content: World-Wide Assay of Natural Radiocarbon. *Science (New York, N.Y.)*, 109(2827):227–8.

Lidberg, M., Johansson, J. M., Scherneck, H.-G., and Milne, G. A. (2010). Recent results based on continuous GPS observations of the GIA process in Fennoscandia from BIFROST. *Journal of Geodynamics*, 50(1):8–18.

Lindborg, T. and Rubio Lind, L. (2006). Long-term development of the super-regional area of Olkiluoto/Forsmark/laxemar. Minutes from the Posiva and SKB workshop, October 12-13, 2006 Rånäs Slott, Sweden. SKB-Report P-06-302, Swedish Nuclear Fuel and Waste Management Co, Stockholm.

Lisiecki, L. E. and Raymo, M. E. (2005). A Pliocene-Pleistocene stack of 57 globally distributed benthic δ^{18}O records. *Paleoceanography*, 20(1):PA1003.

Lokrantz, H. and Sohlenius, G. (2006). Ice marginal fluctuations during the Weichselian glaciation in Fennoscandia , a literature review. Technical Report TR-06-36, Swedish Nuclear and Waste Management Co, Stockholm.

Lüdeke, M. K. B., Badeck, F.-W., Otto, R. D., Häger, C., Dönges, S., Kindermann, J., Würth, G., Lang, T., Jäkel, U., Klaudius, A., Ramge, P., Habermehl, S., and Kohlmaier, G. H. (1994). The Frankfurt Biosphere Model: a global process-oriented model of seasonal and long-term CO2 exchange between terrestrial ecosystems and the atmosphere. *Climate Research*, 4:143–166.

Lunkka, J. P. and Erikkilä, A. (2012). Behaviour of the Lake District Ice Lobe of the Scandinavian Ice Sheet During the Younger Dryas Chronozone (ca. 12800-11500 years ago). Working Report 2012-17, Posiva Oy, Olkiluoto.

Madsen, K. S., Høyer, J. L., and Tscherning, C. C. (2007). Near-coastal satellite altimetry: Sea surface height variability in the North Sea-Baltic Sea area. *Geophysical Research Letters*, 34(14):L14601.

Mathworks (2014). Curve Fitting Toolbox. "`http://www.mathworks.se/help/curvefit/tpaps.html`".

Maune, D., editor (2001). *Digital Elevation Model Technologies and Applications: The DEM User Manual*. American Society for Photogrammetry and Remote Sensing, Bethesda, MD.

Medvigy, D. and Moorcroft, P. R. (2012). Predicting ecosystem dynamics at regional scales: an evaluation of a terrestrial biosphere model for the forests of northeastern North America. *Philosophical transactions of the Royal Society of London. Series B, Biological sciences*, 367(1586):222–35.

Meehl, G. and Stocker, T. (2007). Global climate projections. In Solomon, S., Qin, D., Manning, M., Chen, Z., Marquis, M., Averyt, K., Tignor, M., and Miller, H., editors,

Contribution of Working Group I to the Fourth Assessment Report of the Intergovernmental Panel on Climate Change, 2007, chapter 10, pages 748–845. Cambridge University Press, Cambridge, United Kingdom and New York NY, USA.

Meyer, R., Joos, F., Esser, G., Heimann, M., Hooss, G., Kohlmaier, G., Sauf, W., Voss, R., and U., W. (1999). The substitution of high-resolution terrestrial biosphere models and carbon sequestration in response to changing CO^2 and climate. *Global Biogeochemical Cycles*, 13(3):785–802.

Migliavacca, M., Sonnentag, O., Keenan, T. F., Cescatti, A., O'Keefe, J., and Richardson, A. D. (2012). On the uncertainty of phenological responses to climate change, and implications for a terrestrial biosphere model. *Biogeosciences*, 9(6):2063–2083.

Milanković, M. (1998). *Canon of Insolation and the Ice-Age Problem*. Avod za Udzbenikb i Nastavna Sredstva, Beograd (1998).

Mitrovica, J. and Peltier, W. (1993). The inference of mantle viscosity from an inversion of the Fennoscandian relaxation spectrum. *Geophysical Journal International*, 114:45–62.

Mörner, N.-A. (1981). Crustal movements and geodynamics in Fennoscandia. *Tectonophysics*, 71:241–251.

Mosegaard, K. and Sambridge, M. (2002). Monte Carlo analysis of inverse problems. *Inverse Problems*, 18(3):R29–R54.

Müller, J., Naeimi, M., Gitlein, O., Timmen, L., and Denker, H. (2012). A land uplift model in Fennoscandia combining GRACE and absolute gravimetry data. *Physics and Chemistry of the Earth, Parts A/B/C*, 53-54:54–60.

National Land Survey of Finland (2013). Elevation model 25 m. "`http://www.maanmittauslaitos.fi/en/digituotteet/elevation-model-25-m`".

National Land Survey of Finland (2014). Laser scanning data. "`http://www.maanmittauslaitos.fi/en/maps-5`".

Nelder, J. and Mead, R. (1965). A simplex method for function minimization. *Computer Journal*, 7:308–313.

Öhman, I., Heikkinen, E., and Lehtimäki, T. (2006). Seismic 2D Reflection Processing and Interpretation of Shallow Refraction Data. Working Report 2006-114, Posiva Oy, Olkiluoto.

Öhman, I., Heikkinen, E., and Lehtimäki, T. (2008). Seismic 2D Reflection Processing and Interpretation of Refraction Seismic Data, Extension Area 2007. Working Report 2008-18, Posiva Oy, Olkiluoto.

Palomäki, J. and Ristimäki, L. e. (2013). Facility Description 2012 Summary Report of the Encapsulation Plant and Disposal Facility Designs. Working Report 2012-66, Posiva Oy, Olkiluoto.

Panza, G. F. (1985). Lateral variations in the lithosphere in correspondence of the Southern Segment of EGT. In A., G. D. and Mueller, S., editors, *Second EGT Workshop: The Southern Segment*, pages 47–51, Strasbourg, France. European Science Foundation.

Peltier, W. (1976). Glacial-Isostatic Adjustment — The Inverse Problem. *Geophysical Journal of the Royal Astronomical Society*, 46(3):669–705.

Peltier, W. (1981). Ice age geodynamics. *Annual Review of Earth and Planetary Sciences*, 9:199–225.

Peltier, W. (1984). The thickness of the continental lithosphere. *Journal of Geophysical Research*, 89(B13):11303–11316.

Peltier, W. (1986). Post-glacial rebound and transient lower mantle rheology. *Geophysical Journal of the Royal Astronomical Society*, 87:79–116.

Peltier, W. (2004). Global glacial isostasy and the surface of the ice-age earth: The ICE-5G (VM2) Model and GRACE. *Annual Review of Earth and Planetary Sciences*, 32(1):111–149.

Peltier, W. and Andrews, J. (1976). Glacial-Isostatic Adjustment - The Forward Problem. *Geophysical Journal of the Royal Astronomical Society*, 46:605–646.

Peltier, W. and Tushingham, A. (1991). Influence of glacial isostatic adjustment on tide gauge measurements of secular sea level change. *Journal of Geophysical Research*, 96(B4):6779–6796.

Peltier, W. R., Farrell, W. E., and Clark, J. A. (1978). Glacial isostasy element model. *Tectonophysics*, 50:81–110.

Pesonen, P., Kammonen, J., Moltchanova, E., Oinonen, M., and Onkamo, P. (2011). Archaelogical radiocarbon dates and ancient shorelines – resources and reservoirs. In Ikonen, A. and Lipping, T., editors, *Proceedings of a Seminar on Sea Level Displacement and Bedrock Uplift, 10-11 June 2010, Pori, Finland*, volume 2011-7 of *Posiva Working Report*, pages 119–129, Olkiluoto. Posiva Oy.

Pestunov, A., Fedotov, A., and Medvedev, S. (2014). Qualitative properties of the minimal model of carbon circulation in the biosphere. *Geophysical Research Abstracts*, 16:14720.

Peteet, D. (2000). Sensitivity and rapidity of vegetational response to abrupt climate change. *Proceedings of the National Academy of Sciences of the United States of America*, 97(4):1359–61.

Pohjola, J., Turunen, J., and Lipping, T. (2009a). Creating High-Resolution Digital Elevation Model Using Thin Plate Spline Interpolation and Monte Carlo Simulation. Working Report 2009-56, Posiva Oy, Olkiluoto.

Pohjola, J., Turunen, J., and Lipping, T. (2012a). Statistical Estimation of Land Uplift Model Parameters Based on Archaeological and Geological Shore Level Displacement Data. Working Report 2012-86, Posiva Oy, Olkiluoto.

Pohjola, J., Turunen, J., Lipping, T., and Ikonen, A. T. K. (2009b). Creation and Error Analysis of High Resolution DEM Based on Source Data Sets of Various Accuracy. In Lee, J. and Zlatanova, S., editors, *3D Geoinformation Sciences: Lecture Notes in Geoinformation and Cartography*, pages 341–353. Springer-Verlag, Berlin, Germany.

Pohjola, J., Turunen, J., Lipping, T., and Ikonen, A. T. K. (2012b). Evaluation and assessment of Arctan-based Post-glacial land uplift model. In Nikolakopoulos, K., editor, *4th international workshop of the EARSeL Special Interest Group 'Geological Applications' - Workshop Proceedings, 24-25 May 2012, Mykonos, Greece*, pages 52–60. EARSeL.

Pohjola, J., Turunen, J., Lipping, T., and Ikonen, A. T. K. (2013). Evaluation and Assessment of Arctangent based Post-glacial Land Uplift Model. *EARSel eProceedings*, 12(2):82–93.

Pohjola, J., Turunen, J., Lipping, T., and Ikonen, A. T. K. (2014a). Biosphere development modeling based on statistical framework. *Computers & Geosciences*, 62:43–52.

Pohjola, J., Turunen, J., Lipping, T., and Ikonen, A. T. K. (2014b). The estimation of future surface water bodies at Olkiluoto area based on statistical terrain and land uplift models. Working Report 2014-11, Posiva Oy, Olkiluoto.

Posiva Oy (2013a). Olkiluoto Biosphere Description 2012. Posiva Report 2012-06, Posiva Oy, Olkiluoto.

Posiva Oy (2013b). Safety Case for the Disposal of Spent Nuclear Fuel at Olkiluoto - Models and Data for the Repository System 2012. Posiva Report 2013-01, Posiva Oy, Olkiluoto.

Posiva Oy (2014). Safety Case for the Disposal of Spent Nuclear Fuel at Olkiluoto - Data Basis for the Biosphere Assessment BSA-2012. Posiva Report 2012-28, Posiva Oy, Olkiluoto.

Poutanen, M. (2011). Present bedrock movements and land uplift. In Ikonen, A. and Lipping, T., editors, *Proceedings of a Seminar on Sea Level Displacement and Bedrock Uplift, 10-11 June 2010, Pori, Finland*, volume 2011-7 of *Posiva Working Report*, pages 25–36, Olkiluoto. Posiva Oy.

Påsse, T. (1987). Shore displacement during the Late Weichselian and Holocene in the Sandsjöbacka area, SW Sweden. *Geologiska Föreningens i Stockholm Förhandlingar*, 109:197–210.

Påsse, T. (1990). Empirical estimation of isostatic uplift using the lake-tilting method at lake Fegen and lake Säven, southwestern Sweden. *Mathematical Geology*, 22(7):803–824.

Påsse, T. (1996). A mathematical model of the shore level displacement in Fennoscandia. Technical Report 96-24, Swedish Nuclear Fuel and Waste Management Co, Stockholm.

Påsse, T. (1997). A mathematical model of past, present and future shore level displacement in Fennoscandia. Technical Report 97-28, Swedish Nuclear Fuel and Waste Management Co, Stockholm.

Påsse, T. (2001). An empirical model of glacio-isostatic movements and shore-level displacement in Fennoscandia. SKB-Report R-01-41, Swedish Nuclear Fuel and Waste Management Co, Stockholm.

Påsse, T. and Andersson, L. (2005). Shore-level displacement in Fennoscandia calculated from empirical data. *GFF*, 127(4):253–268.

Punning, Y. M. (1987). Holocene Eustatic Oscillations of the Baltic Sea Level. *Journal of Coastal Research*, 3(4):505–513.

Rantataro, J. (2001). Acoustic-seismic research in the sea area near Olkiluoto in the year 2000. Working Report 2001-11, Posiva Oy, Olkiluoto.

Rantataro, J. (2002). The estimation of sedimentary rock covered area as well as supplementary interpretation of acoustic-seismic research in Olkiluoto area. Working Report 2002-38, Posiva Oy, Olkiluoto.

Rantataro, J. and Kaskela, A. (2009). Acoustic seismic studies in the sea area close to Olkiluoto, 2008. Working Report 2009-122, Posiva Oy, Olkiluoto.

Richardson, A. D., Anderson, R. S., Arain, M. A., Barr, A. G., Bohrer, G., Chen, G., Chen, J. M., Ciais, P., Davis, K. J., Desai, A. R., Dietze, M. C., Dragoni, D., Garrity, S. R., Gough, C. M., Grant, R., Hollinger, D. Y., Margolis, H. A., McCaughey, H., Migliavacca, M., Monson, R. K., Munger, J. W., Poulter, B., Raczka, B. M., Ricciuto, D. M., Sahoo, A. K., Schaefer, K., Tian, H., Vargas, R., Verbeeck, H., Xiao, J., and Xue, Y. (2012). Terrestrial biosphere models need better representation of vegetation phenology: results from the North American Carbon Program Site Synthesis. *Global Change Biology*, 18(2):566–584.

Rostami, K., Peltier, W., and Mangini, A. (2000). Quaternary marine terraces, sea-level changes and uplift history of Patagonia, Argentina: comparisons with predictions of the ICE-4G (VM2) model of the global process of glacial isostatic adjustment. *Quaternary Science Reviews*, 19(14-15):1495–1525.

Saaranen, V., Rouhiainen, P., and Suurmäki, H. (2012). Precise Levelling Campaigns at Olkiluoto in 2010 and 2011. Working Report 2012-64, Posiva Oy, Olkiluoto.

Sabadini, R. and Vermeersen, B. (2004). *Global Dynamics of the Earth*. Kluwer Academic Publishers, Dordrecht.

Sacks, I., Snoke, J., and Husebye, E. (1979). Lithosphere thickness beneath the Baltic Shield. *Tectonophysics*, 56:101–110.

Sandwell, D. T., Smith, W. H. F., Gille, S., Jayne, S. R., Soofi, K., and Coakley, B. (2001). Bathymetry from Space: White Paper in Support of a High-Resolution, Ocean Altimeter Mission. In Chelton, D. B., editor, *Report of the High-Resolution Ocean Topography Science Working Group Meeting*. The College of Earth, Ocean, and Atmospheric Sciences.

Sato, N., Sellers, P., Randall, D. A., Schneider, E. K., Shukla, J., Kinter III, J. L., Hou, Y.-T., and Albertazzi, E. (1989). Effects of implementing the simple biosphere model in a general circulation model. *Journal of the Atmospheric Sciences*, 46(18):2757–2782.

Scherneck, H.-G., Johansson, J. M., Vermeer, M., Davis, J. L., Milne, G. A., and Mitrovica, J. X. (2001). BIFROST project: 3-D crustal deformation rates derived from GPS confirm postglacial rebound in Fennoscandia. *Earth Planets Space*, 53:703–708.

Seifert, T., Tauber, F., and Kayser, B. (2001). A high resolution spherical grid topography of the Baltic Sea - 2nd edition. In *Baltic Sea Science Congress*, Stockholm.

Sellers, P. J., Mintz, Y., Sud, Y. C., and Dalcher, A. (1986). A simple biosphere model (SiB) for use within general circulation models. *Journal of the Atmospheric Sciences*, 43(6):505–531.

Shan, J. and Toth, C., editors (2009). *Topographic Laser Ranging and Scanning: Principles and Processing*. CRC Press.

SKB (2011a). Long-term safety for the final repository for spent nuclear fuel at Forsmark - Main report of the SR-Site project - Volume I. Technical Report TR-11-01, Swedish Nuclear Fuel and Waste Management Co.

SKB (2011b). Long-term safety for the final repository for spent nuclear fuel at Forsmark - Main report of the SR-Site project - Volume II. Technical Report TR-11-01, Swedish Nuclear Fuel and Waste Management Co.

Smith, W. and Sandwell, D. (1997). Global sea floor topography from satellite altimetry and ship depth soundings. *Science*, 277(September):1956–1962.

Steffen, H. and Wu, P. (2011). Glacial isostatic adjustment in Fennoscandia - review of data and modeling. *Journal of Geodynamics*, 52(3-4):169–204.

Steffen, R., Wu, P., Steffen, H., and Eaton, D. W. (2013). On the implementation of faults in finite-element glacial isostatic adjustment models. *Computers & Geosciences*, 62:150–159.

STUK (2013). Disposal of Nuclear Waste. Guide YVL D.5, Säteilyturvakeskus, Helsinki.

Svendsen, J. I. and Mangerud, J. (1990). Seal-level changes and pollen stratigraphy on the outer coast of Sunnmøre, western Norway. *Norsk Geologisk Tidskrift*, 70:111–134.

Tallavaara, M., Pesonen, P., and Oinonen, M. (2010). Prehistoric population history in eastern Fennoscandia. *Journal of Archaeological Science*, 37(2):251–260.

Tappen, J. J., Wasiolek, M. A., Wu, D. W., Schmitt, J. F., and Smith, A. J. (2001). Biosphere Modeling and Analyses in Support of Total System Performance Assessment. In *WM'02 Conference*, number 1, pages 1–13, Tucson AZ, USA.

Thomsen, H. (1981). Late Weichselian shore-level displacement on Nord-Jæren, south-west Norway. *Geologiska Föreningens i Stockholm Förhandlingar*, 103(4):447–468.

Timmen, L., Gitlein, O., Denker, H., Bilker, M., Wilmes, H., Falk, R., Reinhold, A., Hoppe, W., Pettersen, B. R., Engen, B., Engfeldt, A., Strykowski, G., Forsberg, R., Observatory, O. S., and Survey, N. (2004). Observing Fennoscandian geoid change for GRACE validation. In *Joint CHAMP / GRACE Science Meeting, Potsdam, 6.7-8.7.2004.*, pages 1–10.

Tobler, W. (1970). A computer movie simulating urban growth in the Detroit region. *Economic Geography*, 46(2):234–240.

Turveteollisuusliitto (2014). Turvetuotanto –lyhyt välivaihe suon historiassa. "`http://www.turveteollisuusliitto.fi/index.php?id=239`".

Tushingham, A. and Peltier, W. (1992). Validation of the ICE-3G Model of Würm-Wisconsin Deglaciation using a global data base of relative sea level histories. *Journal of Geophysical Research*, 97(B3):3285–3304.

Vermeer, M. and Rahmstorf, S. (2009). Global sea level linked to global temperature. *Proceedings of the National Academy of Sciences of the United States of America*, 106(51):21527–32.

Vestøl, O. (2006). Determination of Postglacial Land Uplift in Fennoscandia from Leveling, Tide-gauges and Continuous GPS Stations using Least Squares Collocation. *Journal of Geodesy*, 80(5):248–258.

Vuorela, A., Penttinen, T., and Lahdenperä, A.-M. (2009). Review of Bothnian Sea Shore-Level Displacement Data and Use of a GIS Tool to Estimate Isostatic Uplift Review of Bothnian Sea Shore-Level Displacement Data and Use of a GIS Tool to Estimate Isostatic Uplift. Working Report 2009-17, Posiva Oy, Olkiluoto.

Wang, H., Wu, P., and Wang, Z. (2006). An approach for spherical harmonic analysis of non-smooth data. *Computers & Geosciences*, 32(10):1654–1668.

Whitehouse, P. (2009). Glacial isostatic adjustment and sea-level change. Technical Report TR-09-11, Swedish Nuclear Fuel and Waste Management Co, Stockholm.

Wu, P., Johnston, P., and Lambeck, K. (1999). Postglacial rebound and fault instability in Fennoscandia. *Geophysical Journal International*, 139(3):657–670.

Yates, D. N., Kittel, T. G. F., and Cannon, R. F. (2000). Comparing the correlative Holdridge model to mechanistic biogeographical models for assessing vegetation distribution response to climatic change. *Climatic Change*, 44:59–87.

Yu, Z. and Eicher, U. (2001). Three amphi-Atlantic century-scale cold events during the Bølling-Allerød warm period. *Géographie physique et Quaternaire*, 55(2):171–179.

Tampereen teknillinen yliopisto
PL 527
33101 Tampere

Tampere University of Technology
P.O.B. 527
FI-33101 Tampere, Finland

ISBN 978-952-15-3409-6
ISSN 1459-2045